DYNAMIC STUDIES ON THE BEARING CAPACITY OF PILES

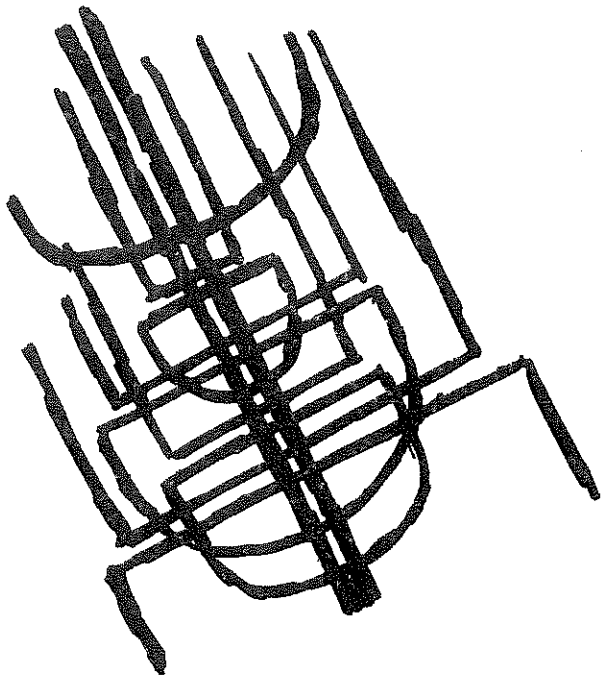

PHASE III VOLUME II

REPORT NO. 48

DIVISION OF
SOLID MECHANICS STRUCTURES AND MECHANICAL DESIGN
SCHOOL OF ENGINEERING CASE WESTERN RESERVE UNIVERSITY

DYNAMIC STUDIES ON THE BEARING CAPACITY OF PILES

Project Report of Phase III

August 1, 1970

by

G. G. Goble

F. Rausche

F. Moses

This research was sponsored by the Ohio Department of Highways and the Federal Highway Administration. The opinions, findings and conclusions expressed in this publication are those of the authors and not necessarily those of the State or the Federal Highway Administration.

Case Western Reserve University
Division of Solid Mechanics,
Structures, and Mechanical Design
University Circle
Cleveland, Ohio 44106

TABLE OF CONTENTS

Volume I

TABLE OF CONTENTS (Continued)

CHAPTER I

Lumped Mass Analysis

1.1 Numerical Procedure

For this analysis, the pile is modeled as a series of discrete masses and springs as shown in Figure 1.1. The problem is to find the displacements during dynamic loading of all elements. Given are either the force acting on the top element or its acceleration, both as a function of time, and various passive force boundary conditions for each element. These passive forces can be regarded as functions of displacement and velocity. In Chapter V a study is presented on the physical model of resistance used, and its limitations.

The piles encountered during this project were, with only a few exceptions, steel pipes of constant cross section. The computer program, therefore, was set up for uniform cross sections and steel elastic properties. However, the changes to a more general pile, for example tapered piles or steel piles filled with concrete, could be easily accomplished and examples of this modification are given in Reference 1.

Consider Figure 1.1. A continuous pile is replaced by n mass elements and n-1 interconnecting springs. The boundary conditions, either acceleration or force, are available from measurements at the middle of the top element. Then stiffnesses

$$k = \frac{EA}{L} n \qquad (1.1)$$

can be assigned to all the springs, and masses

$$M = \frac{1}{n} AL\rho \tag{1.2}$$

to all elements.

Some resistance force, $r_{i,j}$, acts on the i^{th} element at time $t_j = j \cdot \Delta t$. Displacements, velocities, and accelerations of element i at time t_j are $u_{i,j}$, $\dot{u}_{i,j}$ and $\ddot{u}_{i,j}$, respectively. The top element is acted upon by an active force F_j. Velocity and displacement are obtained from the piecewise linear acceleration using:

$$\dot{u}_{i,j} = \dot{u}_{i,j-1} + \frac{1}{2}(\ddot{u}_{i,j-1} + \ddot{u}_{i,j})\Delta t \tag{1.3}$$

and

$$u_{i,j} = u_{i,j-1} + \dot{u}_{i,j-1}\,\Delta t + (\ddot{u}_{i,j} + 2\ddot{u}_{i,j-1})\frac{\Delta t^2}{6} \tag{1.4}$$

Here a comparison with the method developed by Newmark (2) can be made. Instead of Equation 1.4, Newmark proposed the following equation for computing the displacement

$$u_{i,j} = u_{i,j-1} + \dot{u}_{i,j-1}\,\Delta t + (\frac{1}{2} - \beta)\ddot{u}_{i,j-1}\,\Delta t^2 + \beta\ddot{u}_{i,j}\Delta t^2 \tag{1.5}$$

Comparing this equation with Equation 1.4 it can be observed that β is the coefficient obtained by twice integrating a linearly increasing acceleration (e.g. $\ddot{u} = at \rightarrow u = \frac{1}{6} at^3$).

The force in the i-th spring at time t_j is

$$F_{i,j} = k(u_{i+1,j} - u_{i,j}) \tag{1.5}$$

Applying Newton's Second Law to the i-th element, one obtains at a given time j:

$$M\ddot{u}_{i,j} = k(u_{i+1,j} - u_{i,j}) - k(u_{i,j} - u_{i-1,j}) - r_{i,j}$$

or

$$\ddot{u}_{i,j} = \frac{1}{M}\{k(u_{i+1,j} - 2u_{i,j} + u_{i-1,j}) - r_{i,j}\} \tag{1.6}$$

Then $u_{i+1,j}$, $u_{i,j}$ and $r_{i,j}$ (a function of $u_{i,j}$ and $\dot{u}_{i,j}$) will be unknown in this equation. Therefore, Equation 1.4 is applied on both $u_{i+1,j}$ and $u_{i,j}$ to obtain:

$$\ddot{u}_{i,j} = \frac{1}{M + \frac{\Delta t^2}{3}k}\{[\dot{u}_{i+1,j-1}\,\Delta t + u_{i-1,j} + u_{i+1,j-1} - 2(u_{i,j-1} + \dot{u}_{i,j-1}\,\Delta t) + \frac{\Delta t^2}{6}(\ddot{u}_{i+1,j} + 2\ddot{u}_{i+1,j-1} - 4\ddot{u}_{i,j-1})]k - r_{i,j}\} \tag{1.7}$$

Now, the only unknown left is $\ddot{u}_{i+1,j}$ if we determine $r_{i,j}$ by using $\dot{u}_{i,j-1}$ instead of $\dot{u}_{i,j}$ and $\dot{u}_{i,j-1}\,\Delta t$ instead of $u_{i,j}$. Except for the top and bottom element Equation 1.7 can be used to compute $\ddot{u}_{i,j}$. For the first prediction $\ddot{u}_{i+1,j}$ is set to zero. For any later iteration step $\ddot{u}_{i+1,j}$ can be used as obtained in the previous calculation, while $r_{i,j}$ is always computed using the previous results for $u_{i,j}$ and $\dot{u}_{i,j}$. Both $u_{i,j}$ and $\dot{u}_{i,j}$ are readily obtained using Equations 1.3 and 1.4.

For the n-th element, i.e. the pile bottom, 1.7 reduces to:

$$\ddot{u}_{n,j} = \frac{1}{M + \frac{k\Delta t^2}{6}} \{[(u_{n-1,j} - (u_{n,j-1} + \dot{u}_{n,j-1}\,\Delta t + \ddot{u}_{n,j-1}\,\frac{\Delta t^2}{3})]k - r_{n,j}\} \qquad (1.8)$$

where $r_{n,j}$ is the only unknown.

At the pile top force F_j may be prescribed and the acceleration computed. Then

$$\ddot{u}_{1,j} = \frac{1}{M + \frac{k\Delta t^2}{6}} \{[u_{2,j-1} + \dot{u}_{2,j-1}\,\Delta t - (u_{1,j-1} + \dot{u}_{1,j-1}\Delta t) + \frac{\Delta t^2}{6}(\ddot{u}_{2,j} + 2\ddot{u}_{2,j-1} - 2\ddot{u}_{1,j-1})]\,k + F_j\} \qquad (1.9)$$

where the only unknown is $\ddot{u}_{2,j}$ since a passive reaction is not assumed to act on the top element.

If the acceleration $\ddot{u}_{1,j}$ is given as a boundary condition then the force can be calculated from:

$$F_j = M\ddot{u}_{1,j} + k[-u_{2,j-1} - \dot{u}_{2,j-1}\,\Delta t + u_{1,j-1} + \dot{u}_{1,j-1}\,\Delta t - \frac{\Delta t^2}{6}(\ddot{u}_{2,j} + 2\ddot{u}_{2,j-1} - 2\ddot{u}_{1,j-1} - \ddot{u}_{1,j})] \qquad (1.10)$$

where again $\ddot{u}_{2,j}$ can be set to zero for the first step and equal to the previously calculated value for all later iteration steps.

Convergence will be reached when the relative difference between successive results is smaller than a chosen number ε. (The influence of the magnitude ε will be studied in the next section of this Chapter). It is possible to compare displacements, velocities or accelerations. Certainly acceleration will be the most sensitive variable but it was found that a velocity controlled iteration yields good results. In the case of an acceleration input condition on top of the pile, a check is performed on the calculated top force. Thus, the convergence criterion which must be satisfied for all j can be written as

$$\frac{(\dot{u}_{i,j})_{new} - (\dot{u}_{i,j})_{old}}{(\dot{u}_{i,j})_{new}} < \varepsilon \quad i = 1,2,\ldots,n \qquad (1.11)$$

where $u_{1,j}$ might be replaced by F_j.

The frequency of the top boundary condition is an important factor in the choice of the time increment, Δt. It is important that no extreme values of these functions are missed. If Δt is small enough, errors will be negligible (see Fig. 1.4). It is then possible to approximate the continuous boundary function by a sequence of straight lines. Consequently, it should be sufficiently accurate to express accelerations of pile elements as a sequence of straight lines as well. This leads to velocities and displacements being polynomials of second and third order, respectively.

1.2 Analysis Parameter Study

1.2.1 Number of Elements

The numerical method chosen can, at best, be expected to give the solution for the pile modeled as a system with n degrees of freedom. The question, therefore, is how many elements are necessary to accurately represent the continuous pile. For purposes of comparison, using the same acceleration input, time interval and convergence criterion, a pile without reaction forces was analyzed divided into 5, 10 and 20 elements. The exact solution for the continuous pile is easily obtained for this case (see Chapter III) and is given together with the lumped mass solution in Figure 1.2. It should be noted that the actual pile length is not involved in this comparison because it is not a factor in the number of elements needed. As can be seen, while 5 elements represent a poor model, the 10 element system is already a good approximation to the actual solution and 20 elements give noticeable differences only where there are rapid changes of force. It can be deduced that 20 elements will yield a very accurate solution while 10 elements give good qualitative results.

1.2.2 Time Increment

Once the number of elements has been determined the choice of a time increment is constrained. The reason for this is the occurrence of instability of solution whenever the distance traveled by the stress wave in one time increment is constrained. Investigations

into this phenomenon have been undertaken and are discussed by Crandall (3). The suggested limit imposed on Δt is

$$\Delta t \leq L/c \tag{1.12,a}$$

which becomes

$$\Delta t \leq \sqrt{\frac{M}{k}} \tag{1.12,b}$$

using $c^2 \leq E/\rho$.

Now, introducing

$$\phi = \frac{\Delta L}{\Delta t \cdot c} \tag{1.13}$$

as used by Smith (1), $\phi > 1$ will always yield a stable solution. Figure 1.3 shows an exact solution and three other solutions using $\phi = 1/2$ (unstable), $\phi = 1$ and $\phi = 2$. All three solutions were obtained for n = 20. The differences between $\phi = 1$ and $\phi = 2$ are very small and can be accounted for by observing that the input condition is not exactly the same when more time increments are placed on the sequence of straight lines. Figure 1.4 shows what happens to the acceleration input data when used with different lengths of time increment.

1.2.3 Convergence Criterion

Various calculations were performed using different and also calculations without any iteration. It is seen in Figure 1.5 that, whenever enough elements are chosen, say greater than 10, a number .1 will be sufficient and that the iteration starts to improve the solution after 2L/c. These comparisons, however, might yield quite different results when the solutions is carried forward over a longer time interval.

1.2.4 Computation Time

In order to draw conclusions about the accuracy and feasibility of the lumped mass analysis method, the computation time has to be considered. The calculations listed in Table 1.1 were performed on a Univac 1108 Computer. The program was written in Fortran V. The computer time in seconds is an approximation because time is listed only in half seconds. However, it can be seen that solutions using less than 3 seconds are not satisfactory. Using 30 elements did not give substantial improvement while the computation time increase was considerable (9.5 seconds!). The use of 20 elements together with $\phi = 1$ (Δt = .227 milliseconds in this case) gave a satisfactory result and used only 3 seconds. The result could not be much improved by halving the time increment which resulted in almost doubling the computation time. Note that the only satisfactory result for a pure prediction analysis took 2.5 seconds while the result between 2L/c and 4L/c is still quite erroneous as compared to the iterative computation on line 7 which took only 3 seconds. The method of analysis has the advantage of

accuracy and stability within the time domain considered. Only a few rules must be observed in choosing the necessary parameters, i.e. $\phi > 1$, $n > 10$ and $\varepsilon \leq .1$. The application of a predictor-corrector iteration seems justified when considering the increased accuracy in the time region after $2L/c$.

CHAPTER II

Static Analysis

2.1 Introduction

The resistance parameters obtained from dynamic analysis make possible the computation of a load deformation curve to compare to a static load test. The soil parameters describe the shear resistance at the pile soil interface as a function of deformation. Actually, such an analysis should take into account the deformations of underlying soil strata. However, this would require a much better knowledge of the static soil behavior than can possibly be obtained from dynamic measurements. The analysis described below will give results which can be used for correlating dynamic predictions to static measurement and it will provide a valuable tool to obtain an estimate on the pile deformations to be expected. First, the pile is divided into n elements as it was done for the purpose of dynamic analysis in Chapter I. The static soil resistance acting on the ith element is assumed to be directly dependent on the absolute pile displacement and is modeled again by an elastic plastic spring with stiffness $k_{si} = S_{o,i}/q_i$, where $S_{o,i}$ is the ultimate soil resistance and q_i the quake of the shear resistance at the element.

Under these assumptions the load versus deformation curve of the pile will be a piecewise linear function. Once all displacements are larger than the quake the ultimate bearing capacity has been

reached and no more load increase can be obtained.

2.2 Mathematical Formulation

Consider the i-th element in Figure 1.1. Using the same notations as in Chapter I its equilibrium condition can be written as:

$$k(u_{i-1} - u_i) + k(u_{i+1} - u_i) = k_{si}u_i^* \tag{2.1}$$

where

$$u_i^* = \begin{cases} u_i \text{ for } u_i \leq q_i \\ q_i \text{ for } u_i > q_i \end{cases}$$

Thus for $u_i \leq q_i$ Equation 2.1 can be written as

$$-u_{i-1} + (2 + k_{si}/k)u_i - u_{i+1} = 0 \tag{2.2a}$$

and after the displacement has exceeded the quake

$$-u_{i-1} + 2u_i - u_{i+1} = \frac{k_{si}}{k} q_i \tag{2.2b}$$

For the first element on which no reaction forces were assumed to act (Chapter III) the equilibrium equation becomes

$$u_1 - u_2 = F_{top}/k \tag{2.3}$$

where F_{top} is the load applied at the top of the pile. At the tip

$$-u_{n-1} + u_n(1 + k_{si}/k) = 0 \text{ for } u \leq q_n \tag{2.4a}$$

or

$$-u_{n-1} + u_n = (k_{si}/k)q_n \text{ otherwise.} \tag{2.4b}$$

Thus, a system of n equations with n unknowns is obtained which has to be solved for any interval between two consecutive yields of shear resistances. Since shear resistances are acting on n-1 elements this means solving n-1 times.

The procedure followed here uses the same approach as would be followed in a static load test. First some load F_{top} is applied on the top and then the deflections u_i are calculated for all elements, $i = 1, 2, \ldots, n$. The next step is to determine which of the resistance forces will reach the quake first. This can be done by investigating the ratios u_i/q_i. If their maximum happens to be u_j/q_j then the first spring to yield will be located at the j-th element. Because of linearity, the displacements for the instant when the j-th ultimate shear is reached can be calculated from proportionality

$$u_{i,j} = u_i \cdot \frac{q_j}{u_j} \tag{2.5}$$

and the force on top of the pile is

$$F_{top,j} = F_{top} \frac{q_j}{u_j} \qquad (2.6)$$

In this way the first point of the load deflection curve is obtained when plotting $F_{top,j}$ versus $u_{i,j}$.

A new system of equations has to be set up now by writing the j-th equation using eq. 2.2b instead of 2.2a. The new system can be solved when using $F_{top} = F_{top,j} + \Delta F$ where ΔF is an arbitrary load increase and following the same routine as described above.

In this way n-1 systems of linear equation each having n unknowns and n equations have to be solved which can be done conveniently by means of iteration always using the previous result as a starting point.

Results from this analysis were used and are demonstrated in Chapter III of Volume 1 for correlating soil resistance predictions with results from actual static load tests.

CHAPTER III

Wave Propagation in a Pile Under Impact

3.1 Force and Velocity Relation in a Stress Wave

If $u(x,t)$ is the displacement of a particle in a uniform and elastic rod at distance x from some fixed coordinate origin at time t, then the governing differential equation, the so-called wave equation, is

$$\frac{\partial^2 u}{\partial t^2} = c^2 \frac{\partial^2 u}{\partial x^2} \tag{3.1}$$

where $c^2 = E/\rho$. Young's Modulus and mass density of the pile material are E and ρ, respectively. The general solution of the equation is

$$u(x,t) = f(x + ct) + g(x - ct) \tag{3.2}$$

which is easily checked by back substitution. The general solution can be interpreted physically by giving t a fixed value t_1. Then u is a function of x only and can be split into two components: $f(x + ct_1)$ and $g(x - ct_1)$. At a later time t_2

$$f(x + ct_2) = f(x + c(t_2 - t_1) + ct_1) \quad \text{and}$$
$$g(x - ct_2) = g(x - c(t_2 - t_1) - ct_1).$$

If, therefore, a distance $c(t_2 - t_1)$ is subtracted from x then the

station is found at which f has the value at time t_2 that it had at x at time t_1; g will have the same value at $x + c(t_2 - t_1)$ at time t_2 which it had at time t_1 at x. In other words, if f and g are considered to be displacement waves then f travels in the negative x-direction and g travels in the positive x-direction, both having speed c.

Differentiating Equation 3.2 with respect to time leads to an expression for the velocity v(x,t) of a particle

$$v(x,t) = c\left(\frac{\partial f(\eta)}{\partial \eta} - \frac{\partial g(\mu)}{\partial \mu}\right) \tag{3.3}$$

where $\eta = x + ct$ and $\mu = x - ct$. Equation 3.3 can be written as

$$v(x,t) = v_f(x + ct) + v_g(x - ct) \tag{3.4}$$

thus, v can also be described by two waves v_f and v_g which travel in opposite directions.

Now, suppose that the shape of the functions f and g and, therefore, u(x,t) is known at a certain time, t. Then the strain, ε, is obtained by differentiating u(x,t) with respect to x

$$\frac{\partial u}{\partial x} = \varepsilon(x,t) = \frac{\partial}{\partial x}(f(x + ct) + g(x - ct))$$

or

$$\varepsilon(x,t) = \frac{\partial f(\eta)}{\partial \eta} + \frac{g(\mu)}{\partial \mu} \tag{3.5}$$

The advantage of using derivatives with respect to η or μ becomes apparent since these derivatives express the behavior of the derivative with respect to both x and t. Using the rod cross section area A and taking compressive forces positive, the force F(x,t) in the wave can be calculated.

$$F(x,t) = (AE/c)\ (-v_f(x \pm ct) + v_g(x - ct) \qquad (3.6)$$

Thus, there exists a simple relation between particle velocity and force in a stress wave, the force being proportional to the velocity by a factor AE/c. The force will be compressive when the velocities of particles and wave propagation have the same direction and it will be a tension force otherwise.

3.2 Boundary Conditions

So far, only the homogeneous differential equation has been considered and nothing has been said about boundary conditions or external forces. Since the differential equation is linear, superposition is valid, so that a case of complicated boundary conditions can be split into several basic types of easily solvable problems. If the boundary conditions were nonlinear then a result can be obtained by assuming piecewise linear boundary conditions and superimposing their effects. A wave reaching the end of the rod might encounter either prescribed force or displacement conditions. This problem can be split into the case where the wave travels in a rod with homogeneous, i.e. zero force or displacement, boundary conditions plus the case where no wave is present with non zero end forces

or displacements. The case where external forces are acting along the rod may also be treated separately and then superimposed on to the homogeneous solution. Prescribed displacements have to be considered at the end of the rod only. Therefore, four basic conditions must be treated

(i) Wave approaching a free end,

(ii) Wave approaching a fixed end,

(iii) Prescribed force acting at a point along the rod,

(iv) Prescribed displacements at the end of the rod.

Case (i) Wave in a Rod with Free End

Consider Figure 3.1 where on the left a wave $g(x - ct)$ is shown approaching the free end ($x = L$) of the rod. Connected to it on the right is an imaginary rod along which $f(x + ct)$ travels in negative x-direction chosen so

$$f(2L - x + ct) = g(x - ct) \tag{3.7}$$

Therefore,

$$\frac{\partial f}{\partial x} = - \frac{\partial g}{\partial x}$$

Both waves will arrive at $x = L$ at the same time. From superposition the displacement and strain can be calculated

$$u(L,t) = f(L + ct) + g(L - ct) = 2f(L + ct)$$

$$\varepsilon(L,t) = \frac{f(L + ct)}{x} + \frac{g(L + ct)}{x} = 0$$

Thus the boundary condition of a free end is satisfied. The wave $f(x + ct)$ will now travel in negative x-direction through the rod. It is called a reflection wave. As compared to the initiating wave $g(x - ct)$ it will cause displacements of the same sign but forces of opposite sign. The displacement at the free end will be twice that of the approaching wave.

Case (ii) Wave Approaching a Fixed End

An imaginary rod is again used for the case where the displacement of the end of a rod must be zero. In this case, however, the wave traveling in the negative x-direction is chosen so that

$$f(2L - x + ct) = -g(x - ct) \tag{3.8}$$

and, therefore, $\frac{\partial f}{\partial x} = \frac{\partial g}{\partial x}$. As a result of superposition the force at the fixed end will be doubled while the displacements cancel. The reflection wave will propagate displacements of opposite direction but forces of the same sign as the initiating wave.

Case (iii) Prescribed Force Acting at a Point Along the Rod

If a force is applied at $x = x^*$ along the rod then the continuity condition requires

$$u(x^*_L, t) = u(x^*_R, t) \tag{3.9}$$

where x^*_L and x^*_R are on the left and the right side of the loaded

cross section, respectively (Figure 3.2). This can also be written in terms of velocity

$$\frac{\partial u(x^*_L,t)}{\partial t} = \frac{\partial u(x^*_R,t)}{\partial t} \tag{3.10}$$

Also the equilibrium condition has to be satisfied, i.e.

$$AE\left(\frac{\partial u(x^*_L,t)}{\partial x} - \frac{\partial u(x^*_R,t)}{\partial x}\right) = F_A(x^*,t) \tag{3.11}$$

where $F_A(x^*,t)$ is the applied force at $x = x^*$ and time t. Now recalling Equations 3.3 and 3.5, Equations 3.10 and 3.11 can be satisfied by choosing

$$\frac{\partial f(\mu)}{\eta}\bigg|_{x = x^*_L} = \frac{\partial g(\mu)}{\partial \mu}\bigg|_{x = x^*_R} = \frac{1}{2}F_A(x^*,t)/EA \tag{3.12}$$

and

$$\frac{\partial f(\eta)}{\partial \eta}\bigg|_{x = x^*_R} = \frac{\partial g(\mu)}{\partial \mu}\bigg|_{x = x_L} = 0 \tag{3.12}$$

Substituting these two conditions in Equation 3.10 leads to

$$c\left[\frac{1}{2}F_A(x^*,t)/AE + 0\right] = c\left[0 + \frac{1}{2}F_A(x^*,t)/AE\right] \tag{3.13}$$

thus, satisfying the continuity condition.

Similarly it proves that the equilibrium condition is satisfied. Figure 3.2 shows that both waves carry a force of one half of

the applied force while the velocities the same in both waves having the same direction as the applied force and magnitude $\frac{1}{2}F_A(x^*,t)c/EA$.

The case where the force is acting at the end of the rod can be deduced since one of the half-waves is immediately reflected and superimposed on the other. Therefore, a wave will travel away from the end with particle velocity

$$\frac{\partial u(x,t)}{\partial t} = cF_A(t - (L - x)/c) \tag{3.14}$$

and strain

$$\varepsilon(x,t) = F_A(t - (L - x)/c)/AE \tag{3.15}$$

Case (iv) Prescribed Displacements at the End of the Rod

The case of a prescribed displacement condition at a point along the rod will not be discussed since this is equivalent to a rod of shorter length with prescribed end displacement. A displacement prescribed at the end of a rod is equivalent to a prescribed velocity: $v_A(L,t)$. From the force velocity proportionality relation this can be considered a force condition where the force has to be chosen as $F_A(L,t) = v_A(L,t)EA/c$. Thus Case (iii) can be applied.

3.3 Superposition of Waves

In this section certain special cases will be treated where the findings of Section 3.2 are applied. These special cases will be

needed in treating problems where external forces act along the pile together with prescribed end conditions.

(i) Free Pile Under Known Velocity at the Top

Suppose a velocity, $v_A(t)$, which is zero for $t < 0$ is imposed on the top of a pile of length, L. It is desired to know the top force necessary to maintain this velocity when no other forces are acting along the pile.

As long as the wave created by $v_A(t)$ has not yet reached the free end (i.e. for t L/c) a pile particle at a point has velocity

$$v_i(t) = v_A(t - x_i/c)$$

At time $t = L/c$ the wave reaches the free end of the pile and case (i) of Section 3.2 applies. Thus, a reflection wave having velocities of the same sign and forces of opposite signs will travel back up the pile. The velocity at a station $x = x_i$ becomes

$$v_i(t) = v_A\left(t - \frac{2L - x_i}{c}\right) + v_A\left(t - \frac{x_i}{c}\right) \qquad (3.16)$$

for $t \leq \frac{2L + x_i}{c}$.

A new reflection wave will be generated when this "up"-traveling wave reaches the top since here the velocity is prescribed. Case (ii) of Section 2 describes this fixed end situation. This second reflection requires a force; therefore, the proportionality between applied velocity and top forces will no longer hold. The force at the top of

the free pile may be denoted by $F_f(t)$; then for $t < 2L/c$

$$F_f(t) = v_A(t)EA/c$$

and for $2L/c \leq t < 4L/c$

$$F_f(t) = [v_A(t) - 2v_A(t - 2L/c)]EA/c \tag{3.17}$$

At a time $t = 3L/c$ the wave will again be reflected at the bottom end. (It had been reflected at the top at time $2L/c$). At time $t = 4L/c$ the wave has to be reflected again at the top but this time it has the opposite stress due to the previous reflection at tne free end. In general for, $\frac{2Lr}{c} \leq t \leq \frac{2L}{c}(r + 1)$

$$F_f(t) = \frac{EA}{c}[v_A(t) + 2\sum_{j=1}^{r} v_A(t - j\,\frac{2L}{c})(-1)^j] \tag{3.18}$$

where $r = 0,1,2,\ldots$, refers to the time interval considered. Equation 3.18 gives the exact solution for a given top velocity and no reaction forces. This equation can be used as a check on the lumped mass analysis. Comparative results of this kind are shown in Chapter I of this volume. Furthermore, if this solution is subtracted from the measured force, the Measured Delta curve is obtained as defined in Chapter II of the first volume.

Equation 3.16 gives an expression for the velocity at some point in the pile for times $t < (2L + x_i)/c$. The equation can be

extended for times $\frac{2Lr + x_i}{c} \leq t < \frac{2L(r+1) + x_i}{c}$, $r = 0,1.2,\ldots$

$$v_i(t) = \sum_{j=0}^{r} (-1)^j [v_A(t - \{2jL + x_i\}/c) - v_A(t - \{(j+1)2L - x_i\}/c)] \tag{3.19}$$

(ii) External Force Acting on a Pile with Fixed Top and Free Bottom

The force denoted by $R_i(t)$, is assumed to act upwards. If it is acting at $x = x_i$ then the results of Section 3.2 case (iii) apply. Thus, two waves are induced traveling in opposite directions and having particle velocities (at $x = x_i$ and time t)

$$v_r(t) = - \frac{c}{2EA} R_i(t)$$

The forces in the ware are

$$F_r(t) = \pm 1/2R(t)$$

i.e. a compression in the upwards and tension in the downwards traveling wave. The reaction force $F_{top}(t)$ on the fixed top of the pile due to this velocity will be a compression force of twice the magnitude of the force in the wave (Case (ii) Section 3.2). The upwards traveling wave will arrive at the top at a time x_i/c after it is applied, hence

$$F_{top}(t) = R_i(t - x_i/c) \tag{3.20}$$

which is valid for a time as long as it takes the initially downwards traveling wave to reach the top after reflection at the bottom. This reflection at the free bottom end causes the initially downwards traveling wave to change the sign in force (Case (i) Section 3.2) and therefore, is also a compression wave after reflection. Reaching the top at a time $(2L - x_i)/c$ after it was generated by the resistance force, this wave also will produce twice the force at the top which it was propagating. The next wave to arrive at the top will be the initially upwards traveling wave, its sign will be converted so that a tension wave arrives.

This way the reaction at the fixed pile top due to $R_i(t)$ can be calculated for $0 \leq t < 4L/c$

$$F_{top}(t) = R_i(t - \frac{x_i}{c}) + R_i(t - \frac{2L - x_i}{c}) - R_i(t - \frac{2L + x_i}{c}) - R_i(t - \frac{4L - x_i}{c}) \tag{3.21}$$

For later times it can be observed that all the waves which arrived at a time t_1 at the top have in the mean time changed their sign twice thus arriving again with the same sign at a time $t_1 + 4L/c$. This result can be expected since a pile of length L has a lowest natural frequency of $c/4L$, inferring that in the absence of external forces a harmonic behavior can be observed. Therefore, for times

$r\ 4L/c \leq t < (r+1)4L/c$

$$F_{top}(t) = \sum_{j=0}^{r} [R_i(t - \frac{x_i}{c} - j\frac{4L}{c}) + R_i(t - \frac{2L - x_i}{c} - j\frac{4L}{c}) + R_i(t - \frac{2L + x_i}{c} - j\frac{4L}{c}) - R_i(t + \frac{x_i}{c} - (j+1)\frac{4L}{c})] \quad (3.22)$$

and $r = 0,1,2\ldots,n$ indicates the time interval considered.

The problem of obtaining the particle velocities at a point $x = x_h$ when the load, $R_i(t)$ is acting at $x = x_i$ is somewhat more complicated. It can be split in two parts, first considering the wave which is initially moving upwards and then the wave which is initially moving downwards. Both of these waves have a particle velocity $-c/2EA\ R_i(t)$. In order to facilitate the derivation it is further assumed that $x_h > x_i$. Then the velocity $v_{h,up}(t)$ at $x = x_h$ due to the upwards traveling wave obtains its first contribution after a time $(x_h + x_i)/c$, i.e. the time necessary for the wave to reach the top and upon reflection the station $x = x_h$. The wave will again be reflected at the bottom end with no sign change in velocities and reach $x = x_h$ a second time with the same sign in the velocities. Thus, when observing the wave's action at $x = x_h$ for a time $t < 4L/c$

$$v_{h,up}(t) = \frac{c}{EA}[R_i(t - \frac{x_h + x_i}{c}) + R_i(t - \frac{2L + x_i - x_h}{c}) - R_i(t - \frac{2L + x_h + x_i}{c}) - R_i(t - \frac{4L + x_i - x_h}{c})] \quad (3.23)$$

Similarly the influence on the velocity at $x = x_h$ of the initially downwards traveling wave can be determined.

$$v_{h,down}(t) = \frac{c}{2EA}[-R_i(t - \frac{x_h - x_i}{c}) - R_i(t - \frac{2L - x_i - x_h}{c}) + R_i(t - \frac{2L + x_h - x_i}{c}) + R_i(t - \frac{4L - x_i - x_h}{c})] \tag{3.24}$$

Observing that the waves arrive with the same sign of force and velocity after every 4L/c then superimposing the results from Equation 3.23 and 3.24 the velocity $v_h(t)$ due to $R_i(t)$ becomes, for $r\frac{4L}{c} \leq t \leq (r + 1)\frac{4L}{c}$

$$\begin{aligned} v_h(t) = \frac{c}{2EA} \sum_{j=0}^{r} \{ & R_i(t - \frac{x_h + x_i}{c} - j\frac{4L}{c}) \\ & + R_i(t - \frac{2L + x_i - x_h}{c} - j\frac{4L}{c}) \\ & - R_i(t - \frac{2L + x_h + x_i}{c} - j\frac{4L}{c}) \\ & - R_i(t - \frac{x_i - x_h}{c} - (j + 1)\frac{4L}{c}) \\ & - R_i(t - \frac{x_h - x_i}{c} - j\frac{4L}{c}) - R_i(t - \frac{2L - x_i - x_j}{c} - j\frac{4L}{c}) \\ & + R_i(t - \frac{2L + x_h - x_i}{c} - j\frac{4L}{c}) \\ & + R_i(t - \frac{-x_i - x_h}{c} - (j + 1)\frac{4L}{c})\} \end{aligned} \tag{3.25}$$

where again r = 0,1.2,..., indicates the time interval considered.

(iii) Free Pile with a Known Force at the Top

In this case a force $F_A(t)$ is prescribed at the top and no forces act along the pile. It is desired to obtain an expression for the velocity at the pile top $v_{top}(t)$, due to this force. The reflections of waves at both ends of the pile have force but no displacement restrictions. Thus, if the applied wave induces compressive strains then all the reflection waves will have tensile velocities. Reflections will always add to the top velocity on every wave arrival at the top. From proportionality and due to the discussed reflections the result can be readily obtained.

$$v_{top}(t) = \frac{c}{EA}(F_A(t) + 2F_A(t - 2L/c) + 2F_A(t - 4L/c) + \ldots) \tag{3.26}$$

or using the notion above Equation 3.26 can be rewritten to yield for $r\frac{2L}{c} \leq t \leq (r + 1)\frac{2L}{c}$

$$v_{top}(t) = \frac{c}{EA}(F_A(t) + 2 \sum_{j=1}^{r} F_A(t - j\frac{2L}{c})) \tag{3.27}$$

(iv) External Force Acting on a Pile with Free Top and Bottom

The external force may again be denoted by $R_i(t)$ and act at $x = x_i$. The reflections will be of such a nature that the waves arriving at the top always add to the top velocity $v_{top}(t)$ if $R_i(t)$ does not change sign. Hence for $0 \leq t < 2L/c$

$$v_{top}(t) = \frac{-c}{EA}[R_i(t - \frac{x_i}{c}) + R_i(t - \frac{2L - x_i}{c})] \qquad (3.28$$

and for $r\ 2L/c \leq t \leq (r + 1)2L/c$

$$v_{top}(t) = \frac{-c}{EA} \sum_{j=0}^{r} \{R_i(t - \frac{x_i}{c} - j\frac{2L}{c}) + R_i(t - \frac{2L - x_i}{c} - j\frac{2L}{c})\}$$

3.4 Soil Resistance Forces

In this section the relation between the velocity at the top of the pile and the magnitude of reaction forces which are assumed to depend on the pile displacements and pile velocity will be derived. A discussion of this soil model is given in Chapter V. For ease in computation the resistance forces are assumed to act a finite number of stations at uniform spacing so that their application in a lumped mass analysis is possible. The model splits the soil resistance force $R_i(t)$, forces acting at time t and $x = x_i$ into two components: a static component called the shear resistance $S_i(t)$ dependent upon the pile displacements and a dynamic component $D_i(t)$ referred to as the dynamic or damping resistance which is dependent on the velocity at $x = x_i$.

(i) Shear Resistance Forces

The shear resistance force acting at $x = x_i$ and time t has a force displacement relation as illustrated in Figure 2.2 of Volume I. Through the first unloading, i.e. before the velocity becomes positive a second time, this relation is given by:

$$S_i(t) = \begin{cases} k_i u_i(t) & \text{for } u_i(t) < q_i \quad \text{(a)} \\ S_{i,o} & \text{for } u_i(t) > q_i,\ v_i(t) > 0 \quad \text{(b)} \\ S_{i,o} - k_i(\max u_i - u_i) & \text{for } u_i(t) < \max u_i \quad \text{(c)} \end{cases} \tag{3.30}$$

where k_i is the soil stiffness, $S_{i,o}$ is the ultimate shear resistance, $u_i(t)$, $v_i(t)$ are pile displacement and velocity, respectively and $\max u_i$ is the maximum displacement before or at time t. As a theoretical example of how a shear versus time relation can be developed, it is now assumed that only one shear force is acting, that it is caused by a velocity $v_A(t)$ which is applied at the pile top, and that at the pile bottom is a free end. This example will demonstrate the main features of wave propagation effect of a shear force. Subsequent quantitative results, however, will be much easier obtained by a lumped mass analysis. The shear versus displacement relation requires the individual treatment of the three different laws described in Equations 3.30 a, b, c.

Suppose the wave caused by the hammer blow is described by a pile top velocity, $v_A(t)$. Then at a time x_i/c the wave will arrive at $x = x_i$. Thus, $v_i(t)$ and $u_i(t)$, the velocity and displacement of the pile, are zero at $x = x_i$ before x_i/c. When the wave arrives the shear resistance force, $S_i(t)$, will tend to resist the motion of the pile and reduce the applied velocity by sending out waves in both directions along the pile. This reduction in velocity is proportional to the acting shear resistance force, $S_i(t)$, which in

turn is proportional to the actual displacement. Thus, if x_i is far enough from the ends of the pile so that no reflection wave will arrive within the time interval now considered, the actual velocity, $v_i(t)$, at $x = x_i$ is given by

$$v_i(t) = v_A(t - x_i/c) - c/2EA\ S_i(t) \tag{3.31}$$

If the actual displacement, $u_i(t)$, is smaller than the quake, q_i, the shear resistance is given by Equation 3.30a.

$$S_i(t) = k_i u_i(t)$$

but $v_i(t) = \frac{du_i(t)}{dt}$ so that Equation 3.31 can be written as

$$\frac{du_i}{dt} + k_i \frac{c}{2EA} u_i(t) = v_A(t - \frac{x_i}{c}) \tag{3.32}$$

By introducing an integration variable s, an initial condition $u_i(t - x_i/c) = 0$, and by defining $\tau = t - x_i/c$ the solution of Equation 3.32 yields the actual displacement $x = x_i$

$$u_i(\tau) = \int_0^{\tau} v_A(s)\exp\{(-\frac{ck_i}{2EA}(s - \tau)\}ds \tag{3.33}$$

If t_{i1} is defined as the time when $u_i(t)$ becomes equal to q_i, Equation 3.33 is valid for $x_i/c \leq t \leq t_{i1}$. At time t_{i1} the shear force reaches its ultimate value. Therefore, from Equation 3.31

$$v_i(t) = v_A(t - x_i/c) - c/2EA\ S_{i,o} \tag{3.34}$$

and

$$u_i(t) = q_i + \int_{t_{il}}^{t_{i,o}} v_A(t - \frac{x_i}{c})dt - \frac{c}{2EA} S_{i,o}(t - t_{il}) \tag{3.25}$$

This equation is valid until a time $t_{i,o}$ when the maximum displacement is reached. This happens when $v_i(t)$ becomes zero, thus, from Equation 3.34

$$v_A(t_{i,o} - x_i/c) = c/2EA\ S_{i.o} \tag{3.36}$$

These equations assume no reflection waves have reached $x = x_i$.

In most of the cases the velocity $v_A(t)$ stays greater than one half of the proportional resistance forces for a time until the first reflection wave returns from the bottom end. Also the initial portion of the reflection wave which carries the effects of $S_i(t) < S_{i,o}$ has usually passed the station $x = x_i$ before $t_{i,o}$ is reached. Then the above condition Equation 3.36 becomes

$$v_A(t_{i,o} - x_i/c) + v_A(t_{i,o} - \frac{2L - x_i}{c}) = \frac{c}{EA} S_{i,o} \tag{3.37}$$

Here the first term on the left hand side is due to the directly arriving wave caused by impact, the second term is also due to the impact wave but after reflection at the bottom. The term on

the right hand side is due to the effects of both the ultimate shear resistance at time $t_{i,o}$ plus the shear acting at a time $2(L - x_i)/c$ earlier.

After $t = t_{i,o}$ unloading will start i.e. the shear resistance force will decrease by virtue of Equation 3.30c. Unloading effects will be investigated in a later section using a simple example. Their effect at the top of the pile will, in general, be observed at a later time and are, therefore, not considered in detail here.

Examples for shear resistance forces and their effects on the pile top will be given below and in Chapter II of Volume I.

(ii) Dynamic Resistance Force Acting at the Pile

The dynamic resistance is assumed to behave like a linear viscous damper. If the damping constant at a point $x = x_i$ is denoted by d_i and the actual velocity by $v_i(t)$ then the dynamic resistance force $D_i(t)$, defined to be a concentrated force, is

$$D_i(t) = d_i v_i(t) \tag{3.38}$$

The actual velocity at $x = x_i$ is determined by the particle velocities of the two waves in the pile, v_f and v_g, (Equation 3.4) traveling in negative and positive x-direction, respectively. Further, the effect of the damper itself has to be superimposed. The particle velocity at $x = x_i$ due to the dynamic resistance is again determined from Equation 3.12. Thus, if the velocities of the waves arriving at $x = x_i$ at time t add up to $v_{i,a}(t)$ then the actual velocity is

$$v_i(t) = v_{i,a}(t) - \frac{1}{2}D_i(t)\ c/EA$$

and after inserting Equation 3.38 this becomes

$$v_i(t) = v_{i,a}(t)/(1 + d_i c/2EA)$$

Therefore the damping force can be calculated from

$$D_i(t) = d_i(v_{i,a}(t)/(1 + d_i c/2EA)) \qquad (3.39)$$

This dynamic resistance force sends out waves in either direction having particle velocities $-\frac{1}{2}D_i(t)c/EA$. For times $x_i/c < t < \frac{2L - x_i}{c}$ or $x_i/c < t < 3x_i/c$ $v_{i,a}$ consists of the impact wave velocity only. More complicated superpositions occur after one of the waves resulting from $D_i(t)$ or the impact wave reach again $x = x_i$ after having been reflected at top or bottom end of the pile. If the damper is located at the bottom end of the pile then simpler superpositions occur. In this case the initiating wave, $v_{n,a}(t)$, will be reflected at the same time that the damper reacts. Thus

$$v_n(t) = 2v_{n,a}(t) - D_n(t)\frac{c}{EA} \qquad (3.40)$$

and the damping force exerted by a damper located at the bottom end having damping coefficient d_n is determined by

$$D_n(t) = \frac{2v_{n,a}(t)}{1 + cd_n/EA}\, d_n \tag{3.41}$$

If the only wave arriving is that due to the impact then

$$D_n(t) = \frac{2v_A(t - L/c)}{1 + cd_n/EA}\, d_n \tag{3.42}$$

(iii) Dynamic and Shear Resistance Force Together

An important result can be obtained for the specific case where a shear resistance force $S_n(t)$ and a damper having coefficient d_n resist the motion at the pile bottom together. For clarity no other resistance forces are assumed to act along the pile.

Considering only a time after the bottom displacement has become greater than the quake and only before a time 3L/c, i.e. before the impact wave arrives a second time at the bottom, then the only one wave arriving is due to the impact. Thus, becuase of immediate reflection alone

$$v_{n,a}(t) = 2v_A(t - L/c).$$

Due to the shear a reaction wave will be sent upwards having particle velocity

$$v_s(t) = - \frac{c}{EA} S_{n,o}$$

and due to the damper

$$v_d(t) = - \frac{c}{EA} D_n(t)$$

But

$$D_n(t) = d_n v_n(t)$$

where $v_n(t)$ is the actual pile toe velocity given by superposition of all waves. Thus,

$$v_n(t) = 2v_A(t - L/c) - c/EA(S_{n,o} + d_n v_n(t))$$

which leads to

$$v_n(t) = \frac{2v_A(t - L/c) - c/EA\ S_{n,o}}{1 + cd_n/EA} \qquad (3.43)$$

and the damping force $D_n(t)$, therefore, becomes

$$D_n(t) = d_n \frac{2v_A(t - L/c) - c/EA\ S_{n,o}}{1 + cd_n/EA} \qquad (3.44)$$

3.5 Resistance Delta Curves

In Chapter II of Volume I Delta curves were introduced as a means of studying the effects, at the pile top, of the actual resistance forces by means of the Measured Delta curves referred to here as $\Delta(t)$. The effect of resistance forces acting at $x = x_i$ due to the chosen soil model were investigated by means of Resistance Delta curves,

called $\Delta_i(t)$.

All Delta curves are defined to be the effects of the acting resistance forces (depending on pile displacements and velocities) at a fixed pile top when the pile tip is a free end.

In the previous section the resistance forces had been derived for specific cases as a function of time, depending on the impact velocity, $v_A(t)$. In the following paragraphs examples will be given using either a theoretical resistance versus time relation or a simplified top input velocity $v_A(t)$. Since a resistance Delta curve, $\Delta_i(t)$, for a force $R_i(t)$ acting at $x = x_i$ is the force on the fixed top of a pile under action of $R_i(t)$ only, the Delta curve is expressed by Equation 3.22 as derived in Section 3.3. Thus

$$F_{top}(t) = \Delta_i(t) = \sum_{j=0}^{r} \{R_i(t - \frac{x_i}{c} - j\frac{4L}{c}) + R_i(t - \frac{2L - x_i}{c} - j\frac{4L}{c}) - R_i(t - \frac{2L + x_i}{c} - j\frac{4L}{c}) - R_i(t - \frac{4L - x_i}{c} - j\frac{4L}{c})\} \tag{3.45}$$

for $r4L/c \leq t \leq (r + 1)4L/c$ where r, therefore, indicates the time interval considered.

Suppose a shear resistance force acting at $x = x_i$ is given by

$$S_i(t) = H(t - \frac{x_i}{c})S_{i,o} \tag{3.46}$$

This shear resistance force has zero magnitude until $t = x_i/c$ and is constant thereafter, as described by the unit step function $H(t - x_i/c)$. Using Equation 3.45

$$\Delta_i(t) = S_{i,o} \sum_{j=0}^{r} \{H(t - \frac{2x_i}{c} - j\frac{4L}{c}) + H(t - \frac{2L}{c} - j\frac{4L}{c}) - H(t - \frac{2L + 2x_i}{c} - j\frac{4L}{c}) - H(t - \frac{4L}{c} - j\frac{4L}{c})\} \quad (3.47)$$

Both shear resistance force and the corresponding Delta curve are plotted in Figure 3.3 a,b for two cases of shear resistance namely $x_i = L/2$ and $x_i = L$, respectively. In comparing Figures 3.3 a,b with Figures 2.8 and 2.9 of the first volume it can be observed that the simplified resistance law as expressed by Equation 3.46 gives a good approximation of the actual circumstances. In order to study the effect which unloading has on a shear resistance Delta curve a second example will now be given for a shear resistance acting at $x = x_i$ given by

$$S_i(t) = S_{i,o}[H(t - x_i/c) - \tfrac{1}{2}H(t - \frac{2L}{c})] \quad (3.48)$$

This means that a time $2L/c$ the resistance force is assumed to decrease to half its ultimate value. Figure 3.4a shows the shear versus time relation for $x_i = L/2$ and $x = L$. The resistance Δ-curves obtained from applying Equation 3.45 are shown in Figure 3.4b. The terms resulting from applying Equation 3.45 are individually shown before

they are added. Worth noting in this figure is the fact that negative resistance Delta values are obtained for $4L/c < t < 6L/c$ and it can be concluded that negative values in the Measured Delta curve, as for example in Figures 2.5, 2.6 and 2.7 of Volume I will arise from decreasing resistance forces, either shear or dynamic. Obtaining a dynamic resistance force as a function of time is somewhat more complicated even if an idealized velocity input is used.

In order to compute $D_i(t)$ the velocity of the pile particles at $x = x_i$ has to be found. This velocity multiplied by the damping coefficient d_i yields the damping resistance force. If the sum of the particle velocities of the two waves arriving from either direction at $x = x_i$ at time t is denoted by $v_{i,a}(t)$ then the actual velocity of the particles at the damper, $v_i(t)$ can be computed by use of Equation 3.39.

$$v_i(t) = \frac{1}{1 + \frac{d_i c}{2EA}} v_{i,a}(t) = \frac{\alpha_i v_{i,a}(t)}{d_i} \tag{3.49}$$

Thus

$$\alpha_i = \frac{d_i}{1 + \frac{d_i c}{2EA}} \qquad \text{for } i \neq n \tag{3.50}$$

and

$$\alpha_n = \frac{d_n}{1 + \frac{d_n c}{EA}} \qquad \text{for } i = n \text{ from Equation 3.42}$$

It should be noted that the waves arriving from either direction at $x = x_i$ can be the result of a superposition of various other waves. A general derivation of $D_i(t)$ becomes very involved and amounts to a complicated bookkeeping of all the waves traveling through the

pile. Therefore, two special cases will be presented as an illustration of the main features of dynamic resistance forces. A damper at $x = L/2$ and a damper at $x = L$ will be chosen as examples and the computation limited to times $t < 4L/c$.

In order to find the magnitude of the velocities of the arriving waves, applied velocity and velocities due to the damping force will be considered separately. If a velocity, $v_A(t)$, is applied at the top of the pile at time, t, then due to this velocity alone, the velocity at $x = L/2$ for times $t \leq 4L/c$ can be computed from Equation 3.19. This leads to

$$v_{i,A}(t) = v_A(t - L/2c) + v_A(t - 3L/2c) - v_A(t - 5L/2c) - v_A(t - 7L/2c) \quad (3.51)$$

If a damping force, $D_i(t)$, is acting at $x = L/2$ at time t then two waves are generated traveling upwards and downwards away from the location of the damper both having the same particle velocity $-cD_i(t)/2EA$. Due to the initially upward traveling wave, the pile at $x = L/2$, is subjected to the velocity

$$v_{i,up} = \frac{c}{2EA}[D_i(t - L/c) + D_i(t - 2L/c) - D_i(t - 3L/c)] \quad (3.52)$$

The three terms on the right hand side are due to reflection waves arriving. The first coming from the top after the first reflection, the second arriving from the bottom after the second reflection and

the third due to a wave arriving after a reflection at the top, this time having been reflected a third time.

The effects of the initially downward moving wave on the velocity at the damper location can be expressed as

$$v_{i,down} = \frac{c}{2EA}[-D_i(t - L/c) + D_i(t - 2L/c) + D_i(t - 3L/c)] \tag{3.53}$$

Summing up all the effects of applied and resistance waves yields, after simplification, a velocity of the arriving waves for $t \leq 4L/c$

$$v_{i,a}(t) = v_A(t - L/2c) + v_A(t - 3L/2c) - v_A(t - 5L/2c)$$

$$- v_A(t - 7L/2c) + c/EA\ D_i(t - 2L/c) \tag{3.54}$$

But $D_i(t - 2L/c) = \alpha_i v_{i,a}(t - 2L/c)$

$$= \alpha_i[v_A(t - 5L/2c) + v_A(t - 7L/2c)]$$

and therefore

$$v_{i,a}(t) = v_A(t - L/2c) + v_A(t - 3L/2c) - v_A(t - 5L/2c)$$

$$(1 - \alpha_i c/EA) - v_A(t - 7L/2c)(1 - \alpha_i c/EA) \tag{3.55}$$

which leads to $D_i(t)$ by multiplication with α_i.

Figure 3.5a shows the graph of $D_i(t)$ for an assumed constant velocity

of magnitude $v_A(t)/c = 1$ and a damping coefficient $d_i = 2EA/3c$, so that $\alpha_i = EA/2c$. Figure 3.5b shows $\Delta_i(t)$ due to this damping force obtained from applying Equation 3.45 by graphically superimposing the applicable terms as was shown in Figure 3.4.

If a damper is located at the pile bottom then only waves arriving from one direction have to be considered. This leads to simpler computations. The arriving wave velocity for times $t \leq 4L/c$ is then given by

$$v_{n,a}(t) = 2[v_A(t - L/c) - v_A(t - 3L/c) + c/EA\ D_n(t - 2L/c)]$$

or

$$v_{n,a}(t) = 2[v_A(t - L/c) - v_A(t - 3L/c)\ (1 - \alpha_n c/EA)] \tag{3.56}$$

and, therefore, the resistance Delta curve for $t \leq 4L/c$ is

$$\Delta_n(t) = 2\alpha_n[v_A(t - 2L/c)] \tag{3.57}$$

since $D_n(t) = \alpha_n \cdot v_{n,a}(t)$. Both $D_n(t)$ and $\Delta_n(t)$ are shown in Figure 3.5c,d, respectively. Applied velocity and damper coefficients were chosen the same way as in the previous example. This resistance Delta curve seems identical to that for a shear resistance at the tip of the pile. Of course, this is a result of the choice of a constant velocity at the pile top. It was found in analyzing actual records where the velocity showed only a small decrease after the maximum that it is, in fact, difficult if not impossible to distinguish between shear and dynamic

resistance forces. Further detailed discussion of this important point is presented in Chapter IV of Volume I.

3.6 Prediction of Soil Resistance Forces Acting along the Pile under a Hammer Blow

Using the concept of Measured and Resistance Delta curves a prediction scheme will be developed for the magnitude of forces which act along the pile under a hammer blow. Their effects at the pile top are displayed in the Measured Delta curve which is derived from acceleration and force measured at the pile top.

The actual resistance forces are distributed along the pile. For ease in computation it will be assumed that they act as concentrated forces on n equally spaced locations along the pile. The number of unknowns is slightly reduced by assuming that the pile top element has no resistance forces acting, an assumption which is sensible because part of the pile is usually above grade and the topmost soil is usually not in contact with the pile due to transverse pile vibrations. Thus, the magnitudes of (n - 1) quakes, q_i, (n - 1) ultimate shear resistances, $S_{i,o}$, and (n - 1) damping coefficients, d_i, have to be computed.

As outlined in Chapter II of Volume I, the i-th quake will be assumed to be reached when the velocity at the point $x = x_i$ reaches a maximum. If no resistance forces were acting, then this displacement would be the same as the displacement at the top at time t_m, the time when the top velocity has a maximum. Only the bottom end

would obtain twice the displacement due to the reflection of the arriving wave. The effect of the resistance forces can be estimated by considering the Measured Delta curve. In Section 3.5 it was found that a shear resistance force produced a pile top force effect of twice its ultimate shear resistance value at time $t_m + 2L/c$. A damper at the pile toe also yields a top force effect of twice its maximum resistance force at this same time. The Measured Delta curve is equal to the sum of all Resistance Delta curves if the parameters are correct. Thus, $\Delta(t)$ shows, at a time 2L/c after impact, twice the magnitude of the sum of all resistance forces if all the damping force is assumed to act concentrated at the bottom end. The effect of all ultimate shear resistance forces and the effect of the toe damping force on the toe velocity is proportional to their respective wave particle velocities or magnitudes of resistance forces. Thus, the maximum velocity at the pile bottom at time $L/c + t_m$ is

$$\max v_n = 2v_A(t_m) - \frac{c}{EA}\frac{1}{2}\Delta(t_m + 2L/c) \qquad (3.58)$$

where $v_A(t)$ is the top measured velocity and $\Delta(t)$ is the magnitude of the Measured Delta curve at time t.

A good estimate on the bottom end displacement can be obtained by assuming that the ratio of pile top and pile tip displacement is linearly proportional to their respective velocity ratio. Thus

$$q_n = u_n(t + L/c) = u_A(t_m)\frac{\max v_n}{\max v_A} \qquad (3.59)$$

$u_A(t)$ being the pile top and $u_n(t)$ the pile tip displacement. The quakes for locations other than pile top or pile tip are linearly interpolated so that

$$q_i(u_A(t_m) - [u_A(t_m) - u_n(t_m + L/c)]\frac{x_i}{L} \qquad (3.60)$$

Quakes resulting from this calculation which are larger than .12 inch are set equal to this value. The quake, therefore, cannot exceed commonly recommended values for sand (4). A lower bound is not introduced because it is desired to keep the quakes small enough so that the ultimate resistance can be reached at all elements. The prediction scheme for quakes is based on the following considerations:

Examples of Measured Delta curves are shown in Chapter II of Volume I, Figures 2.5, 2.6 and 2.7. All three curves, although obtained from piles having very different behaviors have their maximum value at a time 2L/c after maximum velocity at the top. If skin damping forces are considered small then this means that the maximum shear and damping forces were all reached before or at a time L/c after maximum velocity at the top. Then, the toe shear resistance force must have reached its ultimate value at the same time. This time, however, is the time of maximum velocity at the pile tip. Consequently, the quake of the tip shear resistance force is reached at the time of maximum tip velocity, a result which is extended to all points along the pile. In chapter III and IV of Volume I this point is further discussed.

Although several simplifications have been made in the above described computation, quakes will, in general, result which lead to the ultimate shear resistance at the i-th element at or before a time $t_m + x_i/c$. Therefore, in the absence of dynamic resistance forces, the value of the Measured Delta curve at time $t_m + 2x_i/c$ will be a result of a superposition of the top force effects of the first i ultimate shear resistances plus some small influence of the already increasing shear resistances of lower elements due to the part before maximum velocity. Calling this influence ε_i and defining $t_i = t_m + 2x_i/c$ then

$$\Delta(t_i) = \sum_{j=1}^{i} S_{o,j} + \varepsilon_i \tag{3.61}$$

and for $t_{i-1} = t_m + 2x_{i-1}/c$

$$\Delta(t_{i-1}) = \sum_{j=1}^{i=1} S_{o,j} + \varepsilon_{i-1} \tag{3.62}$$

Subtracting Equation 3.62 from Equation 3.61 leads to

$$S_{o,i} = \Delta(t_i) - \Delta(t_{i-1}) + \varepsilon_i - \varepsilon_{i-1} \tag{3.63}$$

If it is then assumed that the difference $\varepsilon_{i+1} - \varepsilon_i$ is small the i-th ultimate shear resistance has been found. Figure 3.6 serves to clarify this point by use of a theoretical example. Several theoretical Resistance Delta curves (a_i) are shown - corresponding to shear

resistance forces - whose sum corresponds to the Measured Delta curve (b). At times t_i an influence $_i$ from the next lower shear resistance force can be observed. The $S_{o,i}$ were assumed to be equal in this example so that $_i = _{i+1}$ for i n-1.

This computation can be performed the same way for all elements except for the bottom where the effect of all the bottom reflected waves requires a top reaction force of twice the total resistance. Thus, an approximation for the n-th shear resistance force can be computed from

$$S_{o,n} = \frac{1}{2}[(t_n) - (t_{n-1})] \qquad (3.64)$$

where $t_n = t_m + \frac{2L}{c}$ and $t_{n-1} = t_m + \frac{2x_{n-1}}{c}$. This computation scheme will not apply when damping forces have to be considered and when t_m is reached so late that (t_{n-1}) contains already effects of the return of reflection waves from the bottom. In that case an improvement of the above described method for predicting ultimate shear resistance forces can be obtained if the damping effects and the effects due to reflection waves are subtracted from the Measured Delta curve. For doing so the magnitude of damping forces must be known. An estimate of the maximum damping force, max D, can be obtained from the simplified Phase III prediction method as described in Chapter II, Volume I, Section 5 and in Chapter VI, Volume II. If it is assumed that all this damping is concentrated at the pile bottom (actually damping will be distributed but a large percentage is in most cases found to be concentrated at the bottom) then its effects at the top will be proportional to the top velocity shifted over a time 2L/c as shown by the Resistance Delta curve in Figure 2.11 of Volume I. (This

is actually only true for no other resistance forces acting, but since the shear resistance forces are constant except for a small portion before the quake is reached this gives a good approximation).

The doubling effect due to the return of reflection waves from shear resistance can be assumed to be proportional to the Resistance Delta curve for a shear force at the pile bottom. Such a Resistance Delta curve, however, can be assumed proportional to the pile top displacement until t_m and constant thereafter with a time lag of 2L/c.

The resulting Reduced Delta curve is then

$$\Delta_{red}(t) = \Delta(t) - 2 \max D \frac{v_A(t - \frac{2L}{c})}{\max v_A} - S_o \frac{u_A^*(t - \frac{2L}{c})}{q_1} \quad (3.65)$$

where

$$u_A^*(t) = \begin{cases} u_A(t) & \text{for } t < t_m \\ q_1 & \text{for } t > t_m \end{cases}$$

and S_o is the sum of all ultimate shear resistance forces.

Using the Reduced Delta curves the equation for the prediction of ultimate shear resistance forces becomes (see Equation 3.63)

for $i = 1,2,\ldots,n$

$$S_{o,i} = \Delta(t_i) - \Delta(t_{i-1}) \quad (3.66)$$

The damping coefficient for the bottom damper remains to be computed.

From Equation 3.58 it is possible to predict the maximum velocity at the pile tip using both measured velocity and Measured Delta curve. Therefore,

$$d_n = \max D/(2 \max v_A - c/2EA)\ \Delta(t_m + 2Lx_c)) \qquad (3.67)$$

All necessary parameters for performing a lumped mass analysis have now been approximately determined and the top force and all displacements can be calculated using the measured velocity and the predicted soil resistance forces as input. To improve the values an analysis should be performed.

The difference between measured and the pile top force computed in the lumped mass analysis using the predicted soil parameters can again be considered to be a Delta curve. It will be referred to as an Error Delta curve $\Delta_e(t)$, and provide a means of computing corrections on the first predictions. These errors can be due to a pile tip velocity different from the prediction and the assumptions used in reducing the Measured Delta curve can also account for errors. Other errors, however, will also be introduced from assuming that i-th shear resistance force had the same top force effect at time t_{i-1} that $S_{i+1}(t)$ had at t_i(i.e. $\varepsilon_i = \varepsilon_{i+1}$).

The Error Delta curve can be considered a Measured Delta curve which must be the sum of Resistance Delta curves. This time the computation becomes somewhat simplified since for every element both a velocity and displacement versus time relation is available

which can be considered an approximation, whose quality depends on the relative magnitude of the Error Delta curve. Using, again, the concept of Resistance Delta curves it is now possible to set up matrices whose coefficients are influence numbers reflecting the top force effect of a resistance force at time $t_j = 2x_j/c$ at the i-th element. Thus, for the shear resistance forces a matrix C is defined with elements

$$c_{j,i} = u_i^*(t - x_i/c)/q_i + u_i^*(t - \frac{2L - x_i}{c})/q_i \qquad (3.68)$$

where

$$u_i^*(t) = \begin{cases} u_i(t) & \text{for } u_i(t) < q_i \\ q_i & \text{for } u_i(t) \geq q_i \end{cases}$$

As an example of the meaning of $c_{j,i}$

$$\Delta_i(t_j) = S_{o,i} c_{j,i} \qquad (3.69)$$

In the same way for damping forces a matrix E is set up having elements

$$e_{j,i} = (v_i(t - x_i/c) + v_i(t - \frac{2L - x_i}{c}))/\max v_i \qquad (3.70)$$

So that

$$\Delta_i(t_j) = \max D_i e_{j,i} \tag{3.71}$$

This matrix is used later on for distributed damping resistances.

It will be understood that max D_i is the maximum damping force occurring on the first arrival of the impact wave. It is expected that a higher, second maximum is obtained (of about 2 max D_i as can be seen in Figure 2.12 of Volume I) after the impact wave is reflected at the pile bottom. This maximum damping force, max D_i, is known to occur at a time $t_m + x_i/c$ and, therefore, its top force effect will be seen on top at time $t_m + 2x_i/c = t_i$. Thus, $e_{j,i}$ will be a convenient tool for computing damping resistance forces when D_i is not zero along the pile skin. By use of $c_{j,i}$ and $e_{j,i}$ it is now easy to reduce the Error Delta curve by the effect of reflection waves at 2L/c and by the difference, ΔD, between necessary damping (max D) and damping found in the previous analysis (max D^a), thus, if ΔD = max D - max D^a

$$\Delta_{e,red}(t_j) = \Delta_e(t) - e_{j,n}\Delta D \tag{3.72}$$

The corrections on the shear resistance forces can now be computed using the same approach as in the initial shear force prediction

$$\Delta S_{o,i} = \Delta_{e,red}(t_i) - \Delta_{e,red}(t_{i-1}) \tag{3.73}$$

The corrected damping coefficient can be computed from Equation 3.67 where the expression in the denominator on the left hand side

is replaced by max v_n as obtained in the lumped mass analysis.

In order to further improve the predictions another lumped mass analysis can be performed and further corrections obtained and this process continued until the Error Delta is sufficiently small. The number of necessary iteration cycles depends on how well the soil model describes the actual soil behavior. For good agreement between the assumed and actual soil action four iteration steps usually suffice. In many cases, however, the Delta curve portion of the record for 2L/c after impact cannot be reduced to small values. In such cases the computation is terminated after the 8th attempt.

When requiring the Error Delta curve to become smaller than a certain bound it is important to realize the different sensitivity of an Error Delta curve at different times to a change in prediction. As in any other Delta curve an error, S_i, at $x = x_i$ will result in a Delta curve approximately given by

$$\Delta_e(t) = \Delta S_i \qquad \text{for } t_i < t < t_n$$

and

$$\Delta_e(t) = 2\Delta S_i \qquad \text{for } t_n < t < t_{i,o} + x_i/c$$

Thus, the portion of the record for $t_m < t < t_n$ is less sensitive to errors than the later portion of the record. The following criteria, therefore, have been established for a sufficiently small Error Delta curve accounting for the different sensitivities in the record (a further discussion of these criteria is given in the example in the next section).

$$|E_1| = \left| \frac{1}{t_{n-1} - t_2} \int_{t_2}^{t_{n-1}} \Delta_e(t)dt \right| < CR_2 = 0.02 \max F_A \tag{3.74a}$$

$$|E_2| = \left| \frac{1}{t_n - t_{n-1}} \int_{t_{n-1}}^{t_n} \Delta_e(t)dt \right| < CR_2 = 0.05 \max F_A \tag{3.74b}$$

$$|E_3| = \left| \frac{1}{t_f - t_n} \int_{t_n}^{t_f} \Delta_e(t)dt \right| < CR_3 = 0.10 \max F_A \tag{3.74c}$$

where F_A is the maximum measured force

and

$$t_f \leq \begin{cases} 4L/c & \text{for no unloading} \\ t_{n,o} + L/c & \text{otherwise} \end{cases} \tag{3.75}$$

with $t_{n,o}$ being the time of zero velocity at the pile tip. This way it is not required that the predicted and measured top forces match after unloading effects become apparent at the top. It was found in applying the above described error criteria that the $|E_i|$- numbers can be efficiently used to control the computation process: As long as $|E_1|$ is too large the shear resistance forces $S_{i,o}$ along the pile skin have to be corrected, when $|E_2|$ is sufficiently small but $|E_2|$ is not less than CR_2 then either toe damping or toe shear have

to be adjusted by an amount equal to one half of $|E_2|$, and when $|E_2|$ and $|E_1|$ are small then a check on $|E_2|$ determines whether or not the total maximum amount of damping used was correct. This is due to the fact that a Resistance Delta curve for damping decreases with a higher rate after $t_m + 2L/c$ than a Resistance Delta curve for shear forces. Therefore, damping has to be added and shear resistance subtracted at the same time if the predicted force is greater than the measured force for $t > t_m + 2L/c$, i.e. for $E_3 > 0$ the opposite has to be done.

Thus, an improved total damping value will result from

$$\max D_{imp} = \max D - E_3/2 \qquad (3.76)$$

where it is assumed that the shear resistance forces stay constant while the damping forces decrease immediately to zero after $t_m + 2L/c$. This scheme, although quite crude, usually leads to a satisfactory match over the third portion that is t from t_n to t_f as long as the soil model allows a good match in that region.

Once, the inequalities 3.74a, b, c have been satisfied the prediction for all damping at the tip is accomplished.

The assumption of all damping concentrated at the pile tip might yield a good match. However, it is possible and probable that damping locations influence the predicted top force two more methods of damping distribution are tried. One of these methods is to place damping forces uniformly along the skin, i.e. for i = 2,3,...,n-1.

Thus, (n-2) damping forces are chosen to replace the bottom damper. Calculating with the damping maxima, max D_i, occurring before the impact wave reaches the bottom and assuming that the max D_i are one half of the maximum damping effect felt at the top at time 2L/c (see example in Figure 2.12 of Volume I) leads to

$$\max D_i = \frac{\max D_{imp}}{2(n-2)} \tag{3.77}$$

However, a check must be made on whether these damping forces would not result in top force effects larger than specified by the Measured Delta curve. Using the E-Matrix this can be checked

$$\sum_{i=2}^{n-1} \max D_i e_{j,i} < \Delta(t_j) \tag{3.78}$$

If for some time $t = t_j$ this inequality does not hold then max D_j has to be reduced

$$\max D_j \leq \Delta(t_j) - \sum_{i=2}^{j-1} \max D_i e_{j,i} - \sum_{j=j+1}^{n-1} \max D_i e_{j,i}$$

$$j = 2,3,\ldots,n-1 \tag{3.79}$$

Also a check must be made on whether the maximum total damping force on the return of the reflection wave would exceed the necessary total damping force as determined in the first prediction. Again using the E-Matrix this check requires

$$\sum_{i=2}^{n-1} \max D_i e_{n,i} = \max D_{imp} \qquad (3.80)$$

which can be accomplished by adding a max D_n if the left hand side is smaller than the right hand side or to subtract from all max D_i $i = 2,3,\ldots,n-1$ if the opposite holds. If for $j = 2,3,\ldots,n-1$ turns out to be negative then neighboring damping forces have to be reduced until the maximum possible damping forces are found. The corresponding damping coefficients can be found from the previously predicted velocities (which had been used also for computing the $e_{i,j}$). Errors resulting from this assumption must be small since a good match had been determined previously and the maximum velocities for $t < t_m + 2L/c$ will be the same for $\Delta_e(t)$ being small no matter how the match was accomplished. (The particle velocities in the waves due to either resistance forces have to be the same).

The computations for obtaining the ultimate shear resistances, $S_{o,i}$, can be obtained in a similar manner as described above for one damper at the bottom, except that the Reduced Delta curve has to be computed by accounting for all damping forces. Thus

$$\Delta_{red}(t_j) = \Delta(t_j) - \sum_{i=2}^{n} e_{j,i} \max D_i - S_o c_{j,n} \qquad (3.81)$$

The variation of the damping forces and the effects of the reflection wave on damping usually introduces more errors in the prediction than

in the case of only one damper at the bottom. Therefore, if damping is large more computations have to be performed until the final distribution produces a sufficiently small Error Delta curve. Otherwise, the computation is terminated after the 8th iteration.

A third way of distributing damping forces is to place only one damper on the skin at the point where the maximum skin resistance force in the upper half of the pile had been determined in the first prediction. It is computed as follows:

$$\max D_i = \begin{cases} \frac{1}{2} \max D_{imp}; \text{ if } S_{o,i} > \frac{1}{2} \max D_{imp} \\ \max S_{o,i} \text{ plus toe damping; if } S_{o,i} < \frac{1}{2} \max D_{imp} \end{cases}$$

Essentially this computation is the same as when damping forces are distributed uniformly.

Once the final Error Delta curves have been found (these three curves usually differ at and after $t_m + 2L/c$ for all three damping distributions) a linear combination of their $S_{o,i}$ and d_i is used to find a final selection by minimizing the resulting Error Delta curve. If p_i^j stands for the i-th resistance force (either $S_{o,i}$ or d_i) obtained in the j-th damping distribution method and a superscript f is used for the final result, then

$$p_i^f = a_1 p_i^1 + a_2 p_i^2 + a_3 p_i^3 \tag{3.82}$$

where

$$a_1 + a_2 + a_3 = 1 \tag{3.83}$$

and

$$\Delta_e^f(t) = a_1\Delta_e^1(t) + a_2\Delta_e^2(t) + a_3\Delta_e^3(t) \tag{3.84}$$

For $\Delta_e^f(t)$ to become a minimum the coefficients a_1, a_2, a_3 can be determined using

$$\frac{\partial}{\partial a_i}\int_0^{4L/c} (\Delta_e^f(t)^2 w(t)dt = 0 \tag{3.85}$$

where $w(t)$ is a weighting function. Since the errors in the initial portion of the match are due to measuring inaccuracies these effects can be removed from the computation by setting

$$w(t) = 0 \text{ for } 0 \leq t \leq t_2 \tag{3.86a}$$

Also the portion of the record where unloading effects the match, will be disregarded (See Chapter III of Volume I for examples), thus

$$w(t) = 0 \text{ for } t > t_f \tag{3.86b}$$

where t_f is as defined in Equation 3.75. In order to place more emphasis on the improvement of the first 2L/c of the match the rest of the weighting function may be defined as

$$w(t) = \begin{cases} 1 & \text{for } t_2 < t < t_n \\ 1 - \left(\dfrac{t - t_n}{t_f - t_n}\right)^2 & \text{for } t_n < t < t_f \end{cases} \tag{3.86c}$$

However, not too much improvement can be expected from choosing a proper weighting function since it is possible that an application of the least square method results in some $S_{o,i}$ or d_i negative. Since negative values are not allowable the a_1, a_2, and a_3 coefficients have to be adjusted by observing their relative magnitudes. As an example suppose that $a_3 < 0$ and that for some j the ratio $\frac{a_3 p_j^3}{a_1 p_j^1 + a_2 p_j^2} < 0$ and smaller than any other ratio $i \neq j$, $i = 2, 3, \ldots n$, then the new constants, a_1^n, a_2^n, a_3^n can be determined from

$$a_3^n = \frac{1}{p_j^3}(a_1^n p_j^1 + a_2^n p_j^2)$$

$$a_1^n + a_2^n + a_3^n = 1 \qquad (3.87)$$

and

$$a_1/a_2 = a_1^n/a_2^n$$

Using a_1^n, a_2^n, a_3^n in Equation 3.82 leads to the final result if a second coefficient is not negative, in which case the process has to be repeated.

3.7 Computation Example

As a computation example the record obtained from pile F-60 Blow No. 26-A is used. The record, i.e. force and velocity, is shown in Figure 2.1. After subtracting the precompression force, S_p, (for explanation see Chapter IV) in this case 40.6 kip, the

force curve shown in Figure 2.1 of Volume I was obtained.

The pile length below the accelerometer was 59 feet. The pile was of 12-inch diameter pipe with 1/4-inch wall thickness and a cross sectional area of $A = 9.82\ inch^2$.

The wave speed for such a steel pipe pile had been experimentally verified by placing one accelerometer on either end of a 50 feet pile and applying a hammer blow on one end. The wave speed thus determined was $c = 17{,}000$ ft/s and with $\rho = .285/386\ lb(s^2)/in^4$

$$E = c^2\rho = 30.8 \times 10^6 \text{ psi}$$

This dynamic modulus is used in all analyses. The proportionality factor EA/c becomes 17.8 (kip/ft/s), which means that a particle velocity of 1 ft/s corresponds to a 17.8 kip force in the pile.

The maximum pile top velocity encountered in the example problem was 9.1 ft/s which corresponds to a maximum pile top force of 169 (kip). (The yield load of the pile is 220 kip).

The Measured Delta curve is shown in Figure 3.7a and was obtained by subtracting the free pile solution, Equation 3.18, from the measured force record.

It can be observed that $\Delta(t)$ has non zero values before time t_m which are probably due to recording inaccuracies. These values are set to zero until a time 1.2 L/c after which $\Delta(t)$ starts definitely to increase. In some of the records effects of high frequency vibrations are observed which are undesired in the analysis since

they represent only local effects and could lead to misinterpretations. For cancelling out such effects a new, smooth $\Delta(t)$ was obtained by time averaging the original one. The result is shown as curve b in Figure 3.7.

Integrating the top velocity until time t_m leads to a displacement of 0.107 inch. The maximum toe velocity is obtained using Equation 3.58. The maximum top velocity for this case is 9.1 ft/s and $\Delta(t_m + 2L/c) = 422$ kips giving

$$\max v_{n(toe)} = 2 \times 9.1 - \frac{422}{2 \times 17.8} = 6.5 \text{ ft.s}$$

An estimate of the toe displacement at maximum toe velocity can now be obtained using Equation 3.59.

$$u_n(t_m + L/c) = 0.107 \frac{6.5}{9.1} = 0.75 \text{ (inch)}$$

Linear interpolation leads to the quakes shown in Table (2.1). The Phase III prediction for total static resistance is 146 kips and the estimated maximum damping force 65 kips. Reducing the Measured Delta curve by the damping effect leads to curve c in Figure 3.7. This curve is then reduced further in order to remove the effect of initially downward traveling waves from shear resistance forces. The resulting curve (d) is a Delta curve due to the effect of the upward traveling waves from shear resistance forces only. (An infinitely long pile would show the same top force effect due to shear

forces).

This curve can be used to determine the individual ultimate resistance forces by applying Equation 3.66. In Figure 3.7 the $t_i (t_i = t_m + 2x_i/c)$ are marked with dashed lines. Accordingly the $S_{o,i}$ were determined as the differences between the indicated $\Delta_{red}(t_i)$ - values. The last two shear resistances $S_{o,n-1}$ and $S_{o,n}$ are averaged since the accuracy of distinguishing these two forces is small due to the large increase of top forces at $t = t_{n-1}$. Using the maximum toe velocity as calculated above leads to the damping coefficient

$$d_n = 65/6.3 = 10.3 \text{ [kips/ft/s]}$$

All soil parameters predicted so far are listed in Colume 2 of Table 3.2. As a check on the quality of this prediction a lumped mass analysis is performed. The measured pile top velocity and the predicted soil parameters are used and the corresponding pile top force is computed. If the soil model were correct and if the soil parameters were predicted precisely then this computed pile top force would be equal to the measured force (in absence of measurement inaccuracies). In general, however, differences between measured and computed pile top force occur. Subtracting the predicted from the measured curve leads to an Error Delta curve. For the present example curve (a) in Figure 3.8 shows this difference curve.

A remark on this graph is appropriate. For clarity the force

scale was chosen five times larger than in the graphs for the Measured and Reduced Delta curves in Figure 3.7. Considering the first portion of the Error Delta curves (i.e. for $t_m \leq t < t_m + 2L/c$) it can be seen that local peaks and valleys of this curve are preserved and the differences of the Error Delta curves occur only in an averaged manner. Clearly, this is due to the constant behavior of shear resistance forces. The later portion of the graph ($t_m + 2L/c < t$) shows this behavior for Error Delta curves a and b only. Of course, the amount of damping had been changed for obtaining curve c and d. These changes influence only the behavior of this later portion. The high frequency oscillations in the Error Delta curves are due to small time lags from measurement inaccuraries causing a shift between the predicted and the measured force, also the accuracy of reading the original measured force record is responsible as can be seen in Figure 2.1 of Volume I where the relative smoothness of the velocity compared to that of the measured force becomes apparent.

It is not possible to influence the high frequency behavior of the Error Delta curves by applying low frequency resistance forces and a check on the absolute values of $\Delta_e(t)$ could lead to unnecessary computations without convergence. Thus, an average is used. Also, when using the Error Delta curve for computing corrections on the $S_{o,i}$ and d_i only a smoothed $\Delta_e(t)$ is used as in the case of the Measured Delta curve.

The maximum damping force obtained by using $d_n = 10.3$ in the analysis was 70 kips. Using the Error Delta curve for calculating

the $\Delta S_{o,i}$, correcting the damping coefficient and performing another lumped mass analysis leads to the Error Delta curve (b) in Figure 3.8. The damping coefficient is corrected to produce the assumed damping force of 65 kips (i.e. $d_n = 10.3(\frac{65}{70})$). The criteria CR_i of the Inequalities 3.74 are shown in this figure. Here, it also can be observed that over the first and second region the average Error Delta curve stays within the bounds. Thus,

$$|E_1| = CR_1$$

$$|E_2| = CR_2$$

however

$$|E_3| > CR_3$$

and

$$E_3 = 26 \text{ (kips)} > 0$$

E_3 is the average delta value between $t = 2L/c + t_m$ and $t = t_f$. Since the sign of E_3 is positive, it means that not enough shear resistance force was applied. Thus, 13 (kips) total damping will be subtracted and 13 (kips) shear resistance added both at the pile tip.

The Error Delta curve resulting from the redistribution is shown in curve c, Figure 3.8. Error Delta curve c satisfies the conditions in region one and region two but not in region three since $E_2 < 0$ and $E_3 < 0$ this will be corrected by subtracting shear resistance. However, since E_2 was also less than zero no damping is added this time. After

another lumped mass analysis is performed Error Delta curve d is obtained which satisfied all three criteria. The final result is given in column 3 of Table 3.2. As an example for the C and E matrix the displacements and velocities were used from this final match of the first distribution. The resulting matrices are shown in Table 3.1. Ten elements are used in the lumped mass analysis together with $\phi = 2$ (see Chapter I), therefore, $x_i/c = 2\Delta t$. Thus, the influence numbers represent relative displacements or velocities which are taken at time differences of two time increments. ($\Delta t = .178$ milliseconds). It can be observed in the E-matrix that max v_i was not reached exactly at $t_m + x_i/c$ but at $t_m + x_i/c + \Delta t$ a time for which there is no matrix element. Thus, $e_{i,j} = 1.0$ was not obtained. A serious defect is not introduced since the E-matrix recognizes this fact. Note, that at $j = 7$ the influence of the returning wave can be observed in both the C and E Matrix. The C and E matrix are always recalculated when a lumped mass analysis is performed.

The second damping distribution leads to max D_i 55/8 = 6.9 (kips) maximum damping force for the second through ninth element. The Measured Delta curve, however, indicates that the predicted force would become too large in the beginning of the record. Therefore, these damping forces have to be reduced. The result are the parameters listed in Column 4 of Table 3.2.

It can be observed that some damping was used at the pile tip element in order not to exceed allowable top force effects before time $t_m + 2L/c$. The $S_{o,i}$ had been obtained after reducing the Measured Delta curve by means of the E and C - matrix. Figure 3.9 shows the

successively improved Error Delta curve obtained until finally the error criteria were satisfied. The final result is given in Column 5 of Table 3.2.

In the third distribution a max D_3 = 6.4 kips was used corresponding to $S_{o,3}$ which was the maximum shear resistance force at the pile skin in the upper pile half for the first distribution. Likewise, for the pile toe a damper was necessary for max D_n = 57 kips (the total damping determined in the second method was 69.8 kip, therefore, max D_n = 69.8 - 2 x 6.4 = 57.0).

Since the difference between the third and the first method is small for a small damping force at the skin a sufficiently small Error Delta curve (see Figure 3.10 was obtained already from the prediction. Soil resistance parameters obtained from this distribution are given in Table 3.2, Column 6.

In Figure 3.11 the predicted top forces are shown for all three predictions together with the measured force.

Now, the least square procedure can be performed. This leads to

a_1 = 1.48

a_2 = 0.09

a_3 = -0.57

The negative a_3 produces a negative damping parameter, d_3 = -0.3 which is discarded since its effect is small. The final result is tabulated in Column 7 of Table 3.1. Thus, S_o = 157.4 (kip and max D = 52 (kip).

This S_o is the shear resistance acting under impact. But the hammer compression force S_p, had been subtracted from the total record. This static force has to be added to S_o in order to obtain R_o, the total static bearing capacity. As for the distribution it is sensible to add to all $S_{o,i}$ a contribution of this static force proportional to the dynamically predicted value. The total static bearing capacity then becomes R_o = 157.4 + 40.6 = 198.0 (kip). The final distribution and the load test curve predicted from this result are presented in Chapter III of Volume I.

CHAPTER IV

Study on Characteristics of Force and Acceleration Records

4.1 Introduction

As a basis for the studies on pile dynamics presented in this work, two quantities must be available as continuous functions over time, namely force and acceleration measured at the top of the pile. Transducers, signal conditioning and recording devices have been described in References (5,6). Several observations were made which need to be explained. In records taken on a pile driven by a Diesel hammer an increase in force was noticed some time before the impact. This force arises due to pressure building up in the combustion chamber of the hammer. It seemed surprising, therefore, that no acceleration was recorded before the impact. Thus, the proportionality between force and velocity derived from wave theory appeared to be questionable. This and futher details observed in acceleration and force records are discussed in Section 4.2. Another phenomenon which was investigated was the existence of an oscillation appearing in both velocity and force. Since this frequency was not the pile natural frequency several possible models of pile-soil and hammer-pile were studied. The results of these studies are presented in Section 3 of this chapter.

4.2 Observations on Force and Acceleration in Diesel Hammer Records

Because of the proportionality between force and velocity in a stress wave it is advantageous to deal with pile velocities rather than with acceleration. From findings about velocities conclusions can be drawn regarding the measured acceleration. Consider Figure 4.1 showing the measured force and the velocity which was multiplied by the proportionality constant EA/c. The time scale chosen is in L/c units. The time when impact occurs is easily identified from the steep increase in both force and velocity. In this particular record the force starts to build up at a time of the order 10 L/c before impact while the velocity stays zero through the first 9 L/c.

In order to explain this lack of proportionality it is now assumed that the pile is fixed at the bottom end and the force for the first 9L/c is approximated by a piecewise linear function as indicated in Figure 4.2a. This piecewise linear function can be approximated again by superimposing two linear functions $F_{A,1}(t)$ and $F_{A,2}(t)$. For the time until the first reflection wave reaches the top after having been reflected at the bottom, force and velocity must be proportional. Thus, for $t \leq 2L/c$ the velocity is $c/EA\ F_{A,1}(t)$. When the first wave returns from the fixed bottom end its particle velocities will have changed sign. This leads to a decrease in top velocity. At a time 4L/c two reflection waves will reach the top with different signs of velocities. Thus, the pile top velocity can be written as

$$v_{top}(t) = \frac{c}{EA}\left(F_A(t) - 2F_A\left(t - \frac{2L}{c}\right) + 2F_A\left(t - \frac{4L}{c}\right) - \ldots + \ldots\right) \tag{4.1}$$

Using this equation it is seen that for a linearly increasing top force the velocity at the top will oscillate between zero and the value proportional to the force at time 2L/c. Figure 4.2b shows the velocity derived from superimposing the solutions for the two linear force functions. This superposition can only produce a slope in the velocity which is less than or equal to the maximum proportional slope in the force record. A simple calculation can then lead to the maximum acceleration. Suppose max f is the maximum slope encountered in the record before impact then the maximum slope of the velocity, max a, is given by

$$\max a < \max f \frac{c}{EA} \tag{4.2}$$

But max f can be expressed by a force difference F over a time L/c then

$$\max a = \frac{\Delta F}{L/c} \frac{c}{EA} \tag{4.3}$$

and with $c^2 = E/\rho$ and $AL\rho g = W$, the weight of the pile

$$\max a = \frac{\Delta F}{W} g \tag{4.4}$$

In the example of Figure 4.2 ΔF = 5.7 kips and W = 2.0 (kip) so that max a = 2.9 g's. The acceleration is read from a record in which a 1 inch amplitude corresponds to 375 g's (see Figure 4.3). It is, therefore, not surprising that small magnitude accelerations like the 2.9 g's obtained in the example computation were not recognized in

the record.

The results of these considerations can be expressed as follows: The acceleration will reach a noticeable non zero value in the record only when the time derivative of the force becomes large. Second, the velocity of the pile will obtain some value greater than zero which will be dependent mainly on the stiffness of the soil. If this stiffness is infinite then the above derived relations would hold. Third, the proportionality between velocity and force was lost because of the long time over which the force built up. It can be argued that this precompression force is applied in a "static" way, and therefore, should be separated from the dynamic portion of the record if dynamic analysis is to be used. The dynamic record might then be defined from that point at which an acceleration greater than zero can be observed. In most of the records this is the time when a proportionality between force and velocity can be observed. For comparison Figure 2.1 of Volume I shows force and proportional velocity after the precompression force had been subtracted. The record was the same as analyzed above.

The study of the forces recorded before the actual impact occurs leads to another interesting observation. Frequently in pile dynamics it is necessary to predict the hammer impact velocity, max v_h. In the case of a gravity hammer this can be done when the drop height, h, of the hammer is known. Then

$$\max v_h = \sqrt{2hg} \tag{4.5}$$

For Diesel hammers, however, a free fall cannot occur under the action of the fuel compression force. In this case the velocity has to be computed by subtracting the velocity due to these forces. Thus,

$$\max v_h = \sqrt{2hg} - \frac{1}{M_h} \int_{t=0}^{t=t_a} F_{top}(t)dt \qquad (4.6)$$

where M_h is the ram mass and t_a is the time where the "dynamic record" starts. In the example of Figure 4.2 the evaluation of the integral in Equation 4.6 leads to a difference velocity (the second term on the right hand side in Equation 4.6) of 2.7 ft/s (M_h = 3.51 g kips/g) which is substantial compared to the velocity encountered at impact (max v_h = 9.6 ft/s). Although the energy which the hammer supplied does not change due to the compression another kind of energy will be utilized having smaller velocities but being spread over time. This fact might prove essential when applying the wave equation method proposed by Smith (3) where one of the input parameters used is the impact velocity.

A remark on the accuracy of the velocity seems appropriate. The usual recording sensitivity for acceleration is between 300 and 400 g's for one inch amplitude in the record. Records are read with an accuracy of about 1/150 inch. A shift of the assumed zero acceleration line with this amount can produce over the length of the record (usually about 20 milliseconds) a considerable velocity. This effect will be even amplified when considering displacements.

Using the average of two acceleration records taken on opposite sides of the pile should lead to an improvement in accuracy but velocities and displacements can still not be reliable after some time of integration. It was noticed in applying the Phase I simplified theory (see Chapter II, Section 5 of Volume I) that sometimes no zero velocity was reached, which can be explained from the facts under consideration. The Phase II-A method (see Chapter VI of Volume II) will introduce a major improvement because only differences in velocity are considered over a relatively short time and the time of zero velocity is no longer an important parameter.

Another inaccuracy can be observed in Figure 2.1 of Volume I before maximum velocity occurs. The force should be exactly equal to the velocity times EA/c. However, it is noticed that there is a time lag between force and velocity. The reason is a different response time in the signal condition equipment. This time lag often causes large Delta curve values in the beginning of the record which must be discarded in an analysis.

Another interesting observation can be made on records obtained under a single acting Diesel hammer. Such a hammer consists basically of two parts: a cylinder whose top is open and a piston, i.e. the hammer, which falls freely in the beginning and by falling compresses the air in the combustion chamber. When the piston reaches the cylinder bottom fuel is injected so that metal to metal impact between hammer and anvil occurs together with the combustion. Impact plus combustion force will move the pile head. In the first instant both hammer and pile head will move together with the velocity of the

impacting hammer. The hammer cylinder originally resting at the pile top cannot follow this rapid movement, thus it will start to fall under gravity. When assuming that most of the deflection of the pile head is due to penetration into the ground and only a smaller portion is due to elastic deflection of pile and soil, then the hammer cylinder will reach the pile only after the pile has established its final position. The hammer cylinder then will impact upon the pile top and a force and acceleration due to this (smaller) impact can be observed in these records. Figure 4.3 shows a record in its orginal scale. In both force and acceleration the second impact can be observed after a time ΔT. It is now interesting to compute the distance u_f which the hammer cylinder fell freely disregarding any friction in the leads or other losses from the time Δt between the impact of the piston and that of the cylinder

$$u_f = \frac{1}{2} g(\Delta T)^2 \qquad (4.7)$$

and, therefore, in the example of Figure (4.3)

$$u_f = \frac{1}{2} 386(.054)^2 = .562 \text{ [inch]}$$

During the driving operation an average set of .06 inch under one hammer blow was measured. It seems that in cases where the set of the pile is large enough and where a single acting hammer is used more accurate information about the pile set can be obtained

from this observation.

4.3 Studies of Vibration Frequencies Occurring on the Pile Head During Driving

Figure 2.1 of Volume I shows typical force and velocity curves having the above mentioned oscillations about an essentially linear behavior. If the lowest pile natural frequency is responsible only pile length and material properties would be necessary to predict these frequencies but this is not the case. Vibrations might also occur due to the interaction of soil stiffness with pile mass, a system which is respresented in Figure 4.4b. Another explanation for this phenomenon developed herein is that the cushion hammer system supported by the pile exerts forces upon the pile head which are due to its natural frequencies. The model for such a system is shown in Figure 4.4c. In the following the frequencies expected for the discussed models will be investigated and compared to those observed in the record.

The lowest natural frequency of a pile of length L is

$$f_1 = \frac{c}{4L} \tag{4.8}$$

where c is the wave speed.

Assuming the soil stiffness k_s to be approximately

$$k_s = \frac{R_u}{q} \tag{4.9}$$

where the quake q can be chosen as .12 inches and R_u as the ultimate bearing capacity of the pile; then for the system of Figure 4.4b a frequency of

$$f_1 = \frac{1}{2\pi}\sqrt{\frac{R_u}{AL\rho q}} \tag{4.10}$$

would be obtained. In the examples given in Table 4.2 steel piles will be considered having a cross sectional area A = 9.82 (inch^2). For these cases

$$f_2 = 49.4\sqrt{\frac{R_u}{L}}$$

if L is inserted in feet and S_{ult} in kip. The system shown in Figure 4.4c has two degrees of freedom. If the upper cushion stiffness is k and the lower one k·s and if the upper and lower elements have masses r·m and m, respectively then the two natural frequencies can be computed from

$$f_{3,4} = \frac{1}{2}\left[\frac{k}{m}\left\{\frac{1 + r(1 + s)}{2r} \pm \left(\frac{1 + r(1 + s)^2}{4r^2} - \frac{s}{r}\right)^{1/2}\right\}\right]^{1/2} \tag{4.11}$$

The cushion stiffnesses for the transducer cushion (ks) were obtained experimentally. This transducer cushion was built using alternated layers of 3/4-inch plywood and 1/4-inch neoprene sheets. 3 or 5 plywood and 4 or 6 neoprene sheets were used. The pile cushion stiffnesses (k) were obtained from Reference 7. In both cases statically

obtained load versus deflection curves were used and stiffnesses were obtained at the different load levels observed in the force record. All the parameters necessary for computing $f_{3,4}$ are listed in Table 4.1. The correlation of frequencies calculated from all three methods with the observed are listed in Table 4.2.

As an example consider again Figure 2.1 of Volume I representing Pile F-60, Blow No. 26-A. The average frequency observed in the force and velocity record is 409 (cps). The length of the steel pile was 60.5 feet and hence $f_1 = \frac{17,000}{4 \times 60.5} = 70$ (cps) from Equation 4.8. The ultimate resistance obtained in the CRP test was 242 kips which leads to an $f_2 = 99$ (cps) using Equation 4.10. The transducer cushion consisted of 3 sheets of plywood and 4 sheets of neoprene. The average force acting on the pile top during the blow was 150 kips as can be observed in Figure 4.3. From Table 4.1 this gives a transducer cushion stiffness of 7,250 kips/inch. The driving hammer was a Linkbelt 440 which has a cushion stiffness of 9,300 kips/inch under the given circumstances. Thus $s = 7,250/9,300 = 0.78$. Also from Table 4.1 $m = \frac{1.10}{g} \frac{\text{kips}}{g}$ and $r = \frac{4.71}{1.10} = 4.28$. Inserting these values into Equation 4.11 leads to a lower frequency $f_3 = 89$ and a higher frequency $f_4 = 398$ (cps). As in all the other cases presented in Table 4.2 f_4 is the only frequency of a magnitude comparable to the measured one (409 cps in the discussed example). It seems that the only reasonable explanation for the occurence of frequencies higher than 100 cps for the listed cases is that the two degrees of freedom system described above vibrates in its second mode, thus, exerting forces and velocities upon the pile head reflecting this higher frequency.

CHAPTER V
Soil Model Studies

5.1 Introduction

The investigations presented in this Chapter give an insight into the relations between the pile motion and the soil resistance response. This soil response is approximated in Chapter II of Volume I by a simple model, which has also been employed by other investigators in the pile dynamics literature (1, 7). Results in Chapter III of Volume I show that this model does not always describe the soil resistance force, $R_i(t)$, accurately for all times t.

The soil model is shown in Figure 2.2 of Volume I. It consists of a spring and a dashpot in parallel, thus

$$R_i(t) = S_i(t) + D_i(t) \tag{5.1}$$

$S_i(t)$ and $D_i(t)$ are the shear and dynamic resistance, respectively. The index "i" indicates the location where the resistance force acts.

The spring in the soil model is assumed to have elasto-plastic properties such that

$$S_i(t) = k_i u_i^*(t) \tag{5.2}$$

where k_i is the soil stiffness at $x = x_i$ and

$$u_i^*(t) = \begin{cases} u_i(t) & \text{for } u_i(t) \leq q_i \\ \max u_i + q_i - u_i(t) & \text{for } u_i(t) \geq \max u_i \end{cases} \tag{5.3}$$

where $u_i(t)$ is the displacement of the pile at $x = x_i$ and time t; q_i is the quake and $\max u_i$ is the maximum displacement reached at or before time t.

It is further assumed that

$$S_i(t) \geq -k_i q_i \tag{5.4}$$

and that

$$S_n(t) \geq 0 \tag{5.5}$$

i.e. no tension shear forces are allowed to act at the pile tip. This is a reasonable assumption for the soil forces acting against the pile toe plate. The quantity $k_i q_i$ is the ultimate shear resistance force and is denoted by $S_{i,o}$. A typical force versus displacement relation resulting from the definitions in Equations 5.2 through 5.5 is shown in Figure 2.2 of Volume I.

The dynamic or damping resistance force, $D_i(t)$, is linearly proportional to the pile velocity, $v_i(t)$, at $x = x_i$. Thus,

$$D_i(t) = d_i v_i(t) \tag{5.6}$$

where d_i is a damping coefficient. Again, it is assumed that only

compressive resistance forces act at the pile toe. Figure 2.2 of Volume I shows the damping velocity relation graphically.

To investigate the validity of the above soil model, measurements were taken during driving at the pile bottom end. Both force and acceleration records are available. Also the pile tip force was measured as a functionof pile penetration during a static load test. The force was always recorded at some distance above the pile toe plate to which the accelerometer was connected. From these measurements the soil resistance force, $R_n^M(t)$, acting against the pile toe plate during driving can be approximated by

$$R_n^M(t) = F(t) - Ma(t) \qquad (5.7)$$

where $F(t)$ is the measured force, $a(t)$ is the measured acceleration and M is the mass of the pile below the point of force measurement.

Five representative records are selected for investigation. One set of measurements - obtained from a reduced scale pile - is typical for the soil response in coarse grained soils (see Table 1.3 of Volume I for the soil profile). Two records are from full scale pile Ri-50 (see Chapters I and III of Volume I) where the soil surrounding the pile tip was highly cohesive. The records were obtained immediately after driving and also after a waiting period of three days. In a similar manner records were taken on full scale pile Ri-60. This pile had a high point resistance in a sandy gravel layer at the bottom of the pile. Table 1.2 of Volume I gives

the soil profile for both piles Ri-50 and Ri-60.

5.2 Reduced Scale Pile In Sand

The discussion is illustrated in Figure 5.1. At the top of this Figure, a plot is shown of both velocity, $v_n(t)$, and displacement, $u_n(t)$, as obtained by integrating the measured toe acceleration. The measured resistance force $R_n^M(t)$, computed from Equation 5.7 is plotted at the bottom of Figure 5.1. For further discussion the index n is omitted.

The first remarkable observation is that $R^M(t)$ has its maximum at the same time as the velocity v(t). Thus, dynamic forces seem to be present. After its maximum the measured resistance force decreases monotonically. This is in agreement with the decreasing velocity and corresponds after zero velocity to the pile rebound.

The soil model under discussion requires three parameters to describe the behavior of R(t) in terms of u(t) and v(t). These parameters (q, d and S_o) give the theoretical resistance curve such that it agrees with the measured curve at three points. Using the same approach as in Chapter II of Volume I for finding the quake, i.e. assigning the displacement at maximum velocity to be the quake, leads in the example of Figure 5.1 to

$$q = 0.08 \text{ inch}$$

With this choice only two parameters are left to be determined.

Selecting the time of both maximum velocity, t_m, and zero velocity, t_o, for obtaining agreement between measured and theoretical resistance force, then

$$R^M(t_m) = S_n(t_m) + D_n(t_m)$$

and

$$R^M(t_o) = S(t_o) + D(t_o)$$

However,

$$S(t_m) = S(t_o) = S_o$$

and

$$D(t_o) = 0$$

so that

$$S_o = R^M(t_o)$$

and

$$D(t_m) = R^M(t_m) - S_c$$

Thus,

$$d = \frac{R^M(t_m) - S_o}{v(t_m)}$$

In the example of Figure 5.1 the soil parameters become

$$S_o = 6.75 \text{ (kip)}$$

$$\max D = 10.0 - 6.75 = 3.25 \text{ (kip)}$$

$$d = 3.25/8.3 = 0.39 \text{ (kip·sec/ft)}$$

Using now Equation 5.1 through 5.6 the theoretical resistance

curve can be plotted. In Figure 5.1 both R(t) and S(t) are plotted and can be compared with the measured curve. Since no negative damping forces are allowed for the bottom end of a pile R(t) = S(t) when the velocity v(t) is negative. The resistance curves R(t) and $R^M(t)$ agree quite well before and at zero velocity. After this time the theoretical curve decreases at a slower rate than measured. Certainly, a smaller quake could match this portion of the record better, however, such a change would also affect the quality of the match before maximum velocity. Furthermore, the resistance force is very sensitive to changes in either the quake or the displacement during unloading. An error of 0.01 inches in the displacement at the end of the record would amount to a difference of the theoretical resistance force of 12.5% of the predicted ultimate shear resistance. The displacement curve is not very accurate for later times, therefore, not much accuracy can be expected in predicting the quake from the unloading behavior.

To summarize the results obtained from this record: A maximum damping force of approximately one half of the ultimate shear resistance was found. The match between theoretical and measured resistance force is good before zero velocity. The ultimate shear resistance force S_o = 6.75 (kip) compares well with the point resistance under the static load test which is plotted in Figure 6.6a. (7.3 kips at ultimate and 6.6 kips at maximum dynamic displacement). Also soil stiffness and quake are in good agreement.

5.3 Full Scale Pile in Cohesive Soil

Two records taken on a pile in a cohesive soil are shown in Figures 5.2 and 5.3. The records were obtained before and after a waiting period, respectively. The following characteristics are common to both records.

At time zero a force, S_p, can be observed which must be due to the hammer precompression. For further considerations S_p is thought of as a static force independent of velocity and displacement and is, therefore, disregarded. (S_p = 3 kips in Figure 5.2). The resistance forces show a steep rise together with the corresponding velocity. After the maximum, the resistance force rapidly decreases to a magnitude not much greater than S_p. Thereafter, an almost steady strength increase can be observed. This strength increase corresponds to the monotonically increasing displacment while oscillations in the force show some relation to the velocity record.

The velocity shown in Figure 5.2 reaches no zero within the time period considered but a small value at the end of the record. Thus, defining t_o for this case to be the time of minimum velocity the match shown in Figure 5.2 is obtained. The soil parameters, thus determined, are:

$$q = .12 \text{ (inch)}$$

$$S_o = 15 \text{ (kip)}$$

$$d = 1.24 \text{ (kip/ft-s)}$$

This match is very poor immediately after the time of maximum

velocity. Several reasons can be responsible.

(i) The proportionality between damping force and velocity holds only until the time of maximum velocity. Immediately after this time damping forces become very small.

(ii) High pore water pressures are building up during the time of the initial load application and are released slowly, thereafter.

(iii) A strength increase can be observed throughout the resistance force record. Since the velocity is positive and decreasing this strength gain must be due to the displacement gain.

Comparing Figure 5.3 with Figure 5.2 it is observed that higher resistance forces were acting at the pile toe although the displacements were smaller. Thus, a strength gain due to the waiting period can be observed. A match was performed using the same procedure as described before. The soil parameters thus determined are

$$q = .096 \text{ (inch)}$$

$$S_o = 24 \text{ (kip)}$$

$$d = 2.5 \text{ (kip/ft·s)}$$

$$R_o = S_o + S_p = 29 \text{ (kip)}$$

As in Figure 5.2 the predicted soil forces in Figure 5.3 are too large after maximum velocity and agree quite well thereafter.

In Figure 5.6b are shown the two pile tip force versus pile tip penetration curves obtained from static load test and corresponding to the two records just discussed.

At ultimate the point resistance is 14 and 18 (kip) for the cases in Figures 5.2 and 5.3, respectively. This compares to 18 and 24 (kips) from the dynamic measurements. Thus, both dynamic resistances are high by about 25 to 30%.

5.4 Full Scale Pile with High Point Resistance

Two cases where the soil consisted of a very hard gravel and sand layer are shown in Figures 5.4 and 5.5. The resistance force shown in Figure 5.4 can be represented with a fair degree of accuracy by the proposed soil model. A small difference occurs at the second local maximum of the $R^M(t)$ curve. A sensible explanation is a further strength gain due to still increasing displacements. Differences in the unloading portion are again due to the high sensitivity of the soil model to small errors in quake and displacements. This was outlined in Section 5.1.

A time lag between velocity and force (a measurement inaccuracy discussed in Chapter IV of Volume II and Chapter III of Volume I imposes problems on the match in the first portion of the record. In Figure 5.4 this difficulty leads to determining the quake at the time of maximum force.

A different way of matching was used in Figure 5.5; namely by assuming that the quake is greater than maximum displacement and then matching the maximum resistance values. The special feature of

this record is the small displacements (Note the change in scale), and the smooth resistance force curve. Except for a time lag due to measurement difficulties the resistance force essentially follows the behavior of the displacement curve. The fact that this proportional relation holds throughout the record indicates that little or no yielding occurred. Thus, the hammer did not supply enough energy to overcome the soil resistance forces. Small damping forces can be observed at the time of maximum velocity.

The static load tests corresponding to the records of Figures 5.4 and 5.5 had to be terminated before the ultimate load was reached. However, the soil stiffnesses from static and dynamic measurements can be compared. This is shown in Figure 5.6c. Apparently the soil offered a stiffer resistance during the dynamic load application than during the static test. Such a loading rate dependent behavior can be expected. It is interesting to note that the soil lost stiffness during the waiting period; an effect which is reflected in both dynamic and static measurements.

5.4 Summary

The following conclusions can be drawn from the records presented in Figures 5.1 through 5.5.

The present soil model describes the force versus displacement and velocity relation fairly well for granular soils. The unloading portion, however, is difficult to match, although the model might still hold.

Cohesive soils present characteristic resistance force patterns which cannot be described by a simple spring - dashpot model. Further studies on how to model such soils must be conducted, including other independent variables like pore water pressure or soil dynamic effects. The prediction of static capacity from dynamic records can give good results for piles driven into granular soils. In the cohesive soils as in Figures 5.2 and 5.3 it is seen that the shear resistance forces vary throughout the records and no indication is given of the static resistance. A more realistic soil model could improve this situation. In Chapter IV of Volume I further discussion of this problem is given with respect to the results which can be expected by employing the present soil model in a wave analysis. It should be noted that an average value of the measured soil resistance curve immediately after the maximum leads to a reasonable answer. One important observation is made when studying the dynamic and static load versus penetration curves plotted in Figures 5.6b and 5.6c. For cohesive soils a strength increase is observed during the waiting period. The soil stiffness decreased, however, for the granular material. These effects were measured both dynamically and statically, thus, justifying the proposed method of taking dynamic measurements after a waiting period in order to obtain meaningful predictions on the static pile behavior.

CHAPTER VI

Simplified Methods for Predicting Static Bearing Capacity

6.1 Introduction

It was indicated in Chapter I of Volume I that effort was devoted to the development of a simple method for predicting static bearing capacity. Such a method, utilizing in a special purpose computer, would display, in the field, the prediction within a short time after the hammer blow. Thus, decisions could be made to control the driving operation. In the following, two previously developed methods (8) are briefly reviewed. These methods were based on a rigid pile model. Using wave considerations, i.e. employing an elastic pile model, two new computation schemes are derived. Results from all methods are given in Chapter III of Volume I.

6.2 Rigid Body Models

Suppose, a rigid body of mass M is acted upon by a force F(t), and a resistance force R(t). If the acceleration of this mass is denoted by a(t) then the static bearing capacity, R_o, is given by

$$R_o = F(t_o) - M\, a(t_o) \tag{6.1}$$

where t_o is the time of zero velocity. The derivation of Equation (6.1) is given in Chapter I of Volume I. The sign convention is shown in Figure (6.1). Equation (6.1) is referred to as the Phase I

prediction scheme.

The results obtained from the Phase I prediction scheme were promising when compared with the maximum bearing capacity determined in the static load test. However, the results differed substantially from blow to blow and it was found that small changes in t_o often caused large differences in the predictions. Figure 6.2 illustrates this sensitivity of R_o to changes in t_o. In this Figure the measured acceleration and the velocity and displacement obtained by integration are plotted. Also, the measured force and the resistance, R(t), are shown where

$$R(t) = F(t) - M\, a(t) \tag{6.2}$$

The point of zero velocity is indicated by a dotted line in the force diagram. If this point of zero velocity were shifted only a small time increment (due to measurement inaccuracies such a shift is always introduced) then predictions ranging from 150 to 200 kips could be obtained.

This defect of the Phase I prediction method led to an averaging method referred to as the Phase II prediction scheme. Consider the velocity graph in Figure 6.2. A straight line marks the trend of the descending velocity curve. Using the slope of this line instead of $a(t_o)$ in Equation 6.1 the new prediction scheme becomes

$$R_o = F(t_o) - \frac{M}{\Delta T} \int_{t_1}^{t_1 + \Delta T} a(t)dt \tag{6.3}$$

where t_1 was chosen as the time of maximum velocity and the average was taken until the time of zero velocity ($t_1 + \Delta T = t_o$). As a result of the averaging procedure, the variations in the predictions from blow to blow were relatively small. Another method was proposed where the force F(t) is also time averaged, however, results were little affected because of the relatively smooth force records.

6.2 Elastic Pile Models

The above methods used a rigid body as a pile model. To explain and clarify limitations on these methods the traveling wave solution of the linear, one-dimensional wave equation is utilized.

(i) Phase IIA

In Chapter III relations were developed by which the pile top velocity, $v_{top}(t)$, can be expressed as a function of external forces. In particular, if a force, $F_A(t)$, is acting at the pile top then Equation 3.27 can be used to compute $v_{top}(t)$. Similarly, Equation 3.29 expresses the pile top velocity as a function of a resistance force $R_i(t)$ acting at $x = x_i$ and time t at the pile in the upward direction. If it is assumed that n resistance forces act along the pile together with the force applied at the pile top. Then the resulting pile top velocity can be calculated by superimposing the solutions from Equations 3.27 and 3.29. Thus, with r indicating the time interval considered, i.e. $r \frac{2L}{c} \leq t \leq (r + 1)\ 2L/c$,

$$v_{top}(t) = \frac{c}{EA}[F_A(t) + 2\sum_{j=1}^{r} F_A(t - j\frac{2L}{c})$$

$$- \sum_{k=1}^{n}\sum_{j=0}^{r}\{R_k(t - \frac{x_k}{c} - j\frac{2L}{c})$$

$$+ R_k(t - \frac{2L - x_k}{c} - j\frac{2L}{c})\}] \qquad (6.4)$$

It is assumed now that the resistance forces, $R_i(t)$, are only due to shear. Effects of dynamic resistance forces will be included later. Therefore,

$$R_i(t) = S_i(t) \qquad (6.5)$$

and using the simplified expression for a shear force as given in Section 3.5, Equation 3.46, then

$$R_i(t) = S_{i,o}\, H(t - \frac{x_i}{c}) \qquad (6.6)$$

which means that the quake is assumed to be zero. Inserting Equation 6.6 into 6.4 yields

$$v_{top}(t) = \frac{c}{EA}[F_A(t) + 2\sum_{j=1}^{r} F_A(t - j\frac{2L}{c}) - \sum_{k=1}^{n}\sum_{j=0}^{r}\{S_{k,o}H(t - \frac{2x_k}{c}$$

$$-j\frac{2L}{c}) + S_{k,o}H(t - \frac{2L}{c} - j\frac{2L}{c}\}] \qquad (6.7)$$

Now, two different times, t_1 and t_2, are chosen so that

$$t_2 = t_1 + 2L/c \tag{6.8}$$

therefore, if $r\frac{2L}{c} \leq t_1 \leq (r + 1)2L/c$ then $(r + 1)\frac{2L}{c} \leq t_2 \leq (r + 2)\frac{2L}{c}$. The difference between the velocities at both times, Δv_{top}, is

$$\begin{aligned}\Delta v_{top} = v_{top}(t_2) - v_{top}(t_1) = c/EA[&F_A(t_1 + 2L/c) - F_A(t_1) \\ &- 2\sum_{j=1}^{r} F_A(t_1 - j\tfrac{2L}{c}) + 2\sum_{j=1}^{r+1} F_A(t_1 + 2L/c - j\tfrac{2L}{c}) \\ &- \sum_{k=1}^{n}\sum_{j=0}^{r} S_{k,o}\{H(t_1 - 2x_k/c - j\tfrac{2L}{c}) + H(t_1 - \tfrac{2L}{c} - j\tfrac{2L}{c})\} \\ &+ \sum_{j=0}^{r+1} S_{k,o}\{H(t_1 - 2x_k/c - (j - 1)2L/c) + H(t_1 - j\tfrac{2L}{c})\}]\end{aligned} \tag{6.9}$$

This expression can be simplified to yield

$$\begin{aligned}\Delta v_{top} = c/EA[&F_A(t_1 + 2L/c) + F_A(t_1) - \sum_{k=1}^{n}[S_{k,o}\{H(t_1 - 2x_k/c \\ &+ 2L/c) + H(t_1)\}]]\end{aligned} \tag{6.10}$$

The arguments of the step function terms on the right hand side of Equation 6.10 are non negative so that

$$\Delta v_{top} = c/EA[F_A(t_2) + F_A(t_1) - 2\sum_{k=1}^{n} S_{k,o}] \tag{6.11}$$

which can be written as

$$\frac{\Delta v_{top}}{2L/c}\,\frac{L}{c}\,\frac{EA}{c} = \frac{F_A(t_2) + F_A(t_1)}{2} - \sum_{k=1}^{n} S_{k,o} \qquad (6.12)$$

However, $c^2 = E/\rho$ and $AL\rho = M$, M being the mass of the pile. In addition $2L/c = \Delta T$, i.e. the time between t_1 and t_2. Thus, with

$$\sum_{k=1}^{n} S_{k,o} = R_o$$

$$R_o = 1/2(F_A(t_1) + F_A(t_2)) - \frac{M}{\Delta T}\int_{t_1}^{t_2} a(t)dt \qquad (6.13)$$

Equation 6.13 establishes a simple method for computing the static bearing capacity, R_o, if the force and the acceleration at the pile top are known. Because of the similarity between Equations 6.13 and 6.3 this method is referred to as the Phase IIA prediction scheme.

Two differences can be observed between Equations 6.13 and 6.3. First, the force term has to be calculated as an average of the forces where the acceleration average starts and ends. The second difference is the need of restricting ΔT to exactly 2L/c.

In order to understand the actual meaning of the results obtained by applying Equation 6.1, Equation 6.7 has to be differentiated with respect to time and the result, the acceleration of the pile head, substituted into Equation 6.1.

$$a(t) = \frac{c}{EA}\left[\frac{dF_{top}(t)}{dt} + 2\sum_{j=1}^{r}\frac{dF_A(t - j\frac{2L}{c})}{dt} - \sum_{k=1}^{n}\sum_{j=0}^{r}\{S_{k,o}(\delta(t - 2\frac{x_k - jL}{c}) + \delta(t - 2\frac{(j+1)L}{c})\}\right] \quad (6.14)$$

where $\delta(t - a)$ stands for the Dirac δ-function which is zero for $t \neq a$.

Inserting 6.14 into 6.2 and avoiding times t_o such that

$$t_o = \begin{cases} 2\frac{x_e - jL}{c} \\ 2\frac{(j+1)L}{c} \end{cases} \qquad \text{for } j = 0,1,\ldots,r \text{ and } t = 1,2,\ldots,n$$

yields at $t = t_o$

$$R_o = F(t_o) - M\frac{c}{EA}\left[\frac{dF_A(t_o)}{dt} + 2\sum_{j=1}^{r}\frac{dF_A(t_o - j\frac{2L}{c})}{dt}\right] \quad (6.15)$$

The second term consists of the slopes of the force record taken at time intervals of 2L/c. These slopes of the force record change rapidly over short times due to vibrations in the hammer cushion system (see Chapter IV). Therefore, it is not surprising that the results from the Phase I method showed a large change whenever the time t_o was changed by small amounts.

In deriving the Phase IIA prediction scheme dynamic resistance forces were not considered. Such forces can be thought of as being linearly proportional to the pile velocity. Thus, Equation 6.13 is only applicable at all time pairs t_1 and t_2 if either the dynamic resistance forces are identically zero because of special soil pro-

perties or the pile is not moving. Practically, there exists no case of pile driving without velocity dependent forces and the pile motion ceases only after the pile has rebounded and also shear forces reached zero. However, due to the negative particle velocities of waves caused by resistance forces the velocities along the pile are usually small - positive or negative - when the pile top velocity has reached zero. For this reason a good approximation to the prediction of static resistance forces can be found if t_1 is chosen to be the time of zero velocity at the pile top and t_2 at a time 2L/c later.

In analyzing field measurements it was frequently found that zero velocity was not reached even for long times after impact. This non-negative velocity can be explained due to measuring inaccuracies as explained in Chapter IV. In such cases a prediction can be obtained by taking t_1 as the minimum velocity encountered. Since only the difference velocity between t_1 and t_2 affects the result no major error is introduced into the computation.

(ii) Phase III

The studies on wave propagation in Chapter II of Volume I and in Chapter III of Volume II showed that the Measured Delta curve reflects the effects of soil resistance forces at the pile top. Figure 2.5, 6, 7 of Volume I show three such measured Delta curves. Also Resistance Delta curves were investigated which display an approximate pile top force effect of a certain resistance force acting at some point along the pile.

It is now intended to show how the concept of Delta curves can be used to obtain a simple computation scheme for predicting static bearing capacity. In such a simplified analysis it is not possible to find where the resistance forces act. Therefore, the portion of the Measured Delta curve with $t \leq t_m + 2L/c$ (t_m being the time of maximum velocity at the pile top) is of minor interest. However, important information regarding the total amount of static and dynamic resistance forces can be obtained from the Measured Delta curve for $t_m + 2L/c \leq t \leq t_m + 4L/c$.

A first assumption in the derivation of the Phase III prediction scheme is to neglect any influence of skin damping forces. That this assumption is at least a good approximation is proven by the results in Chapter III of Volume I. Next it will be shown how the Measured Delta curve can be modified such that the effect of skin shear forces can be converted to an equivalent effect of pile tip forces. This then will reduce the problem to a pile with only pile toe resistance forces.

Consider Figure 6.3a which shows a theoretical Delta curve for a shear force $S_{n,o}$ acting at the pile tip. (Such a theoretical shear force is discussed in 3.5). A shear force having the same magnitude acting at $x = x_i$ produces a Resistance Delta curve as shown in Figure 6.3b. The difference between these two Delta curves is the earlier pile top effect of the upwards traveling wave generated by the skin force. A modified Delta curve can be obtained by delaying the earlier effects by a time $2(L - x_i)/c$. Figure 6.3c illustrates

this procedure. Analytically, the Modified Delta curve can be obtained from the Measured Delta curve, $\Delta(t)$, and the pile top velocity, $v_A(t)$, using

$$\Delta_{mod}(t) = \Delta(t) + \Delta(t - 2L/c) - 1/2 \frac{v_A(t - 4L/c)}{\max v_A} \Delta(t_m + 2L/c) \tag{6.16}$$

which is valid for $t_m + 2L/c \leq t \leq t_m + 4L/c$, and only if skin forces are of the step shaped type as in Figure 6.3. The third term in this equation is necessary for not delaying effects of the already returning waves after reflection at the bottom end. (This is a similar approach as used in the derivation of $\Delta_{red}(t)$ in 3.6). In further derivations of the Phase III method the subscript "mod" is dropped and it is understood that $\Delta(t)$ means the modified Delta curve.

If all resistance forces act at the bottom end of the pile then their effect can be felt at the pile top at a time L/c later. Thus, the Measured Delta curve is given by

$$\Delta(t) = 2[D_n(t - L/c) + S_n(t - L/c)] \tag{6.17}$$

where the notation of Chapter III is used. The velocity of the pile tip that results from the velocity $v_A(t)$, imposed on the pile top and from both shear and damping forces acting at the tip is given by

$$v_n(t) = \frac{2v_A(t - L/c) - (c/EA)S_{n,o}}{1 + cd_n/EA} \qquad (6.18)$$

where $S_{n,d}$ as defined earlier is the ultimate shear resistance at the pile top. (This is Equation 3.43 derived in 3.5). Equation 6.18 is valid for $L/c \leq t \leq t_{n,o}$, i.e. after the quake is reached until the pile tip velocity becomes zero and unloading starts. The time $t_{n,o}$, i.e. the time of zero velocity at the pile tip, can be determined from Equation 6.18

$$v_n(t_{n,o}) = 0 = 2v_A(t_{n,o} - L/c) - (c/EA)S_{n,o} \qquad (6.19)$$

However, $S_{n,o}$ can be expressed in terms of the Measured Delta curve by using Equation 6.17 and by observing that at time $t_{n,o}$ damping is zero and $S_n(t_{n,o}) = S_{n,o}$. Thus,

$$2v_A(t_{n,o} - L/c) - (c/2EA)\Delta(t_{n,o} + L/c) = 0 \qquad (6.20)$$

or rewritten

$$\Delta(t_{n,o} + L/c) = 4\frac{EA}{c} v_A(t_{n,o} - L/c) \qquad (6.21)$$

Equation 6.21 shows how to find the time of zero velocity at the pile tip from pile top velocity and Measured Delta curve. A comment is appropriate. Suppose that the pile had a fixed bottom end (this is the condition which yields the largest possible pile resistance

forces assuming that there are no forces acting at the pile which could produce a negative pile permanent set). At a fixed end reflection waves are generated such that no movement occurs. This constraint requires a reaction force, $R_f(t)$, of twice the magnitude of the forces in the wave. Therefore,

$$R_f(t) = 2\frac{EA}{c} v_A(t - L/c) \tag{6.22}$$

if it is assumed that the only wave arriving is due to the hammer impact. The Measured Delta curve resulting from a fixed end is then

$$\Delta(t) = 4\frac{EA}{c} v_A(t - 2L/c) \tag{6.23}$$

Hence, whenever the Measured Delta curve exhibits a value four times larger than the force proportional velocity at a time 2L/c earlier then no motion of the pile tip will occur at a time L/c earlier.

In the usual case of pile driving a motion of pile will always occur before the fixed end condition, Equation 6.23, is satisfied. Such a motion is necessary to activate the resistance forces. Once, however, the resistance forces have reached a value large enough or once the applied velocity, $v_A(t - 2L/c)$, became small enough then Equation 6.21 will be satisfied. (An exception is the case where the hammer applied forces are so large that the motion will not

cease before time t_m - 3L/c; this case will be discussed later).

Once the time of zero velocity at the pile tip has been determined, the ultimate shear resistance force can be found using Equation 6.17

$$S_{n,o} = \frac{1}{2}\Delta(t_{n,o} + L/c) \tag{6.24}$$

Also, the maximum damping, max D, force which acts at the pile tip at the time of maximum tip velocity can be found. Since the effect of the maximum pile tip velocity is felt at time t_m + 2L/c at the pile top one obtains again from Equation 6.17

$$\text{max } D = \Delta(t_m + 2L/c)/2 - S_{n,o} \tag{6.25}$$

To illustrate the prediction scheme as developed so far a computation example is given. The acceleration and force record used is the same as in the computation example in Section 3.7. In Figure 6.4 both Measured and modified Delta curve are shown together with the force proportional to velocity and the curve obtained by multiplying the velocity by 4c/EA and shifting it over 2L/c. The point where both curves intersect is at a time 3.81 L/c and at a Delta curve value of 292 kips. This intersection represents the solution to Equation 6.21. The maximum Delta is 422 kips, thus

$S_{n,o}$ = 146 (kip) (from Equation 6.24)

max D = 65 (kip) (from Equation 6.25)

The precompression force, S_p = 41 kips, had to be subtracted in this method as well as in the wave analysis (see Chapter III) so that the prediction of static capacity becomes:

$$R_o = 146 + 41 = 187 \text{ (kip)}$$

For the same record analyzed by wave analysis the results were:

$$R_o = 198 \text{ and max } D = 52 \text{ (kip)}.$$

Special consideration was necessary for cases with low driving resistance in the Phase IIA derivation. In such cases no zero velocity was encountered at the pile top throughout the analyzed record. A similar difficulty can arise in the Phase III method. Suppose, that $t_{n,o} \geq 3L/c + t_m$ then the fixed end condition 6.23 is not satisfied within the considered time interval ($t \leq 4L/c + t_m$). An approximate prediction scheme for such cases is to neglect presumably small dynamic force effects at the pile top at time $3L/c + t_m$ (the maximum damping effect is displayed in the Measured Delta curve at time $2L/c + t_m$). This assumption is derived from studies at piles with low shear resistance and relatively high damping as discussed in Chapter V. In order to avoid using a local extreme value for predicting the ultimate shear resistance an average Delta is taken over some time before and after $t_m + 3L/c$. Thus,

$$S_{o,n} \simeq \frac{c}{2L} \int_{t_m + 2.5L/c}^{t_m + 3.5L/c} \Delta(t)dt \qquad (6.26)$$

An example to this computation scheme is given in Figure 6.5. It can be observed that $(4EA/c)v_A(t - 2L/c)$ is always greater than $\Delta(t)$, within the time interval $t_m + 2L/c \leq t \leq t_m + 4L/c$. The predictions, taken from Figure 6.5 are:

$$\max D = 72 \text{ and } S_{n,o} = 46 \text{ (kip)}.$$

The Phase III method is used as an initial estimate on the magnitudes of shear and damping forces in the wave analysis, discussed in Chapter II of Volume I. Table 6.1 gives the results from both Phase III and the predictor analysis for the cases discussed in Chapter III of Volume I. It can be seen that the Phase III method gives good results in most cases.

CHAPTER VII

Computer Program

In the following a brief description is given of the computer program used for predicting the soil resistance forces from measurements of both pile top force and acceleration. The program is demonstrated using block diagrams and short descriptions. Only the main features of the program are discussed. Emphasis is placed on a description of both input and output.

The program consists of two parts. The first part is an ALGOL 60 routine employed for reading the dynamic data and the pile parameters. All necessary arrays are declared in this program, thus, dynamic allocation is possible.

The second part of the program consists of several FORTRAN V subroutines. A subroutine MAIN controls the actual computation process.

1. ALGOL Program PREDIC

One force record and two acceleration curves (see MAIN) are needed as dynamic input. The continuous records are digitized by placing points on the traces such that linear interpolation between these points closely resembles the original record. Both the time and the function values are then determined in units of 0.02 (inch).

Frequently, the portion of the record before impact (the acceleration is still zero while the force is already increasing as shown in Chapter IV is long. It would be unreasonable to include

this portion of the record in the dynamic analysis. Therefore, an input parameter SUB is included which is the time at which to start the dynamic computations. Also, the maximum time is limited by an input value MAXT.

The following input is necessary:

N1,N2,M	The number of values of the first acceleration, second acceleration and force trace, respectively.
S1,S2,S3,S4	Four string variables describing pile, blow, soil, and transducers, respectively.
SUB,MAXT	Time at which to start and terminate computations, respectively.
UA1,UA2	Calibration constants for first acceleration (A1) and second acceleration trace (A2), respectively.
UF,UT	Calibration constants for force values and length to time conversion, respectively.
MASS	Mass of pile
AE,LE	Cross sectional area and length of pile, respectively.
TF(J)	Force time vector in units (J = 1,2,...,M).
FO(J)	Vector of force values in units (J = 1,2,...,M).
T1(J)	Accel. -1 time vector in units (J = 1,2,...,N1).
A1(J)	Vector of accel. -1 values in u's (J = 1,2,...,N1).
T2(J)	Accel. -2 time vector in units (J = 1,2,...,N2).
A2(J)	Vector of accel. -2 values in u's (J = 1,2,...,N2). (If N2 = 0 then no values for T2(J) and A2(J) have to be given).

Procedure:

From MASS and LE together with $\phi = 2$ and N = 10 (N being the number of elements to be used in the lumped mass analysis) the time increment DET is computed (see Chapter I). From the total time interval (MAXT - SUB) one obtains NT, the number of time increments necessary. PREDIC now calls MAIN.

2. FORTRAN Subroutines

MAIN controls the computation process. The following subroutines are called:

ANALYS	For lumped mass analysis (see Chapter I).
DISTRI	For computing shear resistance distributions.
LEASTS	For performing a Least Square Analysis.
PILEPL	For plotting results.
RESIST	For finding soil resistances (Eqs. 3.30, 38).
SMOOTH	For smoothing a given function.
STATIC	For finding a theoretical load versus penetration curve (see Chapter II).

In the following these subroutines and MAIN are discussed in more detail.

(a) ANALYS (see Chapter I)

Problem: For given pile top acceleration (velocity, displacement), pile properties and resistance force parameters find the pile top force and displacements along the pile.

Input:	A(1,J)	Pile top acceleration (J = 1,2,...,NT)
	V(1,J)	Pile top velocity (J = 1,2,...,NT)
	D(1,J)	Pile top displacement (J = 1,2,...,NT)
	K	Element stiffness
	MA	Element mass
	N	Number of pile elements
	NT	Number of time increments
Procedure:		see Block Diagram

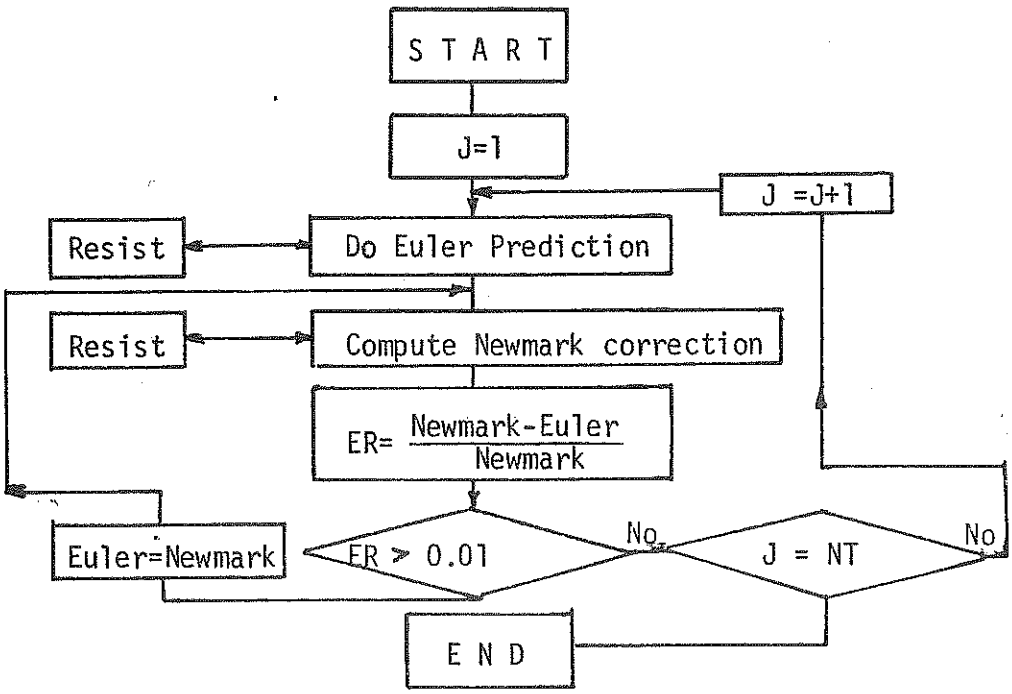

(b) DISTRI (see 3.6)

Problem: Compute corrections on predicted shear resistance forces and damping coefficients for given Error Delta curve and displacements and velocities from corresponding analysis.

Input:

DN(J)	Error Delta curve
RE(I)	Previous ultimate shear resistance forces
CO(I)	Previous damping coefficients
ITIME(I)	Time value at which full effect of ultimate shear resistance RE(I) can be felt at pile top.
V(I,J)	Velocity of i-th element at time J*DET
D(I,J)	Displacement of i-th element at time J*DET
DAMP(I)	Damping force to effect pile top at time ITIME(I).
DET	Time increment
N,NT	As introduced in PREDIC

J = 1,2,...,NT I = 1,2,...,N

Procedure:

Compute C- and E-Matrix. Compute differences ΔD between proposed and actually obtained damping forces. Reduce Error Delta curve by ΔD effects. Reduce Error Delta curve by the effects of returning reflection waves due to shear forces. Compute corrections on ultimate shear resistance forces and find new damping coefficients.

(c) LEASTS

Problem: Compute coefficients A1, A2, A3 such that

$$A1 + A2 + A3 = 1$$

and

$$\int \{\Delta(t)\}^2 dt \text{ becomes a minimum}$$

where

$$\Delta(t_j) = A1*DN1(J)+A2*DN2(J)+A3*DN3(J)$$

Input:

DN1(j)	Error Delta curve for first damping distribution
DN2(J)	Error Delta curve for second damping distribution
DN3(J)	Error Delta curve for third damping distribution
DET	As in PREDIC
NT	As in PREDIC
	J = 1,2,...,NT

Procedure:

Generate a weighting function w(t).

Set up Normal Equations.

Solve Normal Equations.

Output: A1, A2, A3.

(d) PILEPL

Problem: Plot measured and predicted pile top force as a function of time.

Input:

FTOP(J)	Measured pile top force
F(1,J)	Predicted pile top force
NT	As introduced in PREDIC
	J = 1,2,...,NT

(e) RESIST (see Equations 3.30,38)

Problem: Compute shear and damping resistance force for element INOW at time JNOW*DET.

Input:

INOW	Element number
JNOW	Time increment number
RE(INOW)	Ultimate shear resistance of element INOW
QO(INOW)	Quake of element INOW
CO(INOW)	Damping coefficient of element INOW
V(INOW,J)	Velocity at element INOW
D(INOW,J)	Displacement at element INOW J = 1,2,...,JNOW

Procedure:

Solve Equation 3.30.

Solve Equation 3.38.

Output:

RESI	Shear resistance at element INOW and time JNOW*DET
DI	Damping resistance at element INOW and time JNOW*DET.

(f) SMOOTH

Problem: Time average a given curve to obtain a smooth curve.

Input:

ROUGH(J)	Original function.
ISTART	First value of ROUGH to be included in smoothing.
ISTOP	Last value of ROUGH to be included in smoothing.
ITVAL	Time interval DET*ITVAL is to be used as interval over which to integrate for smoothing. Odd integer

CUT — Option: CUT = 1 means no change of function before ISTART. CUT = 2 means set all function values to zero before ISTART.

Procedure:

Integrate ROUGH over time interval ITVAL*DET and divide result by ITVAL*DET. This yields the new function value at the middle of the time interval. The new function is called SMOOTH.

Output: SMOOTH(J) — New smooth function between ISTART and ISTOP.

Either SMOOTH(J) = 0
or SMOOTH(J) = ROUGH(J)
} for J < ISTART

and SMOOTH(J) = ROUGH(J) for J > ISTOP

(g) STATIC (see Chapter II)

Problem: For given static soil resistance parameters and pile stiffness compute static load versus deflection curve.

Input:

RE(I) — Shear resistance force at i-th element

QO(I) — Quake at i-th element

K — Stiffness of pile element

N — As introduced in PREDIC.

I = 1,2,...,N

Procedure: see Block Diagram

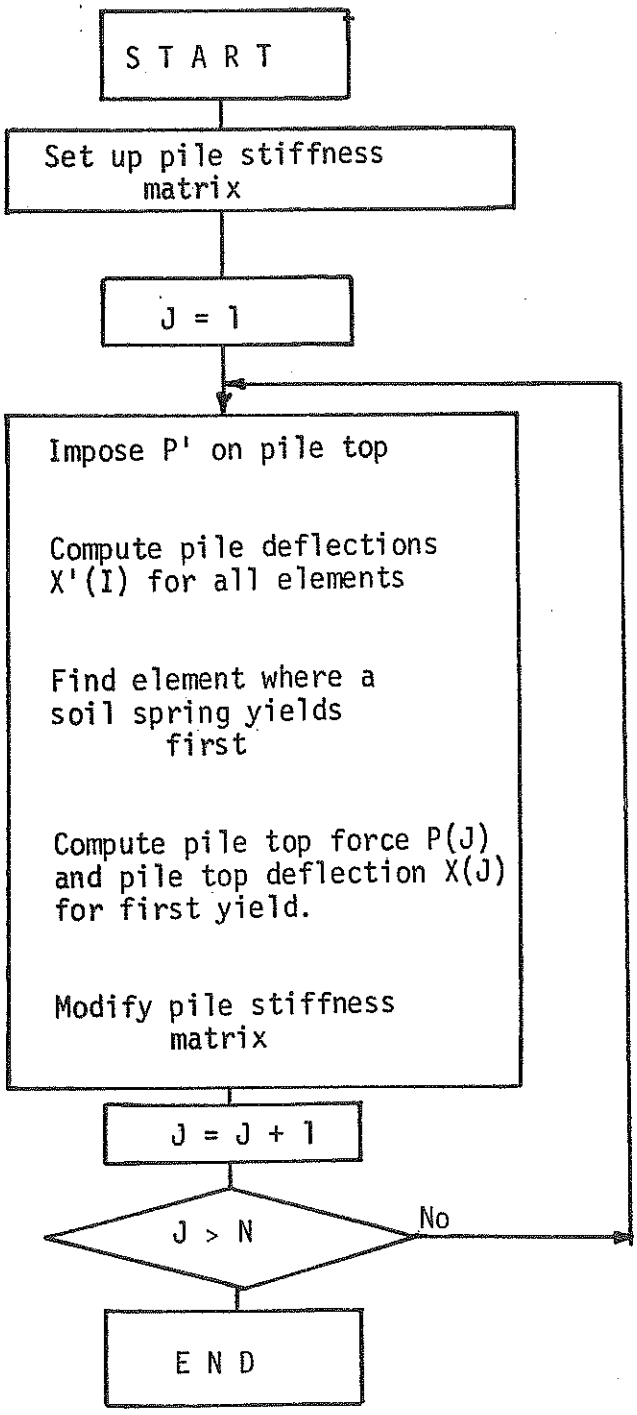

(h) MAIN (see Chapter III)

Problem: For given pile properties and both measured force and acceleration find shear and damping resistance distribution for a best match of predicted with measured top force. Also, predict static load versus deflection curve. Plot and print pile top forces both measured and predicted. Print predicted pile displacements, velocities and forces below pile top.

Input:

A1(J)	Acceleration 1	measured at opposite sides of pile
A2(J)	Acceleration 2	
FTOP(J)	Measured pile top force	
DET	Time increment	
N	Number of pile elements	
NT	Number of time increments	
LE	Length of pile	
AE	Pile cross sectional area	
MASS	Pile Mass	

Procedure: see Block Diagram

"Prepare" stands for the following manipulations:

Use E = 30.8 (psi) and compute pile element stiffnesses K. Compute element mass MA. Average both acceleration curves. Integrate acceleration twice. Subtract precompression force from force record.

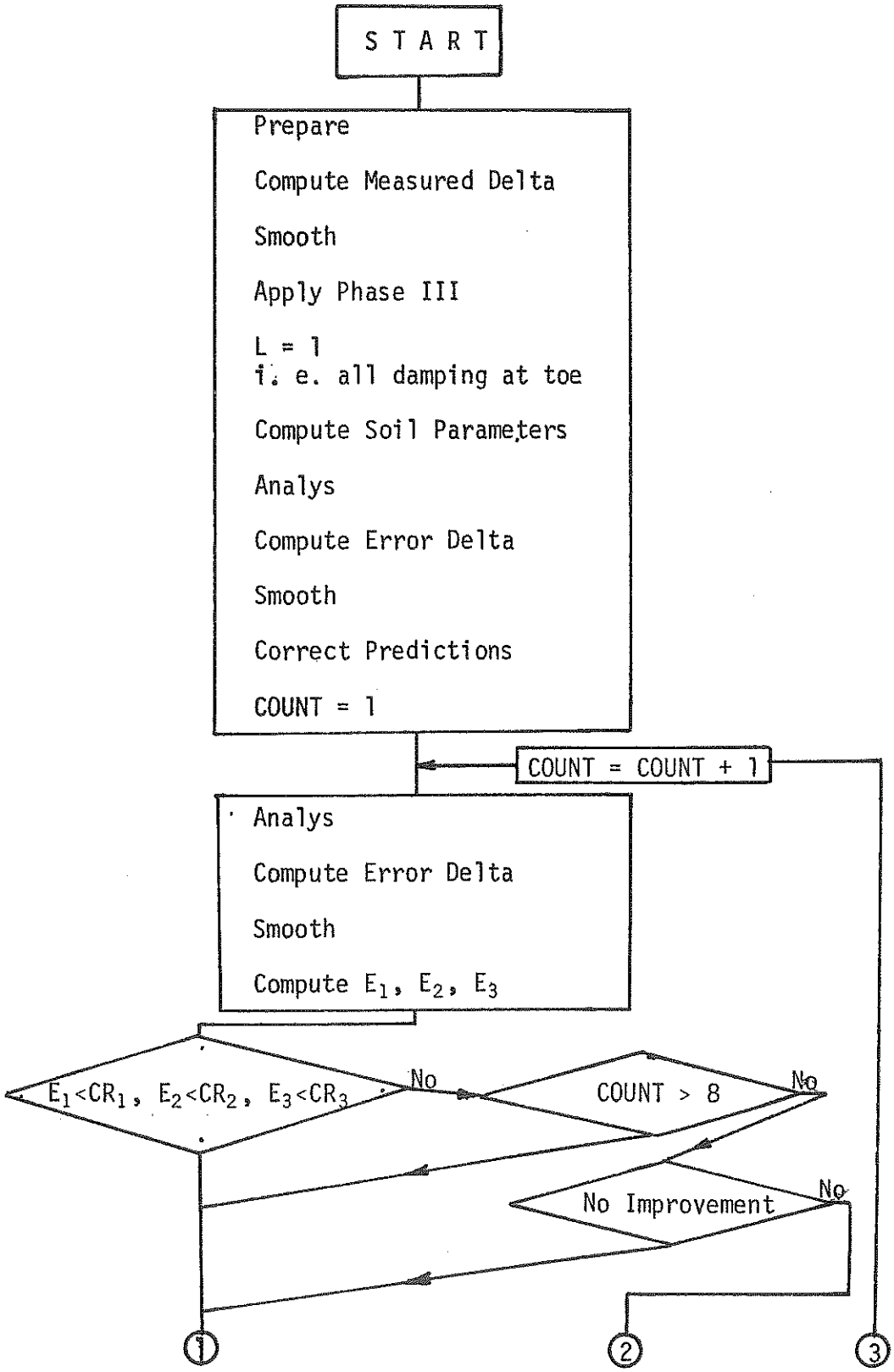
START
Prepare
Compute Measured Delta
Smooth
Apply Phase III
L = 1
i. e. all damping at toe
Compute Soil Parameters
Analys
Compute Error Delta
Smooth
Correct Predictions
COUNT = 1
COUNT = COUNT + 1
Analys
Compute Error Delta
Smooth
Compute E1, E2, E3
E1<CR1, E2<CR2, E3<CR3
No
COUNT > 8
No
No Improvement
No
1
2
3

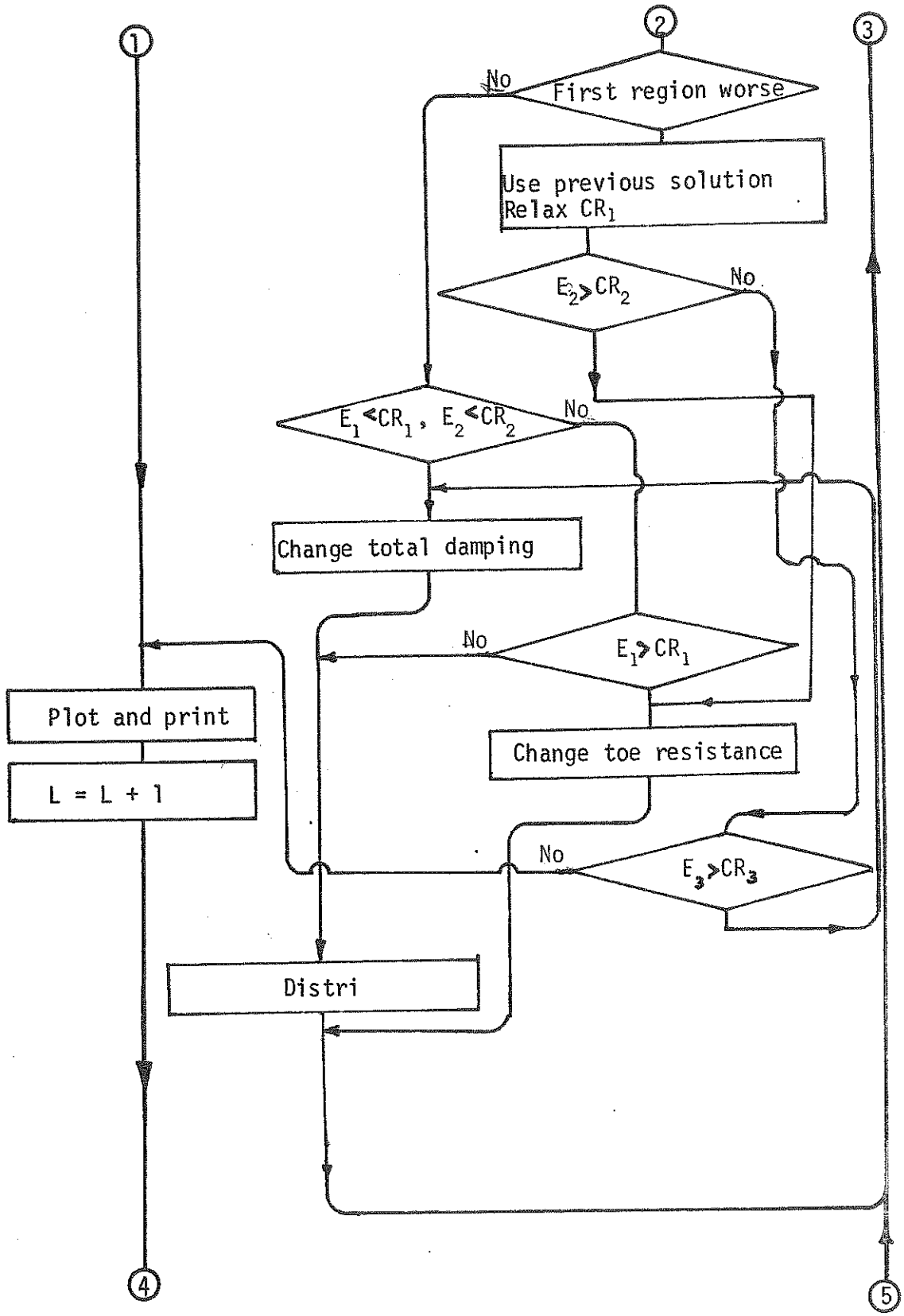
1
2
3
No
First region worse
Use previous solution
Relax CR1
E2>CR2
No
E1<CR1, E2<CR2
No
Change total damping
No
E1>CR1
Plot and print
L = L + 1
Change toe resistance
No
E3>CR3
Distri
4
5

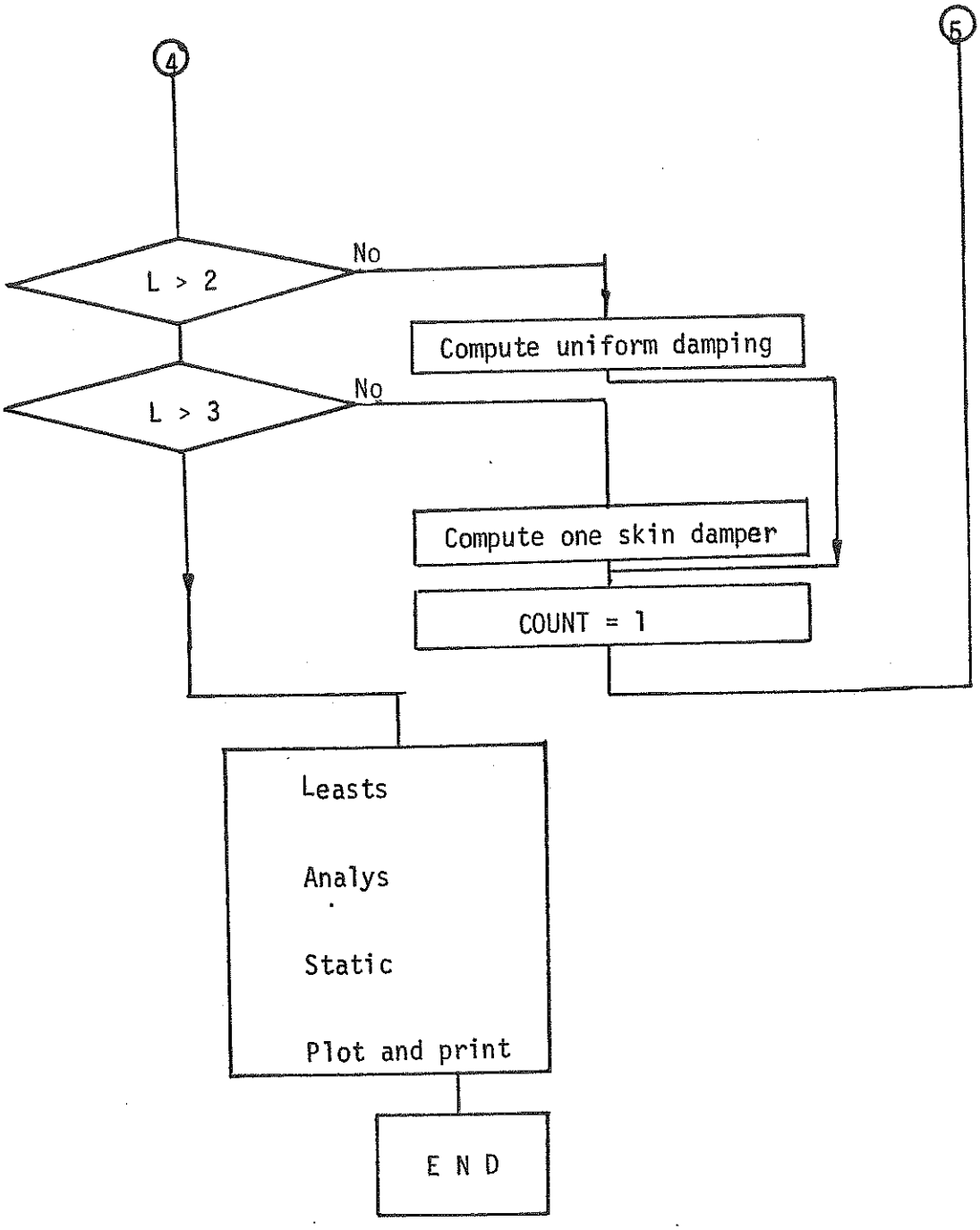
4
5
L > 2
No
Compute uniform damping
L > 3
No
Compute one skin damper
COUNT = 1
Leasts
Analys
Static
Plot and print
E N D

References

1. Smith, E. A. L., "Pile Driving Analysis by the Wave Equation", Journal of Soil Mechanics and Foundations, American Society of Civil Engineers, 86, August, 1960, p. 35-61.

2. Newmark, N. M., "A Method of Computation for Structural Dynamics", Proceedings, ASCE, 85, EM3, 1959, p.67.

3. Crandall, S. H., "Engineering Analysis", McGraw-Hill, 1956, p. 396.

4. Olson, R. E. and Flaate, R. S., "Pile Driving Formulas for Friction Piles in Sand, "Journal of the Soil Mechanics and Foundation Division, ASCE, Vol. 93, No. SM6, November 1967, p. 279-296.

5. LaPay, W. S., "Dynamic Pile Behavior - Literature Survey and Response Studies", Master's Thesis, Case Institute of Technology, 1965.

6. Goble, G. G. and Rausche, F., "Pile Load Test by Impact Driving", paper presented to the Highway Research Board Annual Meeting, January 1970, Washington, D. C.

7. Samson, C. H., Hirsch, T. L. and Lowery, L. L., "Computer Study of the Dynamic Behavior of Piling", Journal of the Structural Division, Proceedings, ASCE, Paper No. 3608, ST4, August 1963.

8. Tomko, J. J., "Dynamic Studies on Predicting the Static Bearing Capacity of Piles", Ph. D. Dissertation, Case Western Reserve University, 1968.

No. of Computation	No. of Elements (L in Ft.)	$= \frac{\Delta L}{\Delta tc}$ (Δt in Ms)	Convergence Crit. ε	Time Consumption in Seconds	Plotted in Figure
1	5(15.6)	1(.908)	.01	1/2	-
2	5(15.6)	2(.454)	.01	1	-
3	5(15.6)	4(.227)	.01	2	1.2
4	10(7.8)	2(2.77)	.01	2	1.2
5	10(7.8)	2(.227)	No Iteration	1	-
6	20(3.9)	$\frac{1}{2}$(.454)	.01	2 (unstable)	1.3
7	20(3.9)	1(.227)	.01	3	1.2, 1.3
8	20(3.9)	2(.113)	No Interation	$2\frac{1}{2}$	1.5
9	20(3.9)	2(.113)	.01	$5\frac{1}{2}$	1.3, 1.5
10	20(3.9)	2(.113)	.1	5	1.5
11	30(2.6)	2(.076)	.1	$9\frac{1}{2}$	-

TABLE 1.1: COMPARISON OF VARIOUS LUMPED MASS ANALYSES USING THE SAME INPUT BUT DIFFERENT PARAMETERS

C-Matrix: Influence of i-th Shear Resistance on $\Delta(t_j)$

j \	1	2	3	4	5	6	7	8	9	10
1	0	0	0	0	0	0	0	0	0	0
2	0	1.00	.67	.15	.01	0	0	0	0	0
3	0	1.00	1.00	.69	.16	.02	0	0	0	0
4	0	1.00	1.00	1.00	.71	.17	.02	0	0	0
5	0	1.00	1.00	1.00	1.00	.74	.18	.03	0	0
6	0	1.00	1.00	1.00	1.00	1.00	.77	.19	.03	.01
7	0	1.01	1.01	1.01	1.02	1.02	1.02	.80	.20	.05
8	0	1.13	1.14	1.09	1.16	1.17	1.18	1.19	.85	.39
9	0	1.66	1.67	1.51	1.71	1.74	1.76	1.77	1.55	1.54
10	0	2.00	2.00	2.00	2.00	2.00	2.00	2.00	2.00	2.00

E - Matrix: Influence of i-th Damping Force on $\Delta(t_j)$

1	0	0	0	0	0	0	0	0	0	0
2	0	.87	.96	.39	.05	.01	0	0	0	0
3	0	.61	.87	.96	.38	.05	.01	0	0	0
4	0	.65	.61	.87	.95	.37	.05	.01	0	0
5	0	.64	.66	.62	.88	.95	.38	.07	.01	0
6	0	.44	.65	.66	.61	.88	.95	.40	.08	.02
7	0	.36	.44	.63	.65	.61	.90	1.01	.46	.14
8	0	.71	.62	.55	.88	.86	.84	1.19	1.24	.81
9	0	1.18	.121	1.02	1.19	1.39	1.38	1.38	1.74	1.91
10	0	1.04	1.14	1.24	1.08	1.16	1.34	1.29	1.47	1.75

TABLE 3.1: C-and E-MATRIX

Column No. 1 Soil Parameter Element No.		2 First Damping Distribution Initial	3 First Damping Distribution Final	4 Second Damping Distribution Initial	5 Second Damping Distribution Final	6 Third Damping Distribution Initial & Final	7 From Column 3,5,6 Final Distribution
$S_{o,i}$	1	0	0	0	0	0	0
	2	0	0	0	0	0	0
	3	12.0	6.4	6.4	4.0	4.4	0
	4	4.8	0	0	0	0	0
	5	18.2	0	0	0	0	0
	6	15.7	34.1	34.0	24.7	32.9	34.0
	7	19.1	1.1	0	17.4	5.4	0
	8	17.5	0	0	14.6	0	1.6
	9	38.7	56.4	49.2	55.7	54.9	57.2
	10	38.3	56.4	57.3	50.9	54.9	57.3
d_i	1	0	0	0	0	0	0
	2	0	0	0	0	0	0
	3	0	0	.36	.36	.71	0
	4	0	0	.53	0	0	0
	5	0	0	.36	.36	0	.03
	6	0	0	.99	1.00	0	.08
	7	0	0	.55	.55	0	.05
	8	0	0	0	0	0	0
	9	0	0	1.18	1.13	0	.10
	10	10.0	7.71	1.14	.99	8.00	7.00

TABLE 3.2: SOIL PARAMETERS PREDICTED (F-60, BLOW NO. 26-A)

CUSHION STIFFNESSES k in kips/inch

Applied Force kips	Transducer 3-4	5-6	Oak 15/15/5 (Delmag D-12)	Phenol 11"ϕ/2.5" Link Belt 440
100	4,600	3,500	1600	8,600
150	7,250	5,500	2400	9,300
200	10,000	8,000	3300	11,600

WEIGHTS of RAM and ANVIL in kips

	Ram and Anvil	Capblock and Adaptor
Delmag D-12	3.50	1.20
Link Belt 440	4.71	1.10

TABLE 4.1 : CUSHION STIFFNESSES AND HAMMER WEIGHTS

PILE	BLOW NO.	LENGTH FT.	P_{ult} KIPS	AVG. KIPS	HAMMER	$f_1 = \frac{c}{4L}$ 1/s	$f_2 = 49.4\sqrt{\frac{P}{L}}$ 1/s	f_3 1/s Equ. 3	f_4 1/s Equ. 3	MEAS. 1/s	ERROR %
F-30	13	33	104	100	Link Belt 440	129	88	75	360	400	10
	14		104	100			88	75	360	400	10
	15		104	110			88	78	367	409	10.3
	16		104	110			88	78	367	402	8.7
	1-A		114	120			92	81	375	409	8.3
	5-A		114	110			92	78	367	409	10.3
	6-A		114	110			92	78	367	409	10.3
	7-A		114	110			92	78	367	409	10.3
F-50	18	51.5	224	140	Link Belt 440	83	103	86	390	418	6.7
	19		224	140			103	86	390	422	7.6
	20		224	140			103	86	390	422	7.6
	10-A		238	190			106	99	443	425	-4.1
	13-A		238	20			106	102	454	418	-8.0
	14-A		238	190			106	99	443	427	-3.7
	15-A		238	140			106	86	390	427	8.7
F-60	17	60.5	204	180	Link Belt 440	70	91	97	431	435	.9
	18		204	140			91	86	390	427	9.5
	19		204	150			91	89	390	418	4.8
	22-A		242	140			99	86	390	414	5.8
	26-A		242	150			99	89	398	409	2.7
	27-A		242	130			99	83	382	418	6.2

TABLE 4.2 : MEASURED AND CALCULATED FREQUENCIES ON TOP OF PILE

TABLE (4.2) continued

PILE	BLOW NO.	LENGTH FT.	P_{ult}	AVG. KIPS	HAMMER	$f_1 = \frac{c}{4L}$ 1/s	$f_2 = 49.4\sqrt{\frac{P}{L}}$ 1/s	f_3 1/s Equ. 3	f_4 1/s Equ. 3	MEAS. 1/s	ERROR %
TO-50	III-2	50	69	140	Delmag D-12	85	58	68	272	313	13.1
	III-3		69	110			58	50	239	292	18.1
	IV-2		69	110			58	60	239	298	19.2
	3-A		95	180			68	77	314	303	-3.6
	I-4A		95	200			68	82	333	313	-6.4
TO-60	IV-9	60	43	120	D-12	71	42	62	250	274	8.8
	II-5-A		86	100			59	57	228	285	20.0
	III-1-A**		86	90			59	51	198	244	18.9
TO-50-c*	I-9-A**	50	130	230	D-12	60	23	88	338	324	8.0

* Concrete filled pile here c = 12,000 ft/s was used.

** Transducer cushion with 5 plywood and 6 rubber sheets.

DATA SET NO.	MAXIMUM DAMPING FROM PHASE III kips	MAXIMUM DAMPING FROM ANALYSIS kips
3	14	15
5	44	50
6	25	23
7	40	41
8	60	52
9	42	25
10	65	57
11	13	17
13	44	57
14	57	88
15	68	70
16	98	106
17	55	54
18	102	125
19	65	58
20	59	61
21	80	87
22	67	106
23	96	93
24	44	48

TABLE 6.1: COMPARISON OF MAXIMUM DAMPING FORCE AS PREDICTED FROM PHASE III AND FROM WAVE ANALYSIS

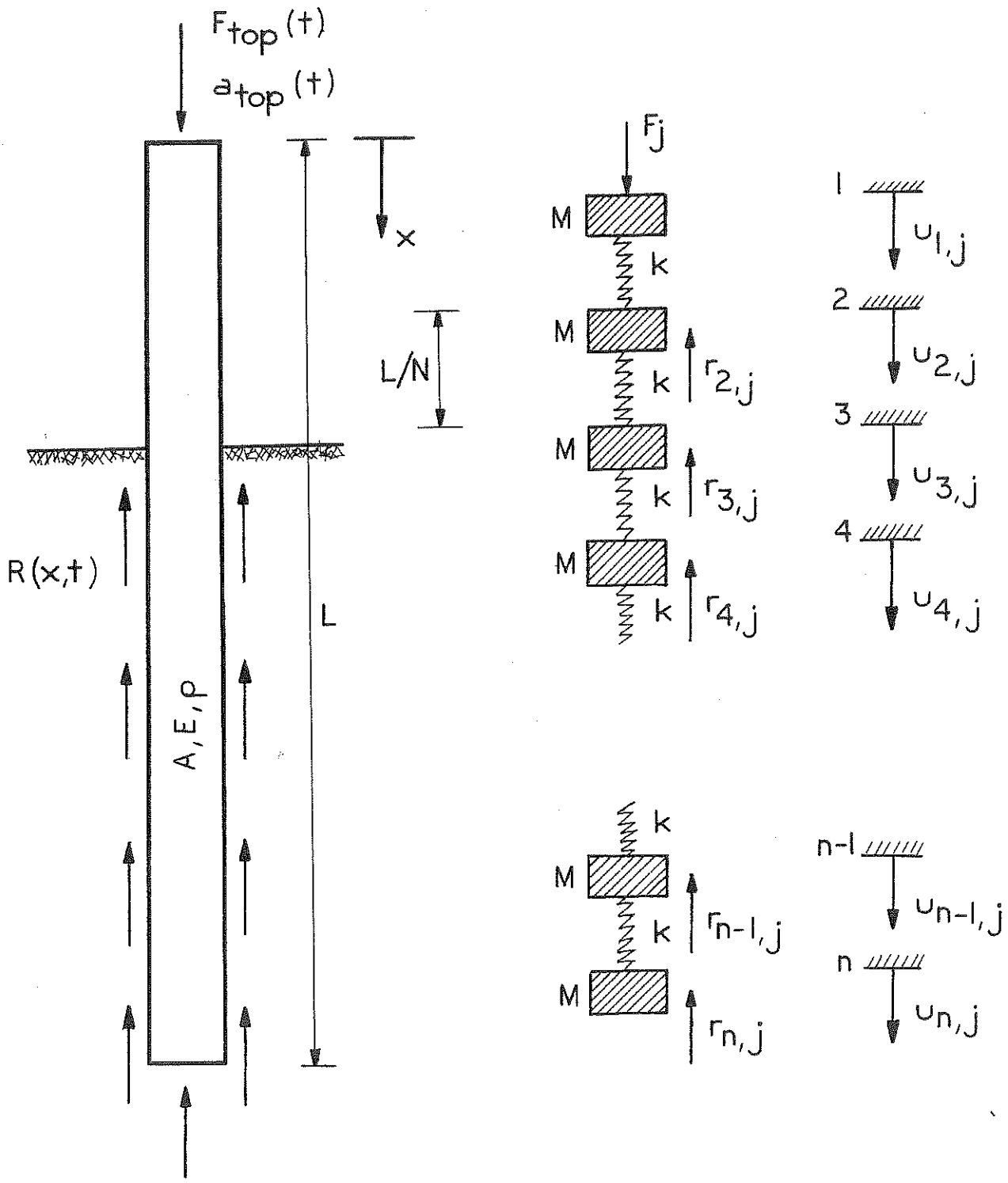

FIGURE 1.1: CONTINUOUS PILE AND SPRING-MASS MODEL

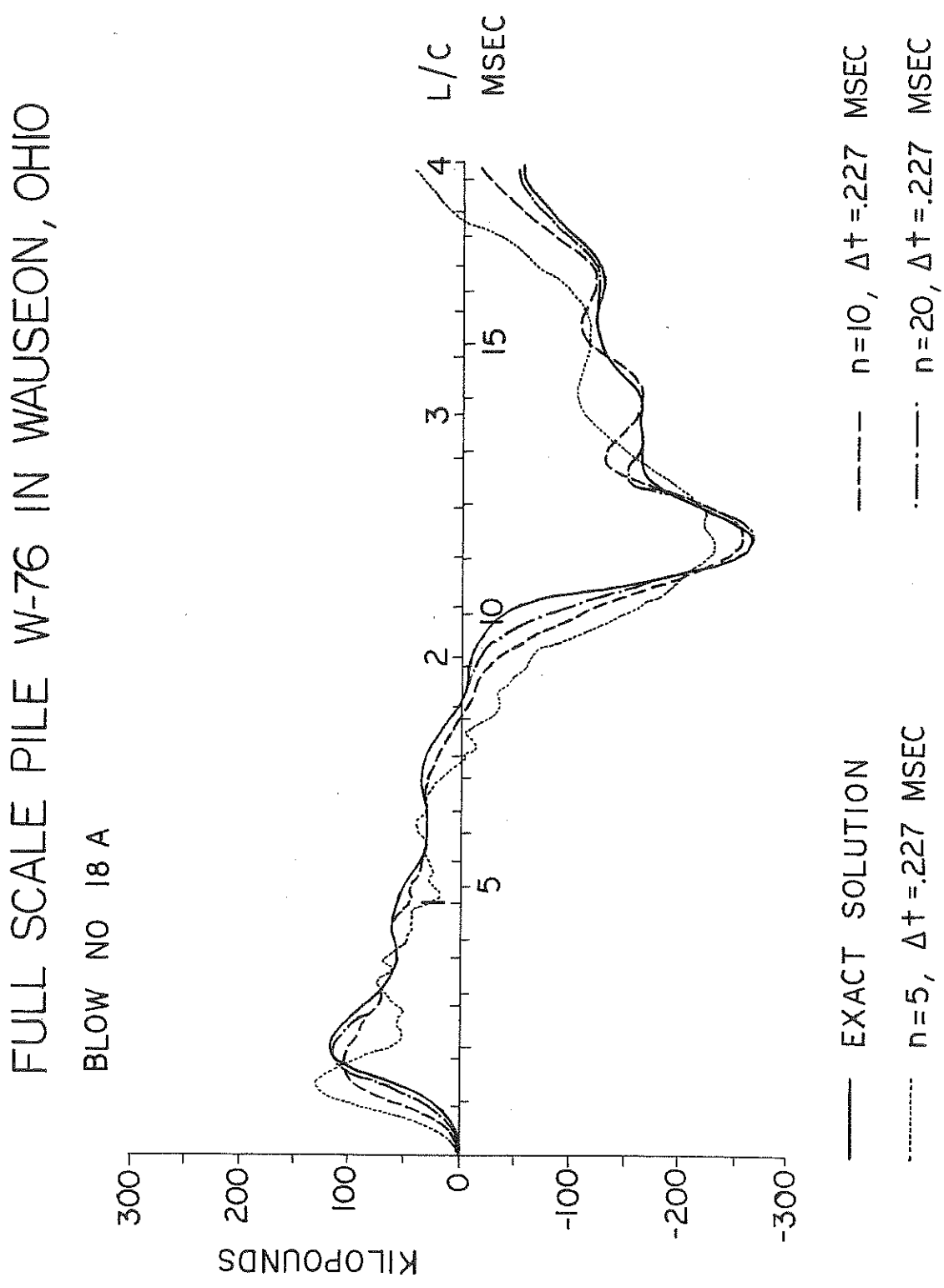

FIGURE 1.2: COMPARISON OF ANALYSIS RESULTS USING DIFFERENT NUMBERS OF ELEMENTS

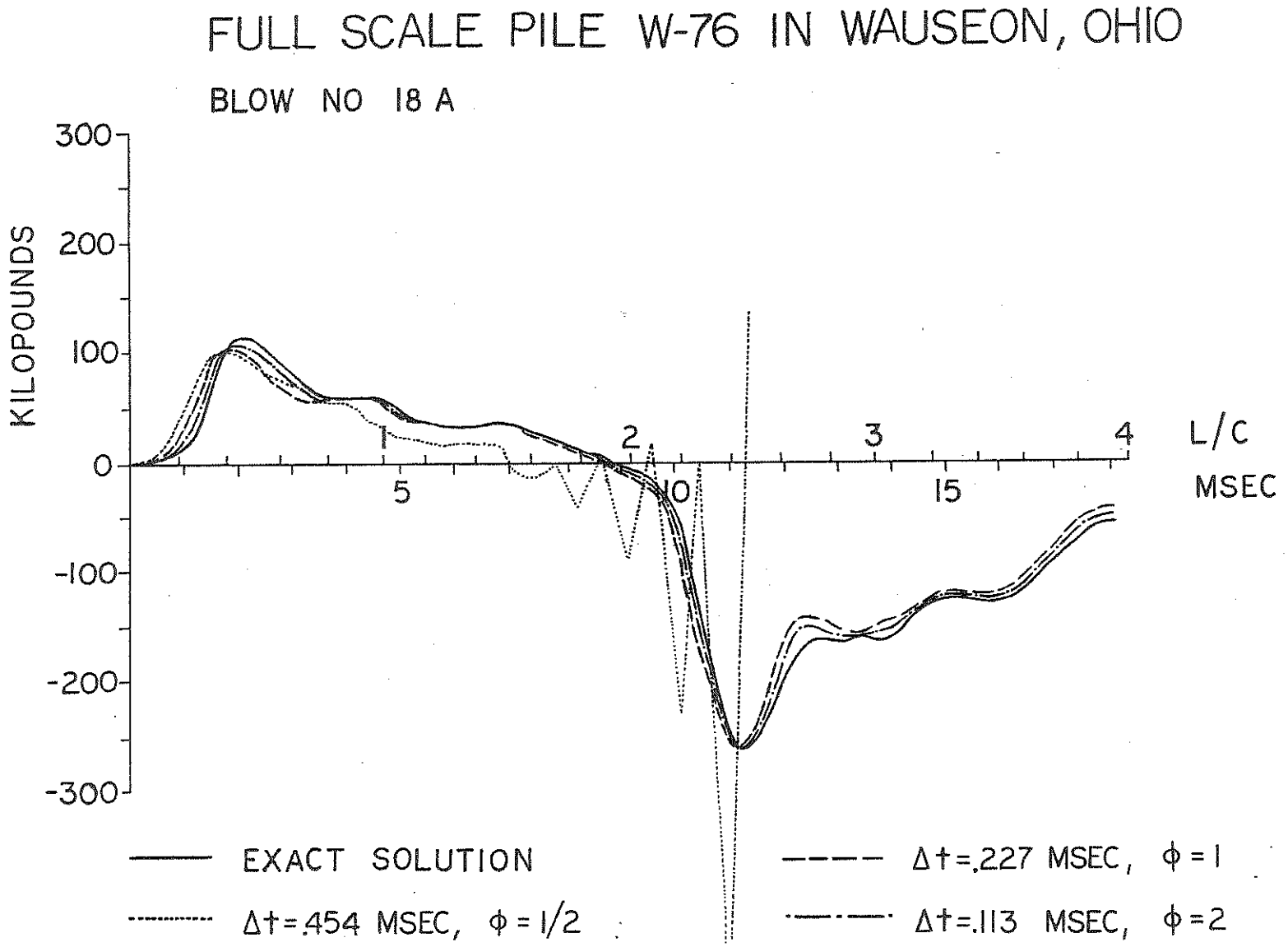

FIGURE 1.3: COMPARISON OF ANALYSIS RESULTS USING DIFFERENT TIME INCREMENTS, n = 20 and ε = .01

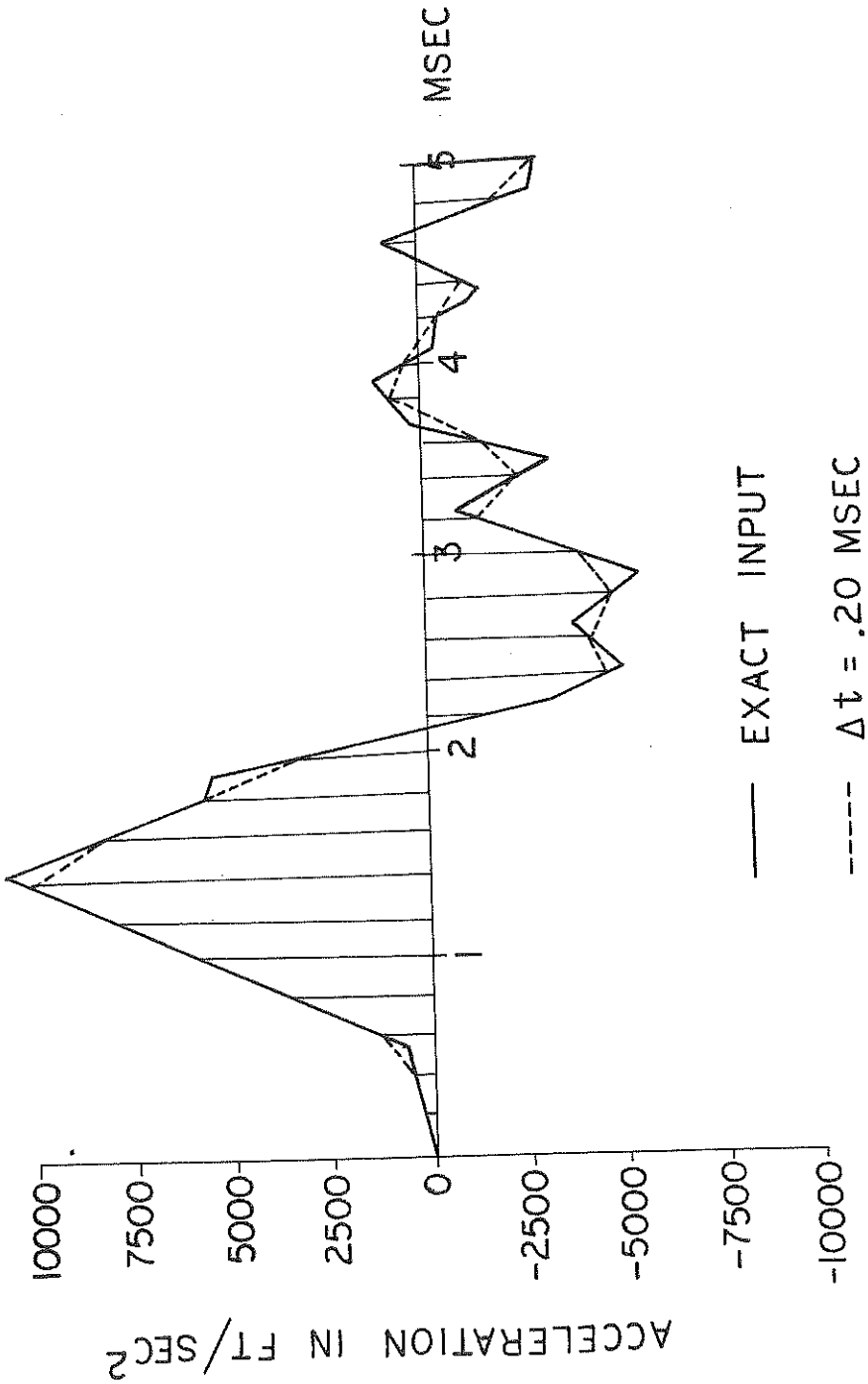

FIGURE 1.4: POSSIBLE DEVIATIONS FROM EXACT INPUT USING FINITE STEP SIZES

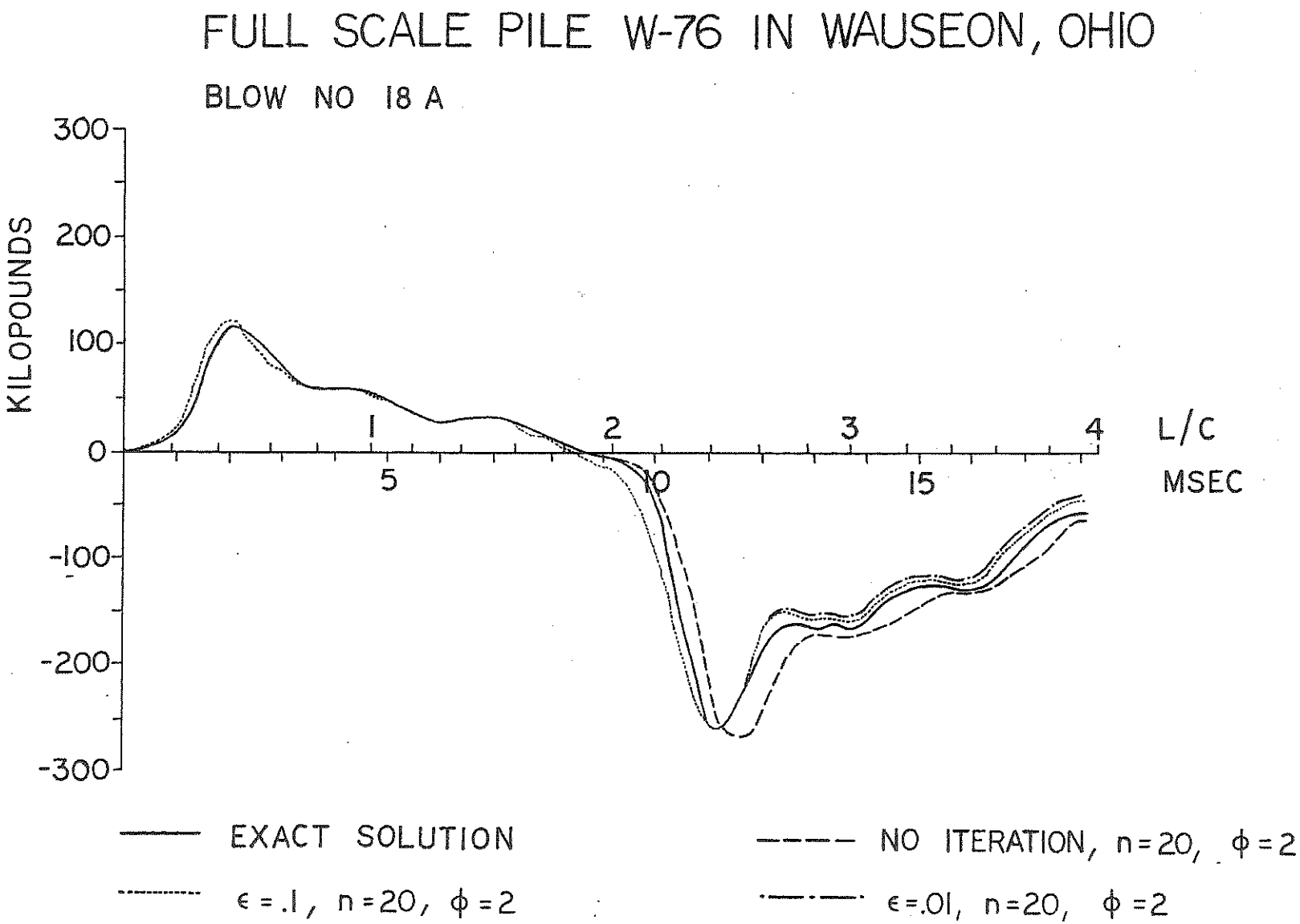

FIGURE 1.5: COMPARISON OF ANALYSIS RESULTS USING DIFFERENT CONVERGENCE CRITERIA

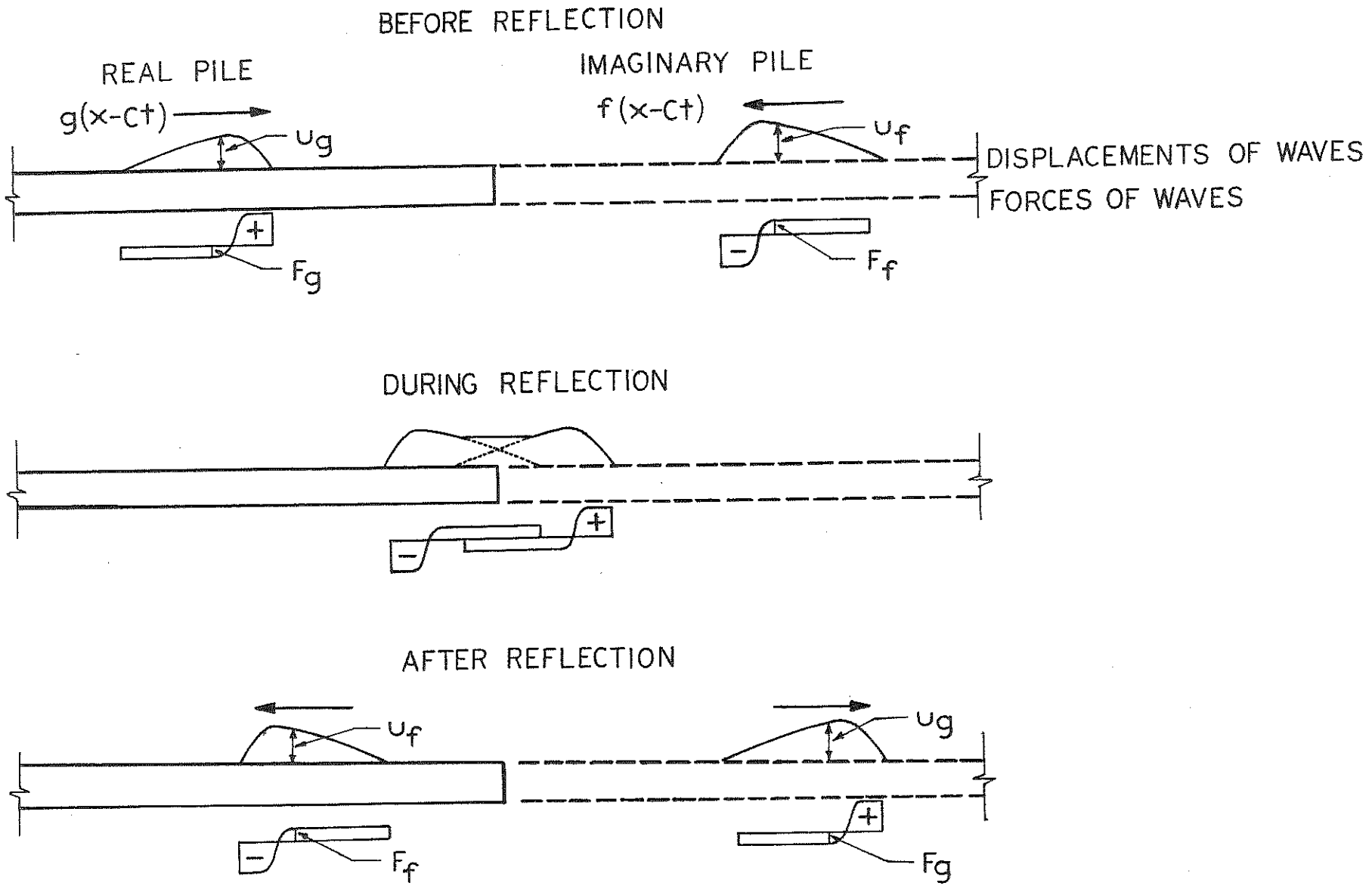

FIGURE 3.1: TREATMENT OF FREE END BOUNDARY CONDITION

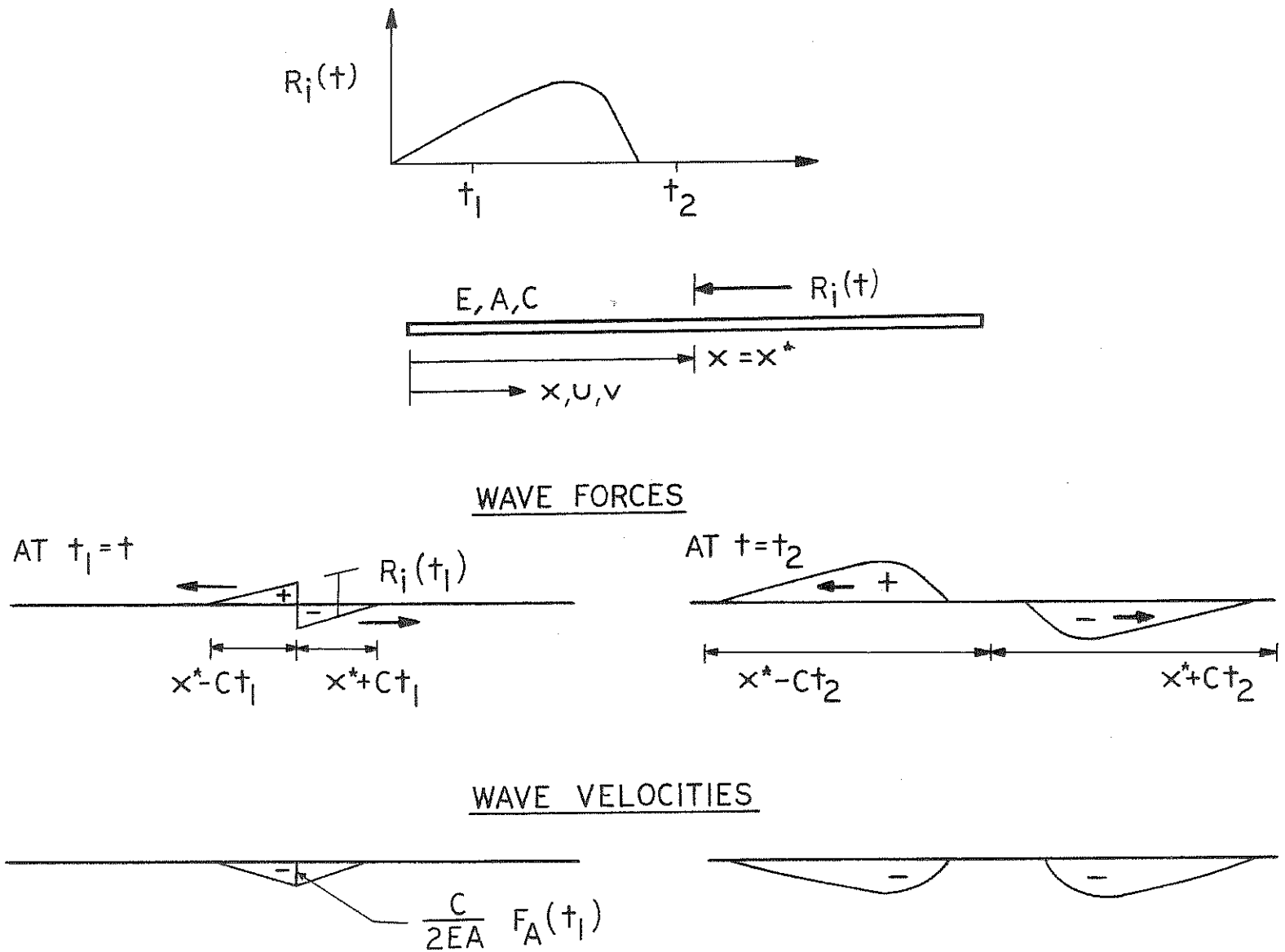

FIGURE 3.2: IMPACT FORCE APPLIED AT AN INTERMEDIATE POINT ALONG THE PILE

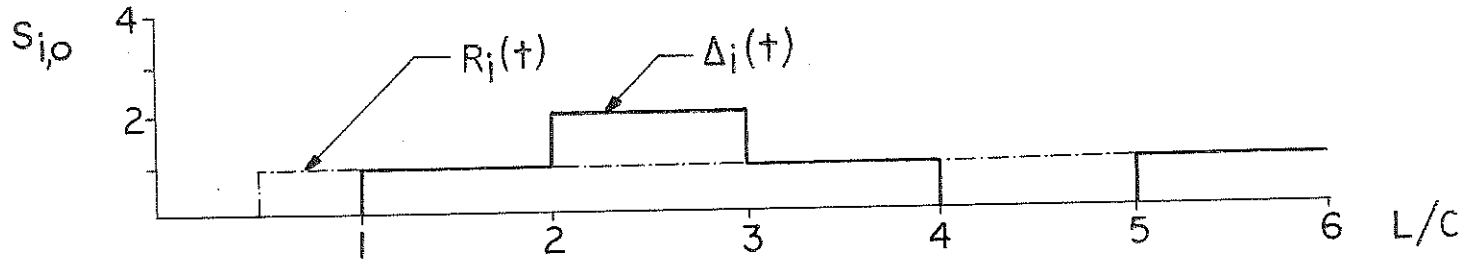

A. SHEAR RESISTANCE FORCE AT $x = L/2$

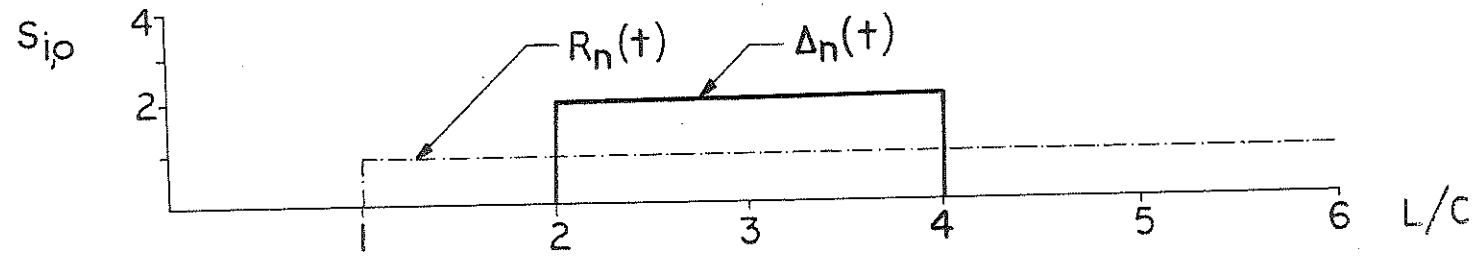

B. SHEAR RESISTANCE FORCE AT PILE BOTTOM

FIGURE 3.3: RESISTANCE DELTA CURVES FOR THEORETICAL SHEAR FORCES AT MIDDLE AND BOTTOM OF PILE

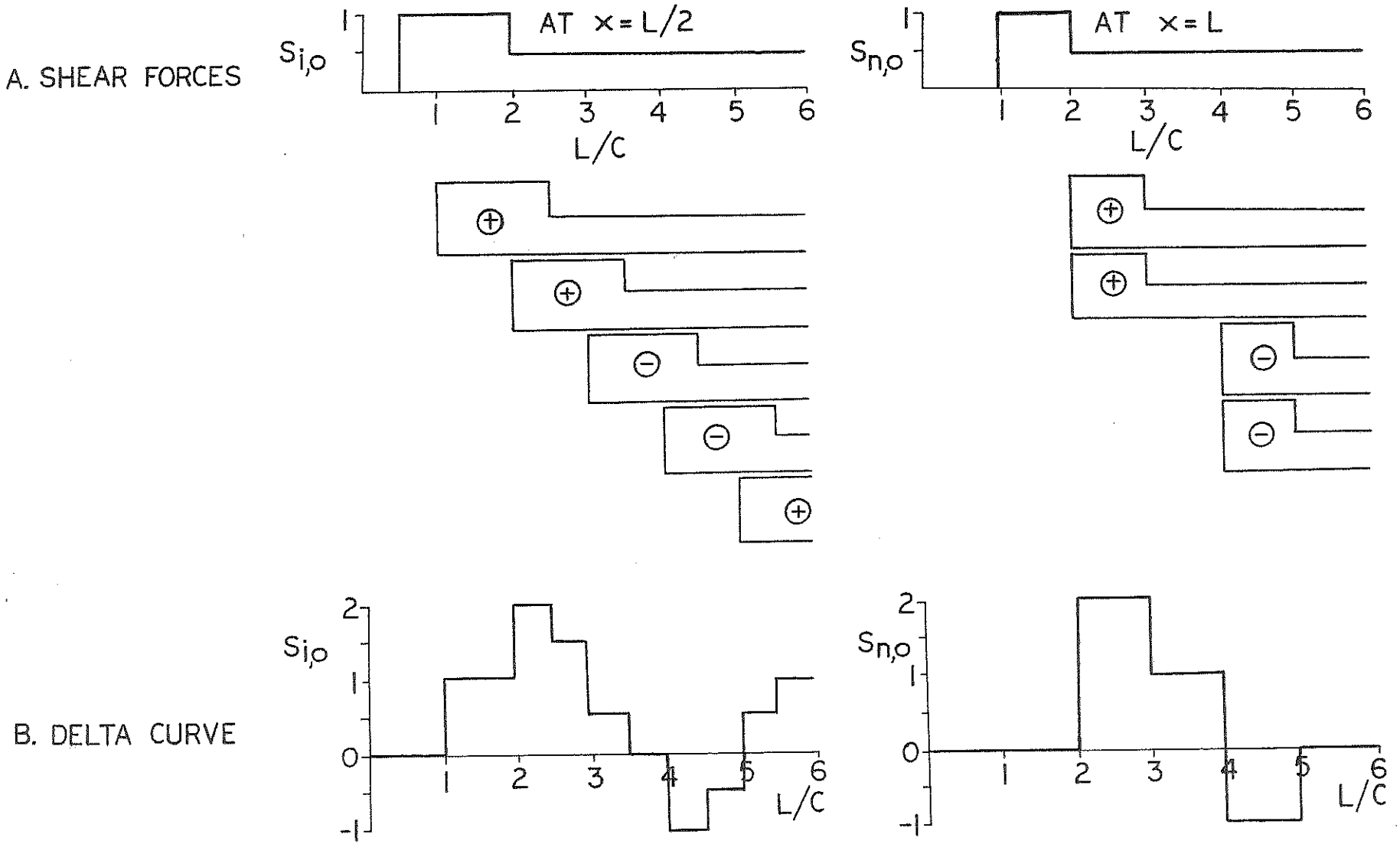

FIGURE 3.4: RESISTANCE DELTA CURVES FOR THEORETICAL SHEAR FORCES WITH UNLOADING

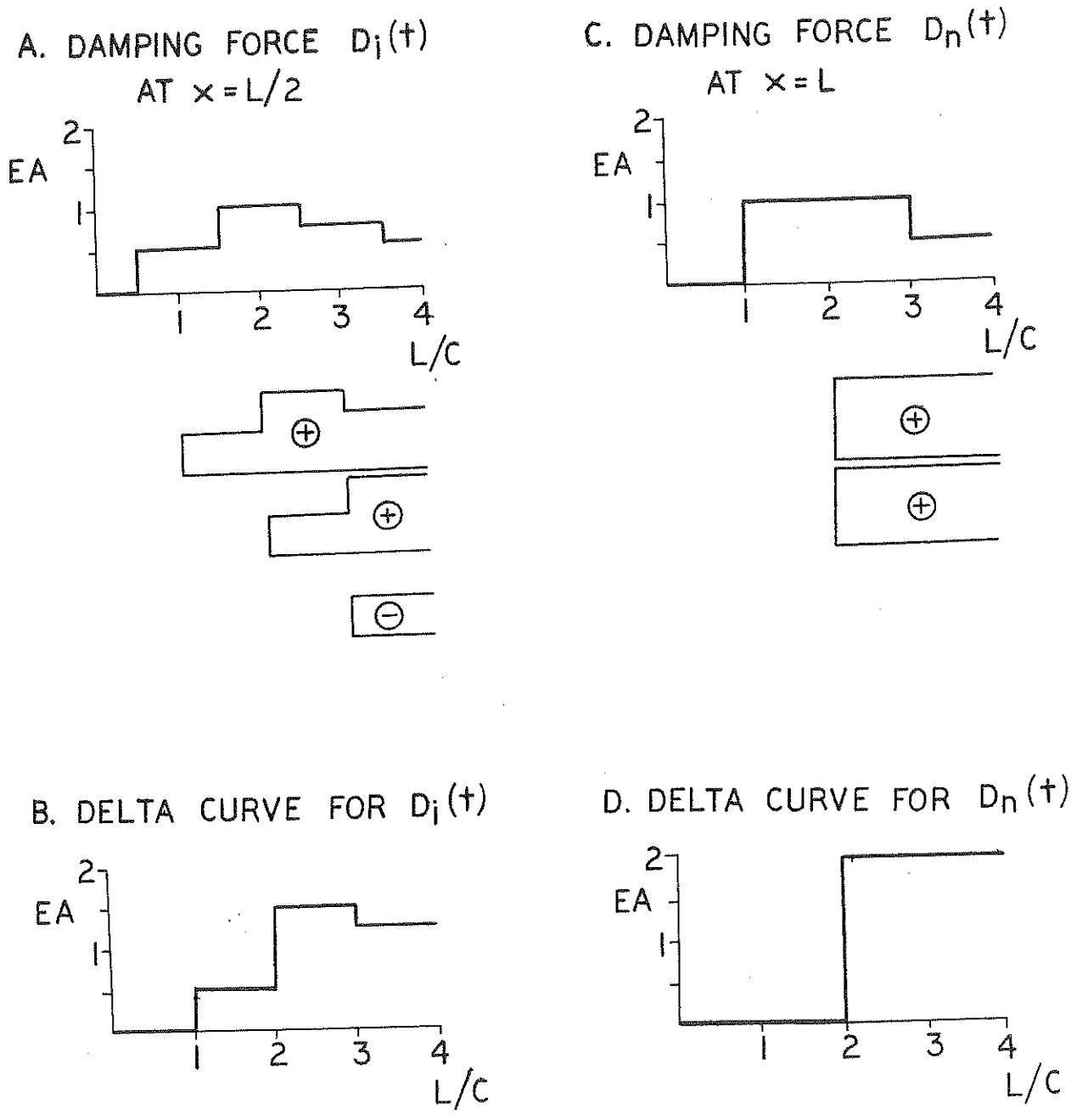

URE 3.5: RESISTANCE DELTA CURVES FOR DAMPING WITH CONSTANT VELOCITY AT PILE TOP

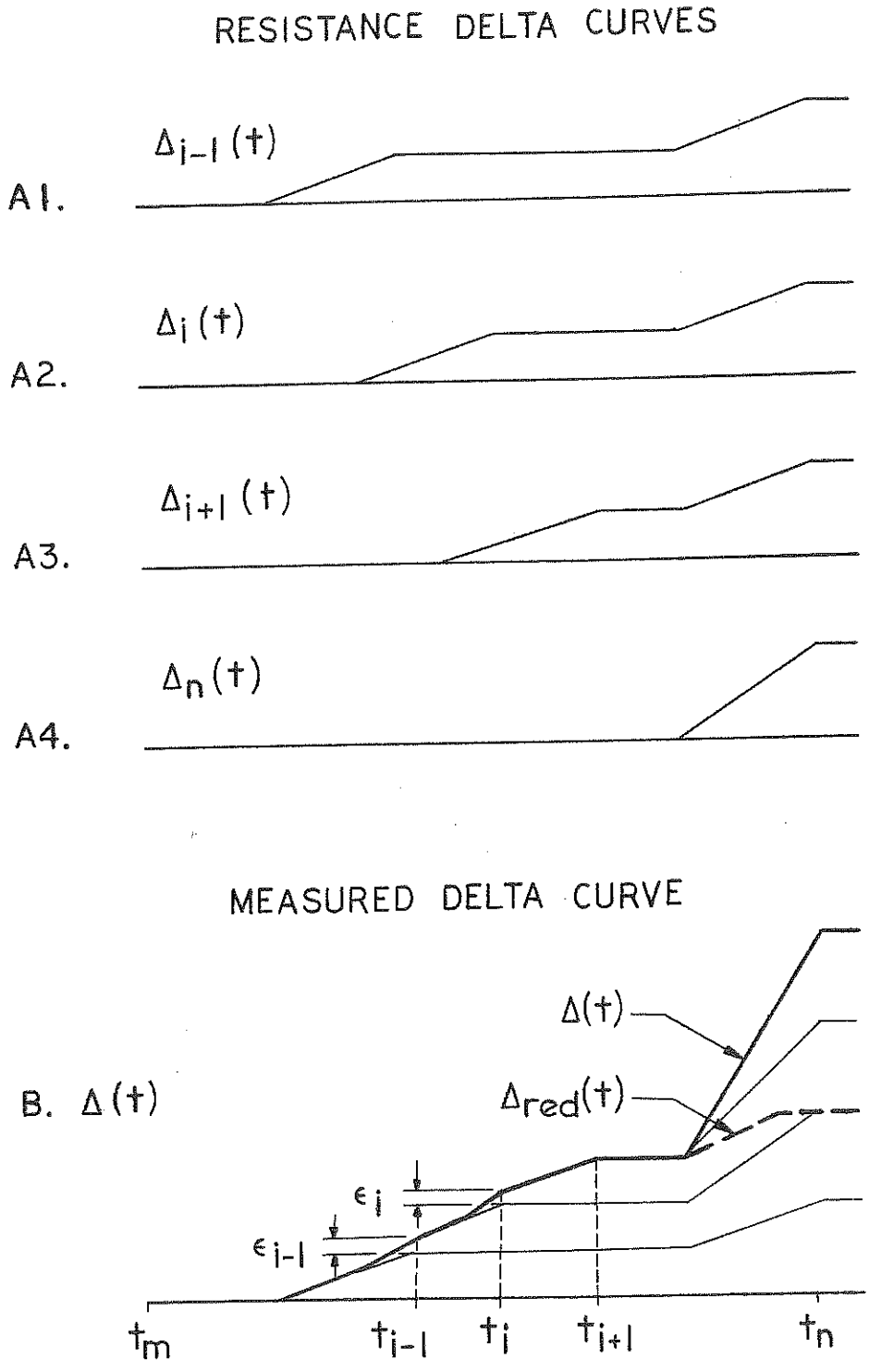

FIGURE 3.6: PREDICTION OF SHEAR RESISTANCE FORCES FROM MEASURED DELTA CURVE IN ABSENCE OF DAMPING FORCES

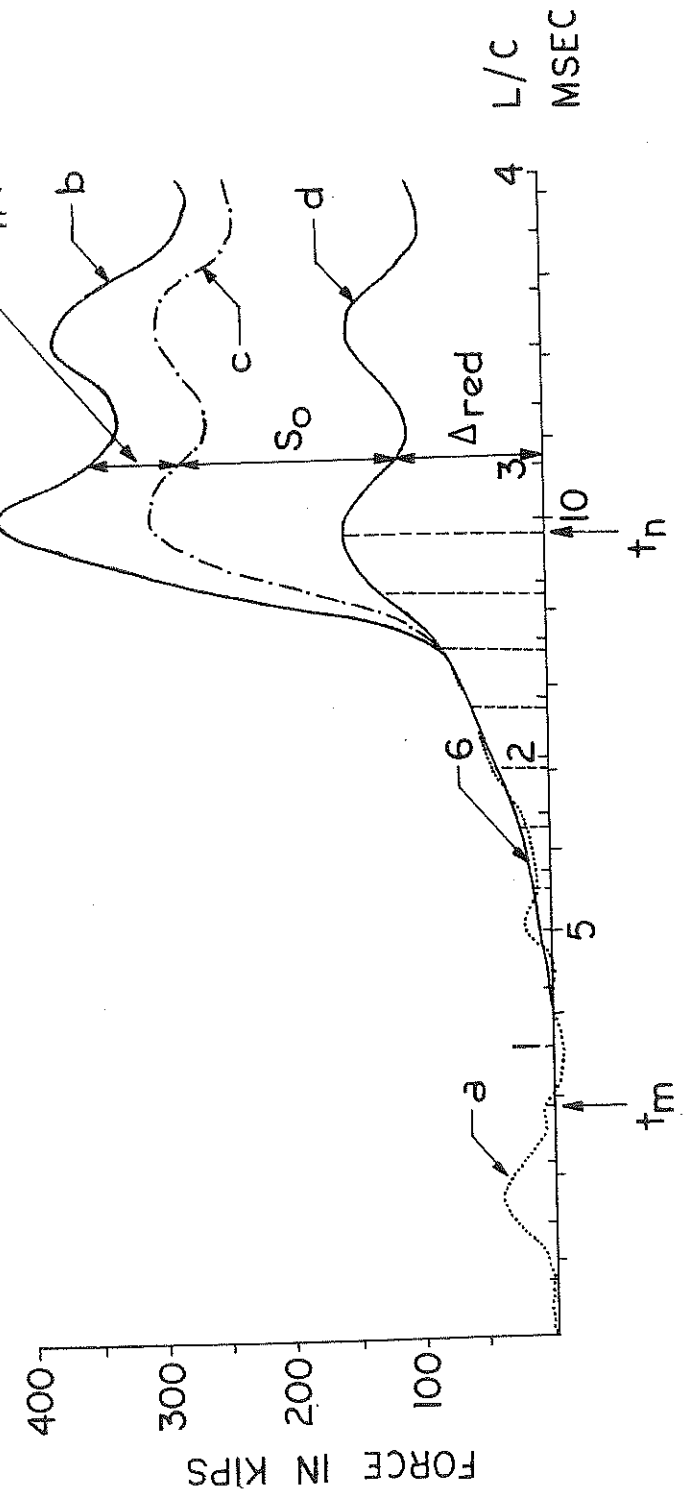

FIGURE 3.7: GRAPHICAL REPRESENTATION OF INITIAL PREDICTION SCHEME

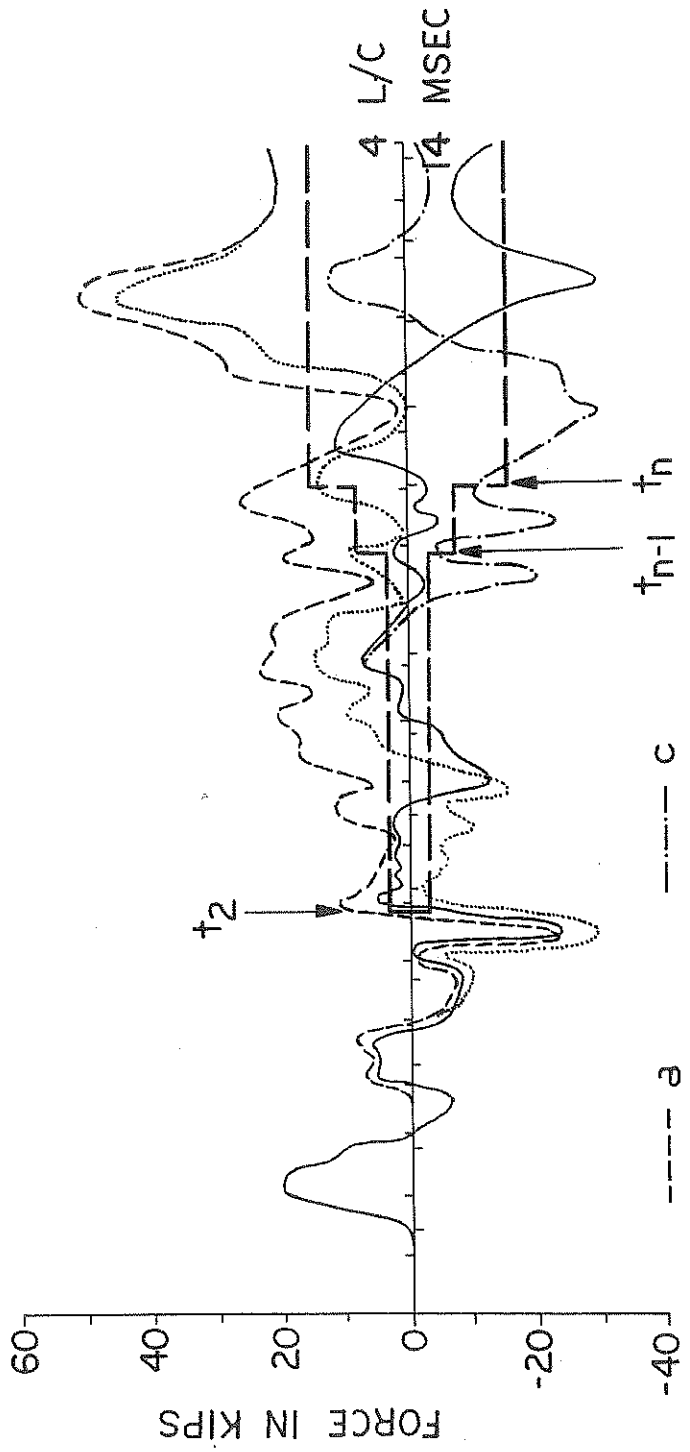

FIGURE 3.8: ERROR DELTA CURVES FROM PREDICTION PROCESS FOR DAMPER AT PILE TIP

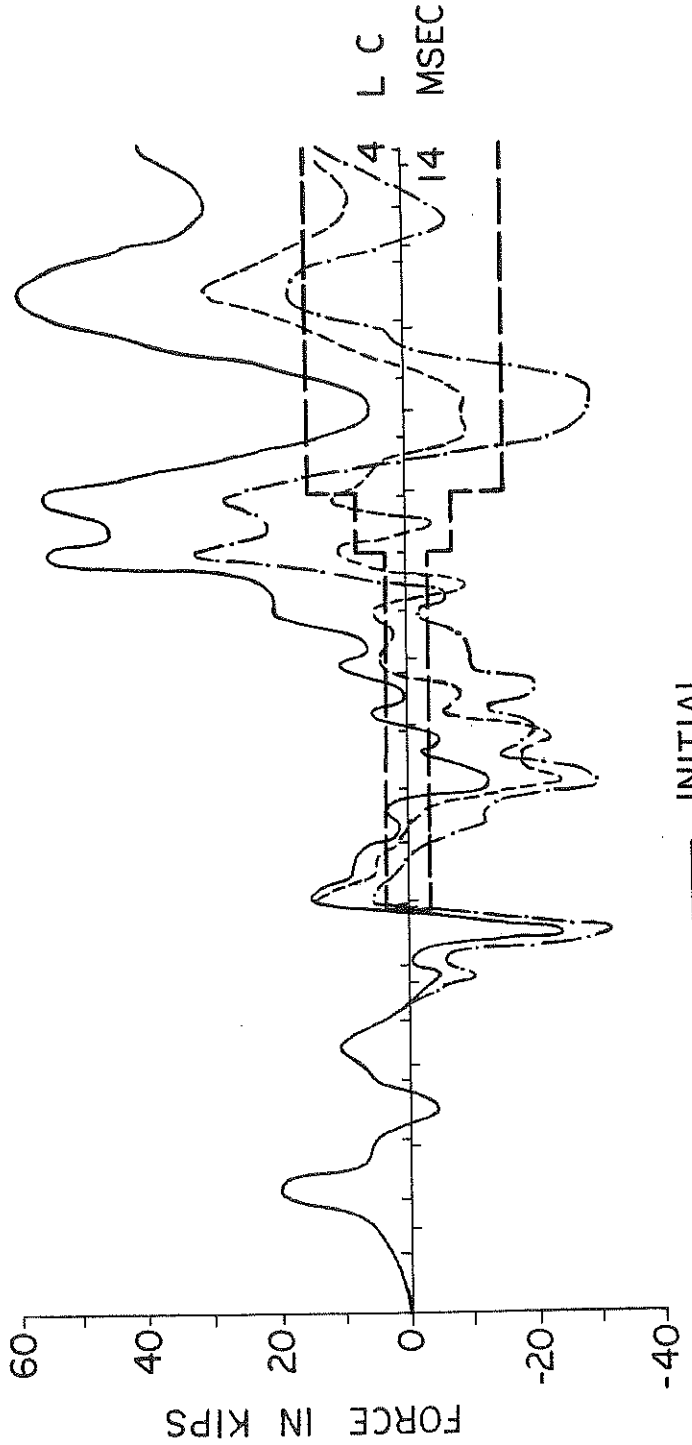

FIGURE 3.9: ERROR DELTA CURVES FROM PREDICTION PROCESS FOR DISTRIBUTED DAMPING

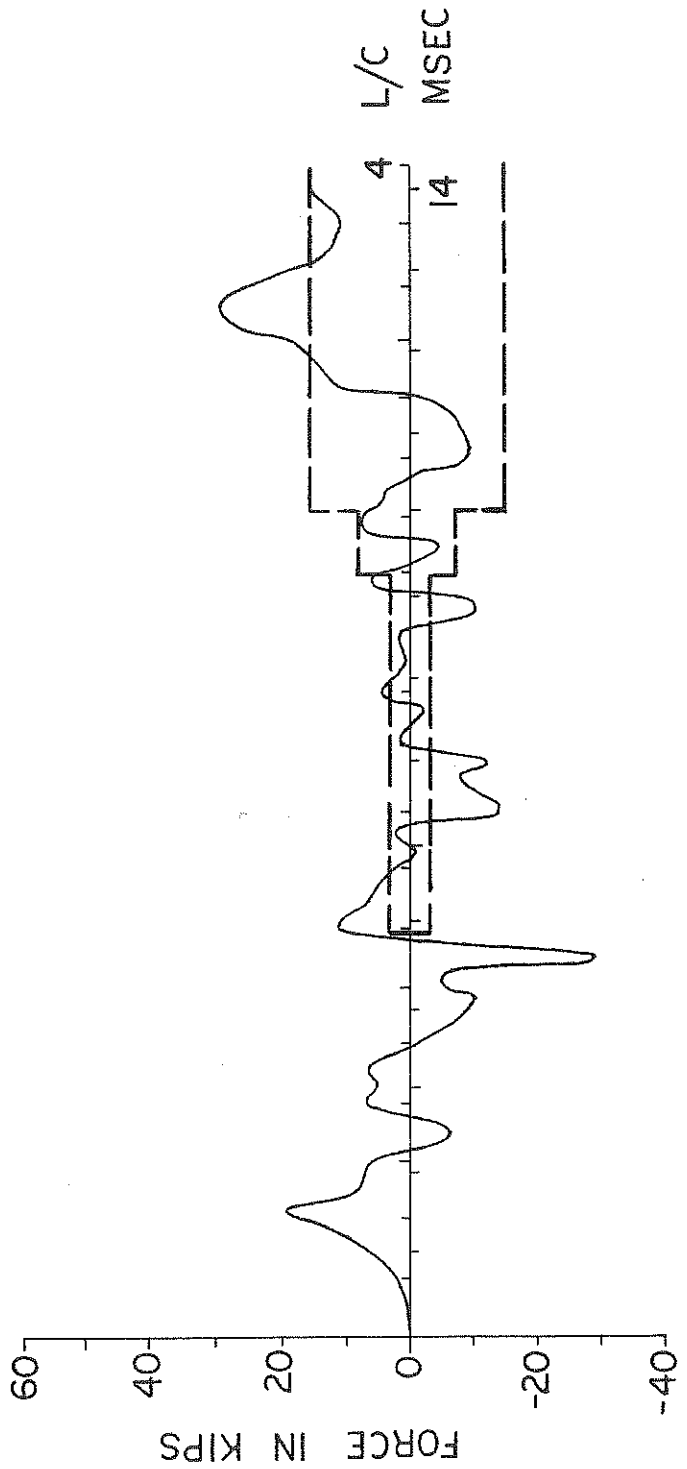

FIGURE 3.10: ERROR DELTA CURVE FOR ONE SKIN AND ONE TOE DAMPER

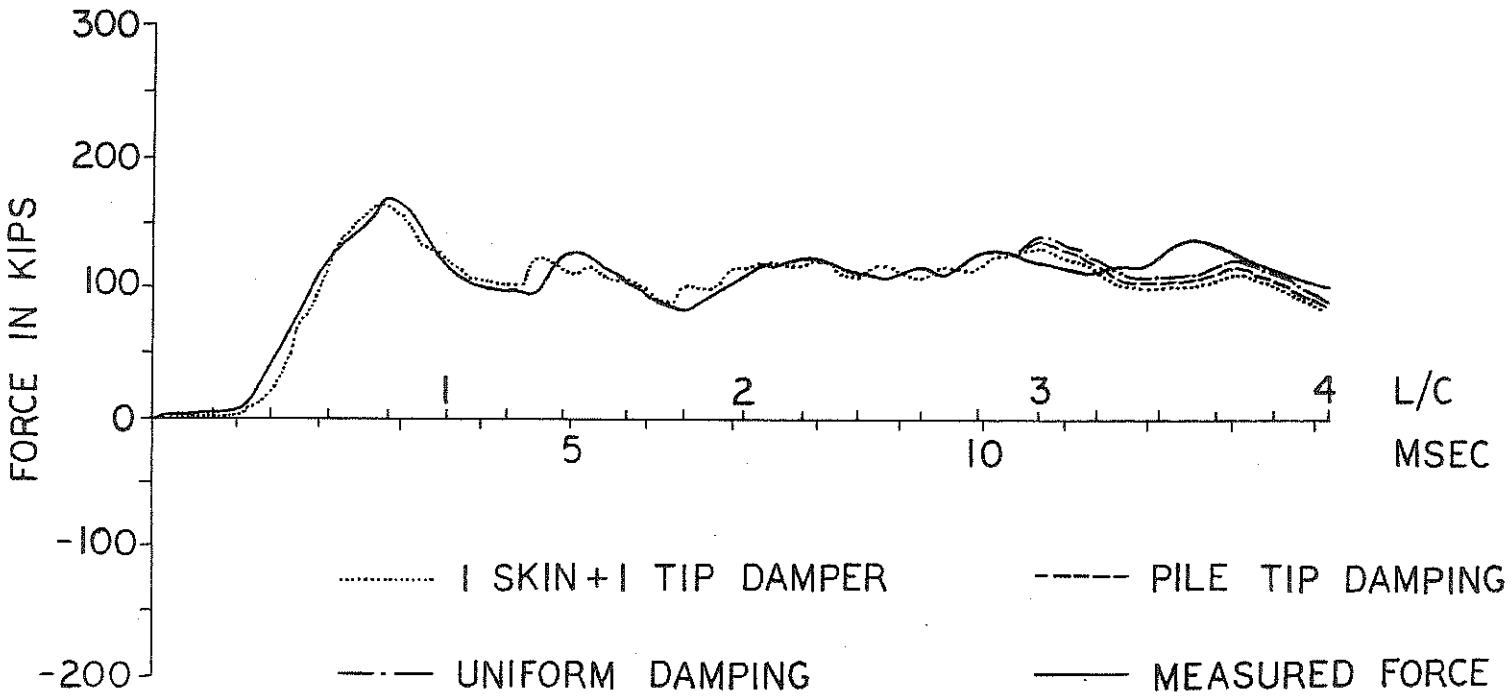

FIGURE 3.11: PREDICTED PILE TOP FORCE FOR THREE DIFFERENT DAMPING DISTRIBUTIONS COMPARED WITH MEASURED PILE TOP FORCE

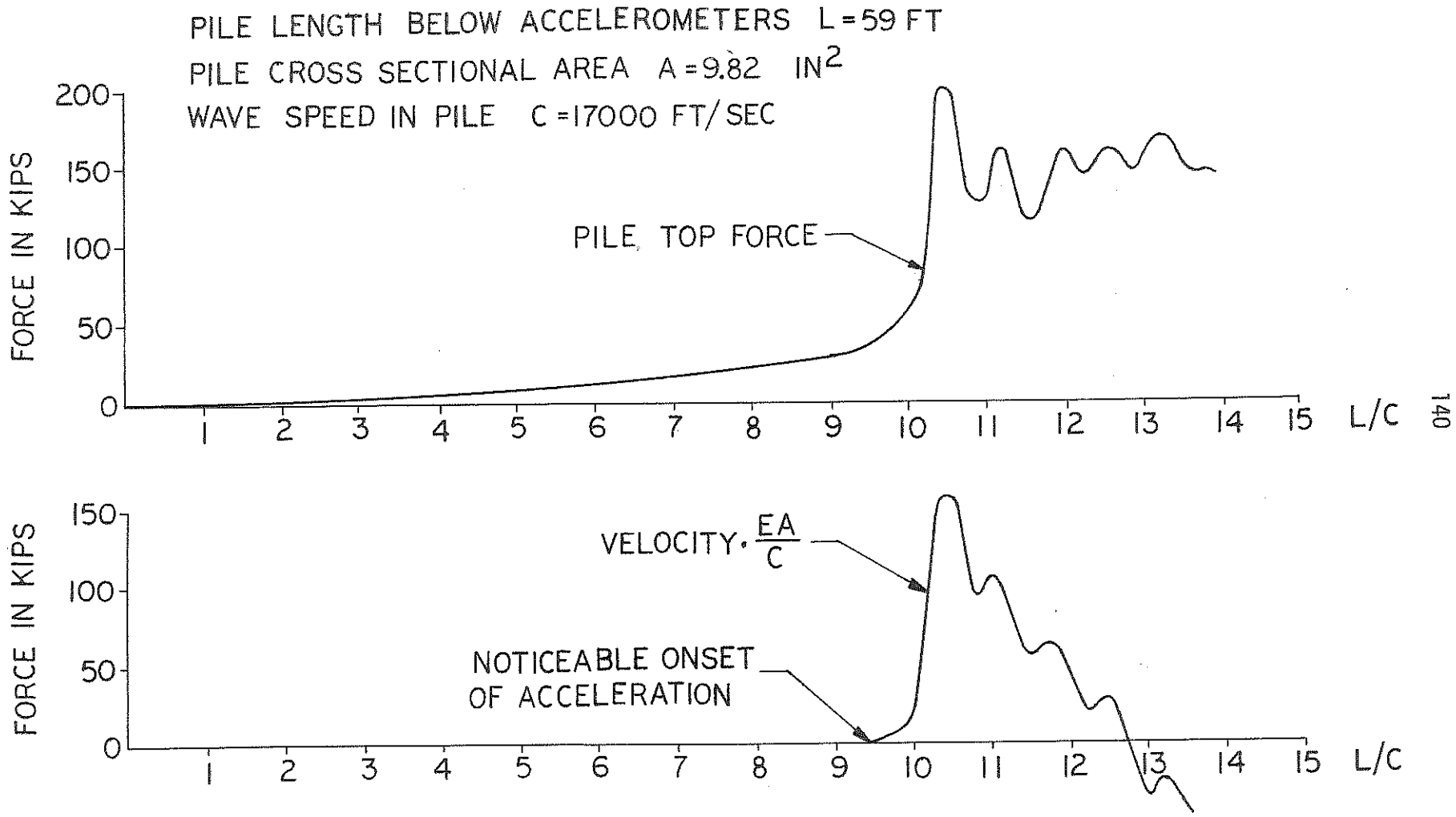

FIGURE 4.1: MEASURED FORCE AND VELOCITY OF PILE F-60 NO. 26.A

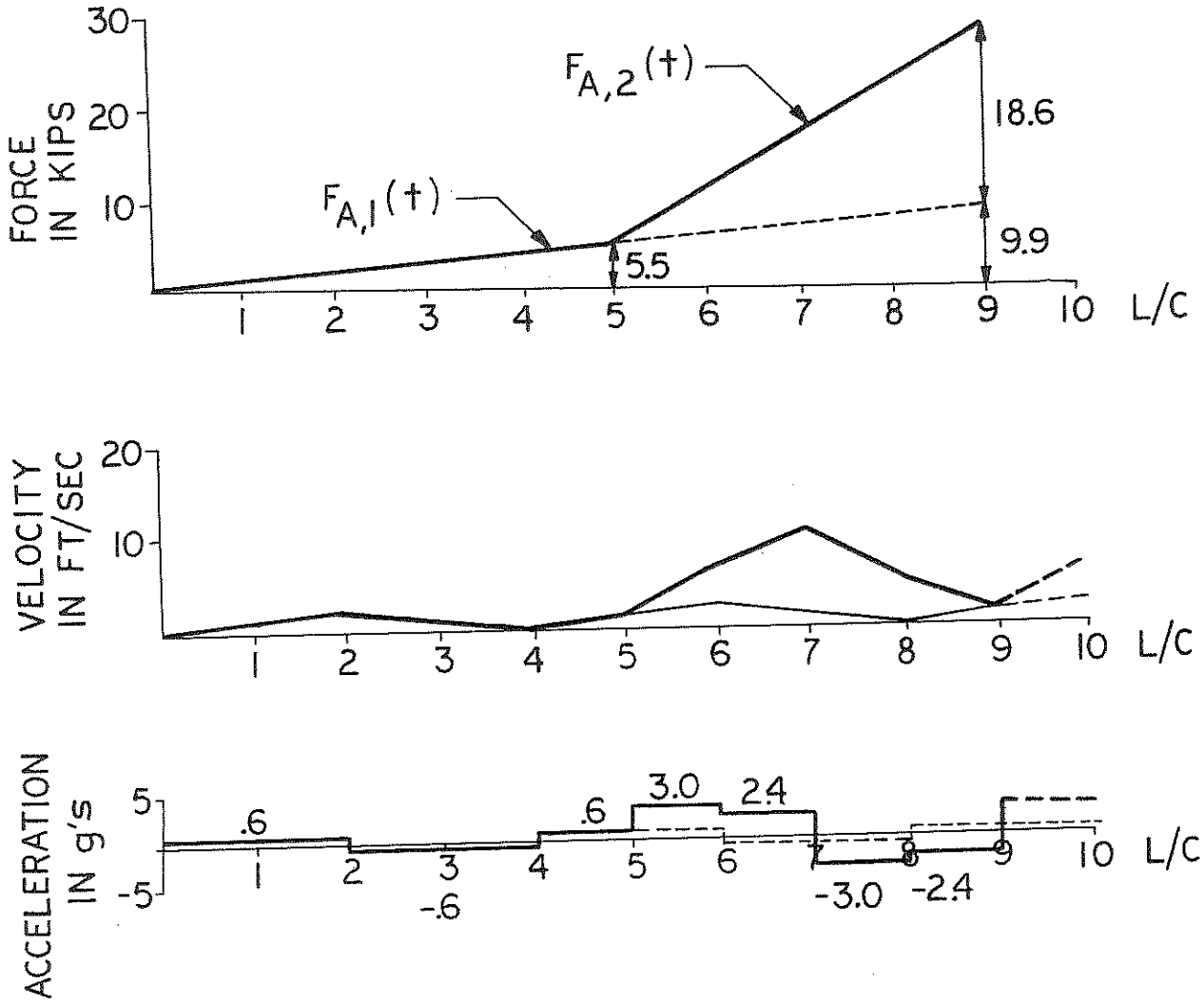

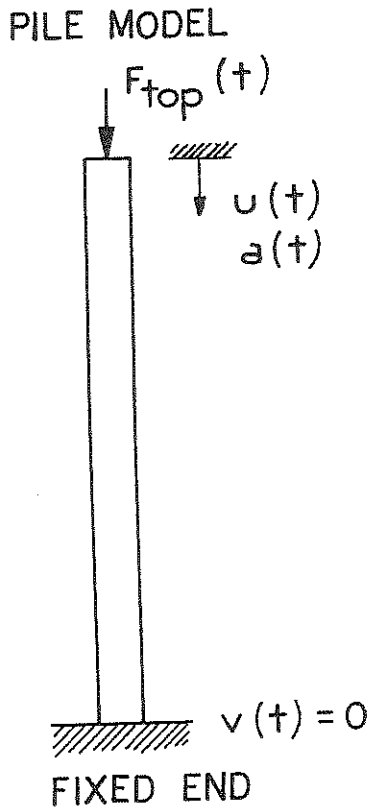

FIGURE 4.2: VELOCITY AND ACCELERATION AS DERIVED FROM FORCE OVER INITIAL PORTION OF RECORD

Pile F-60 Blox No. 26-A

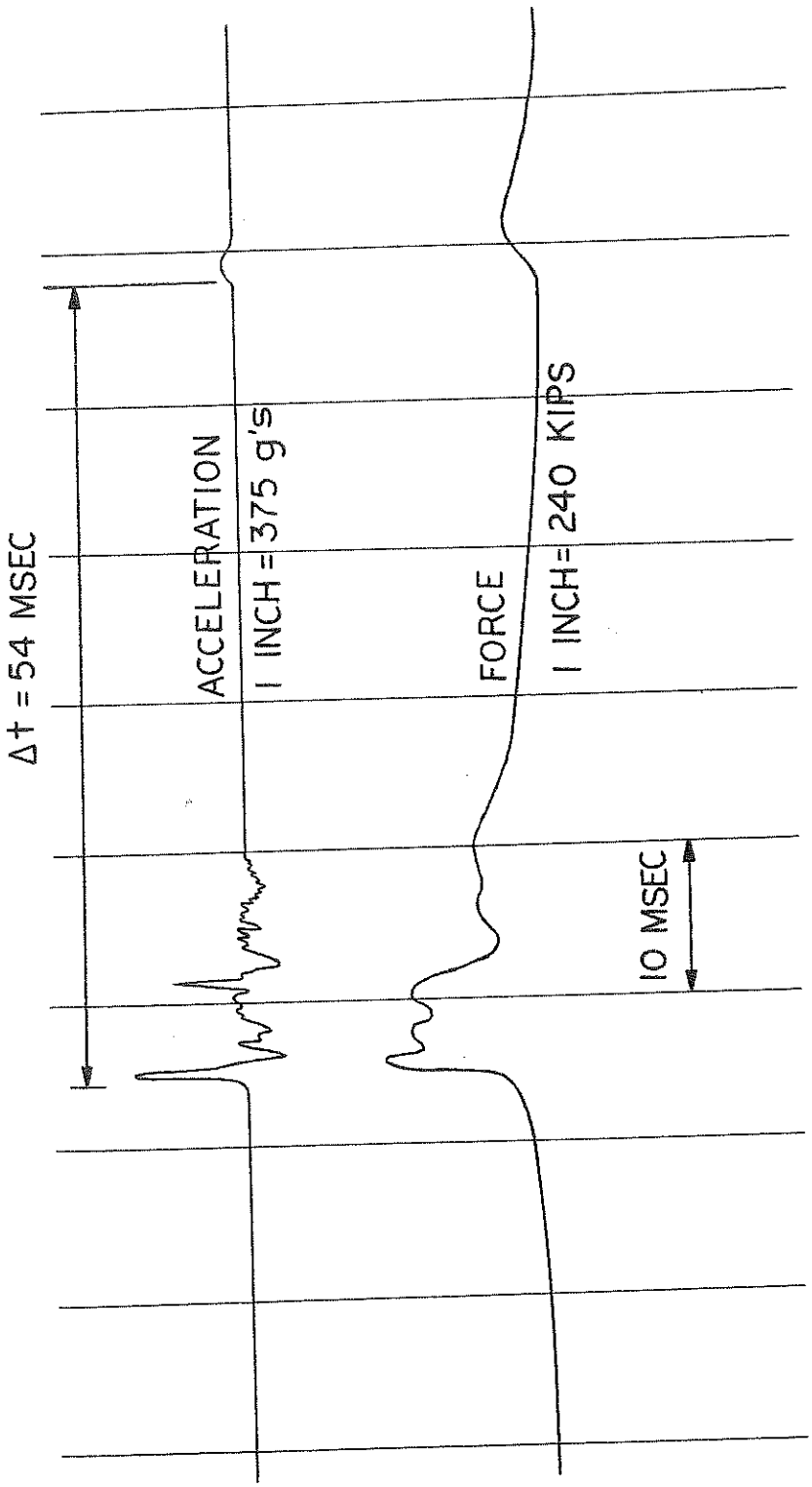

FIGURE 4.3: FORCE AND ACCELERATION IN ORIGINAL SCALE

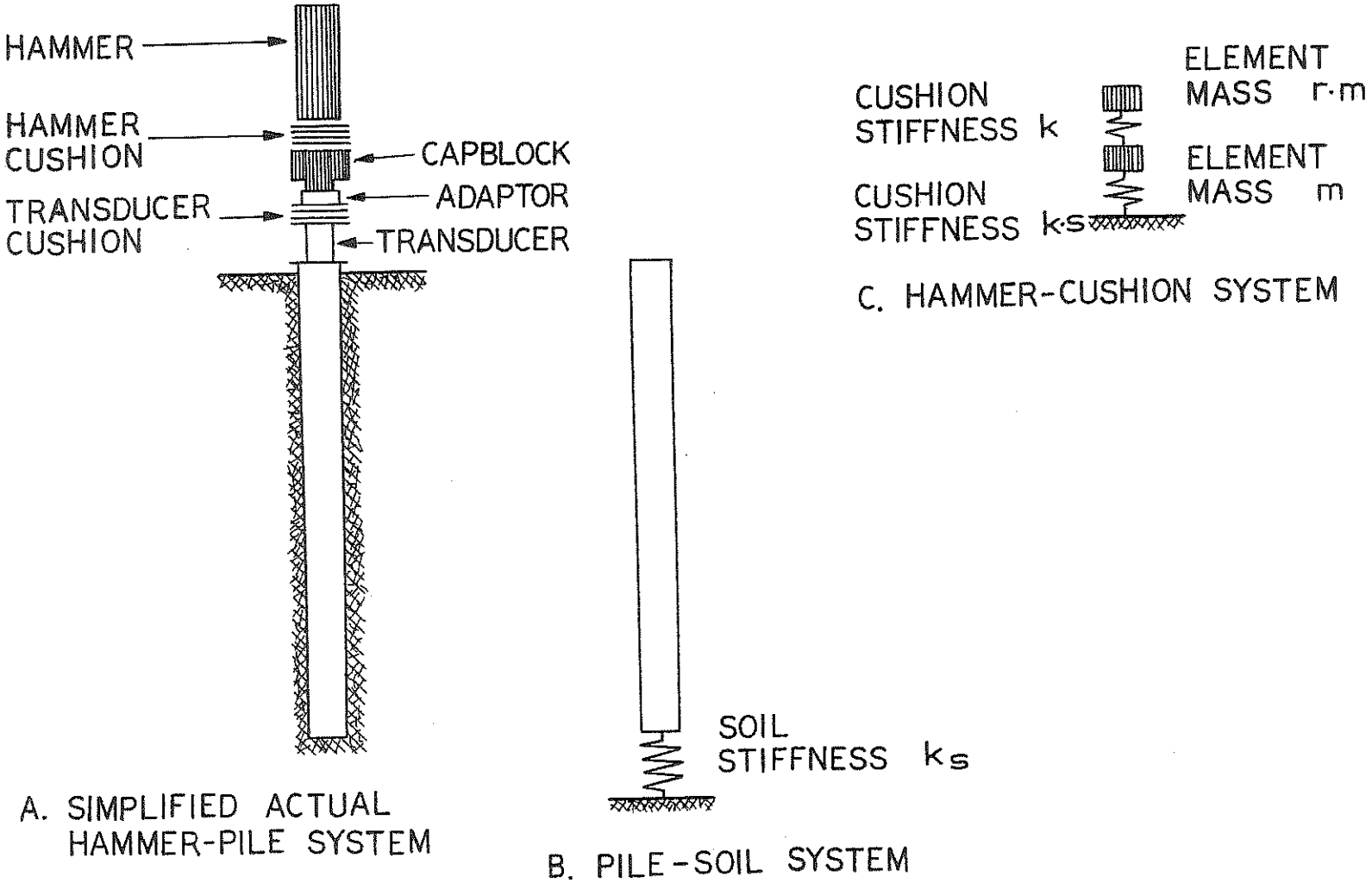

FIGURE 4.4: SIMPLIFIED MODELS OF HAMMER PILE SYSTEMS

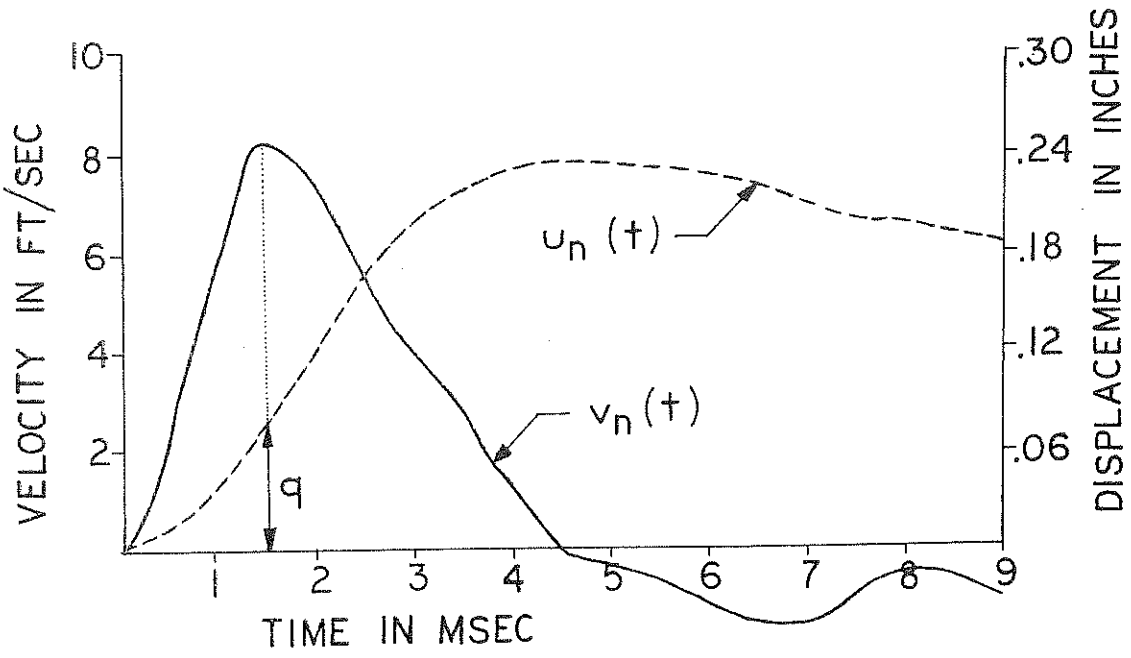

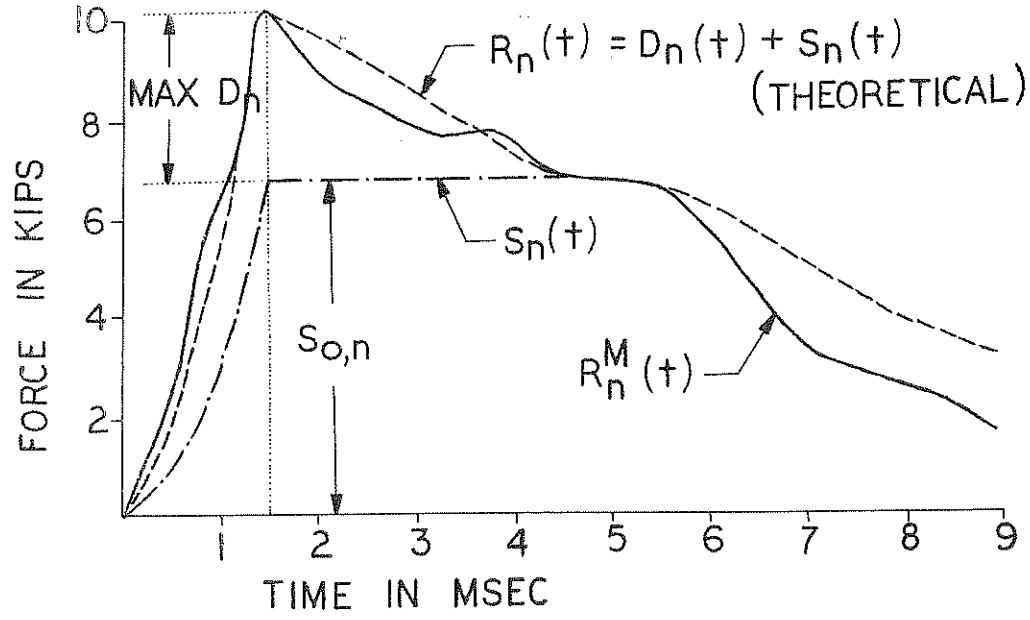

FIGURE 5.1: SOIL RESISTANCE FORCES AT PILE TIP 6-T-20, BLOW NO. 1-A

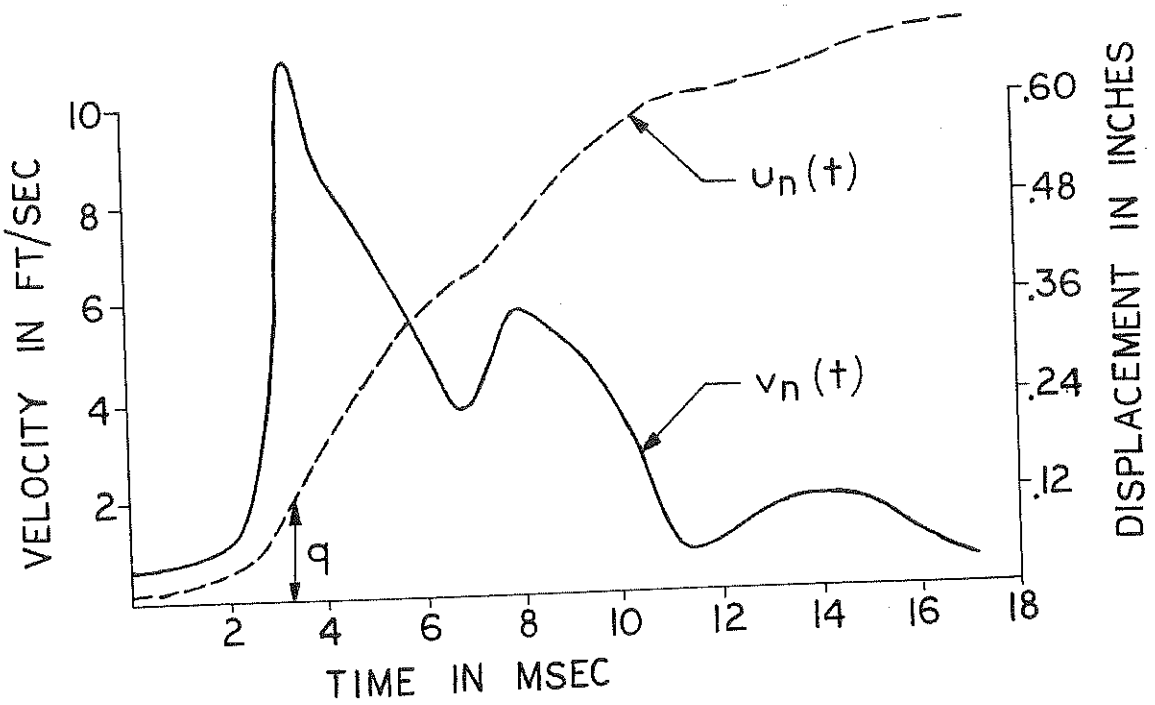

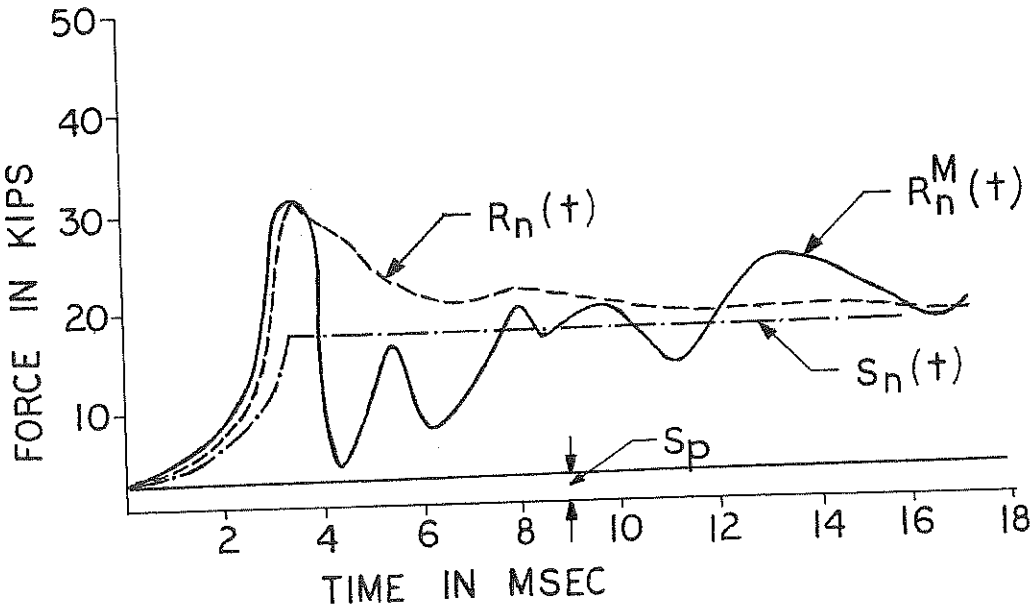

FIGURE 5.2: SOIL RESISTANCE FORCES AT PILE TIP Ri-50, BLOW NO. 22

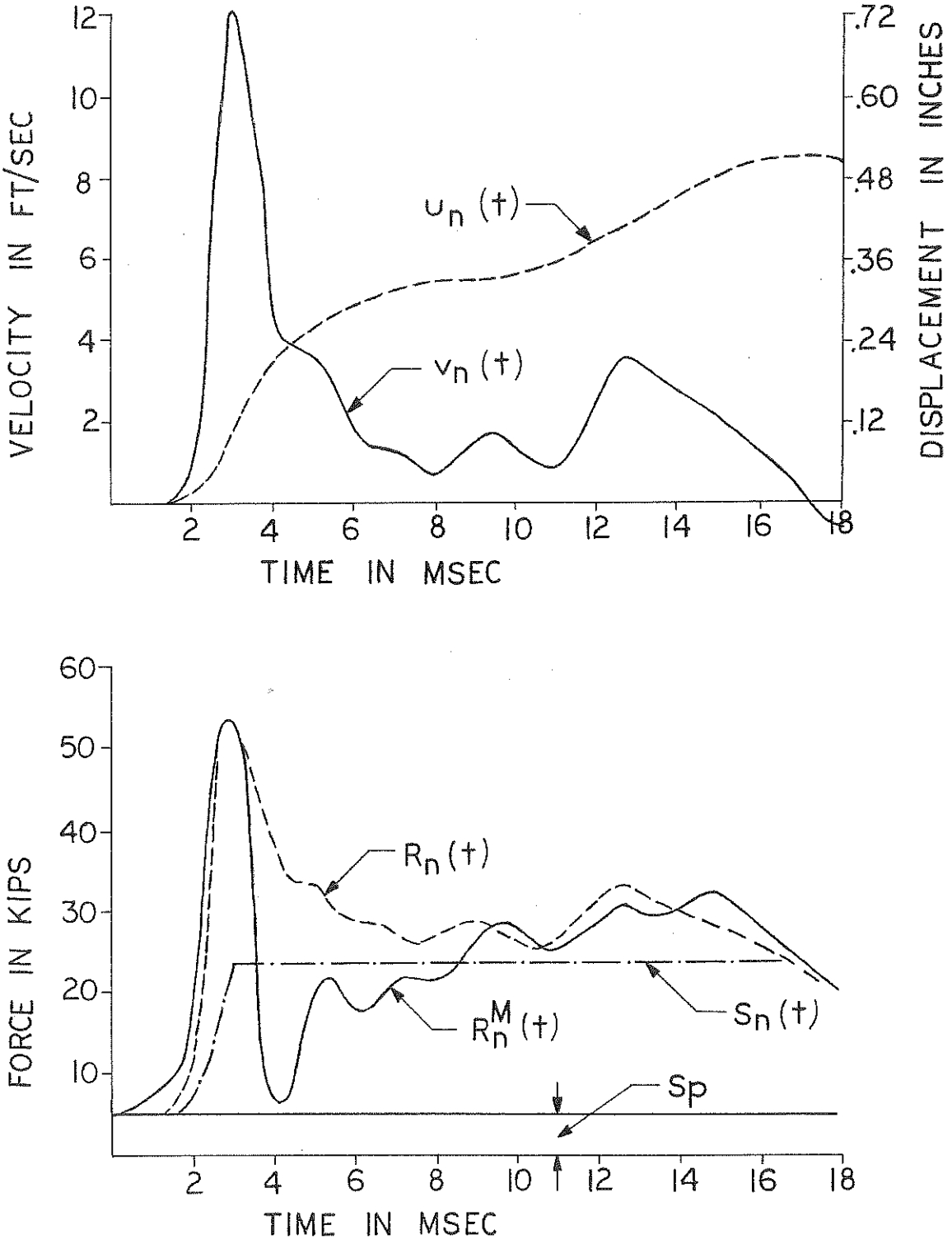

FIGURE 5.3: SOIL RESISTANCE FORCES AT PILE TIP Ri-50 BLOW NO. 8-A.

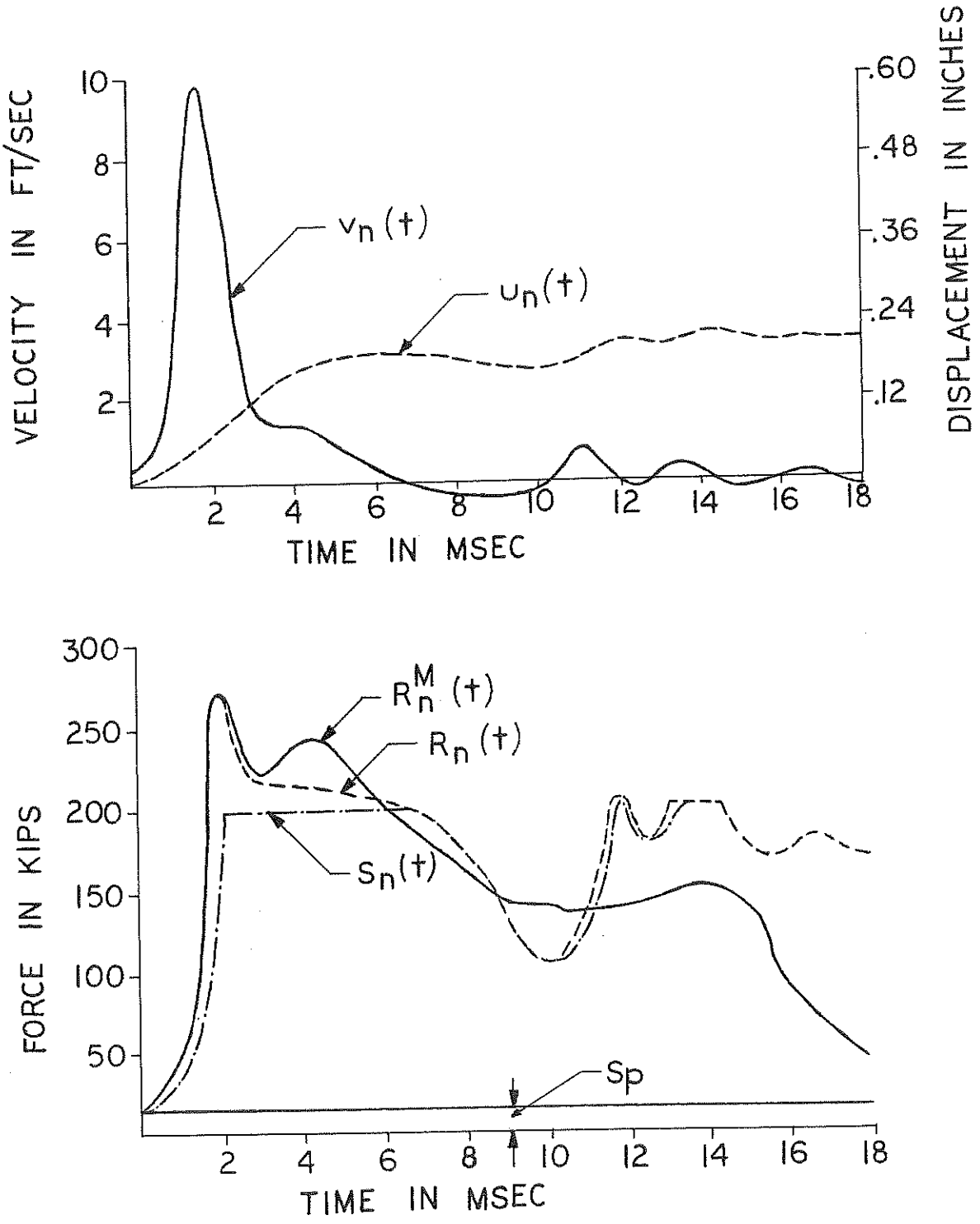

FIGURE 5.4: SOIL RESISTANCE FORCES AT PILE TIP Ri-60, BLOW NO. 22

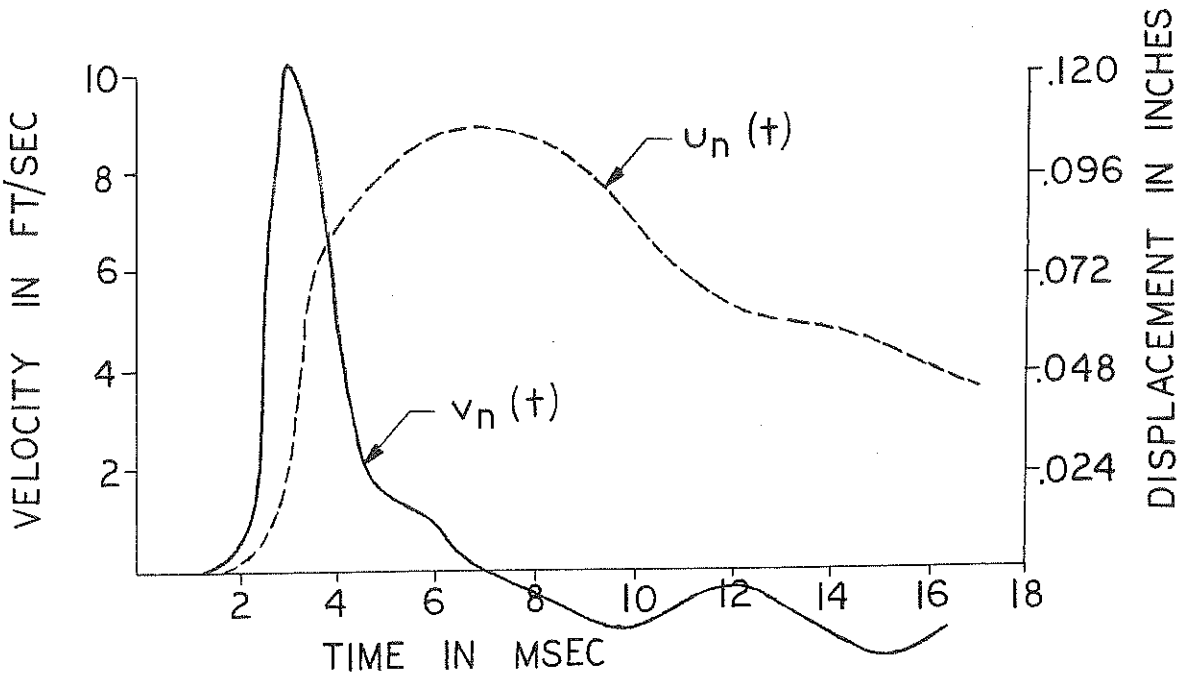

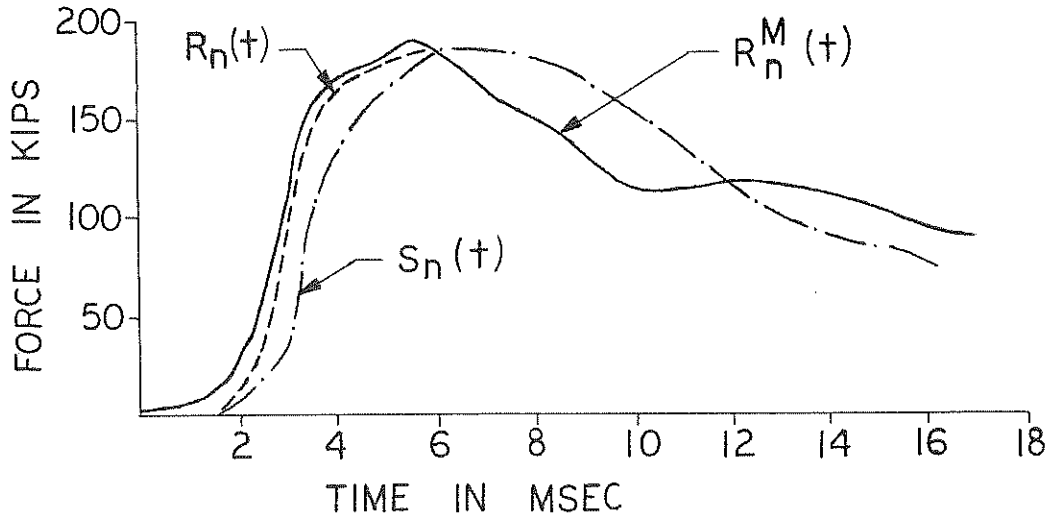

FIGURE 5.5: SOIL RESISTANCE FORCES AT PILE TIP Ri-60, BLOW NO. 8-A

A. 6-T-20 SAND

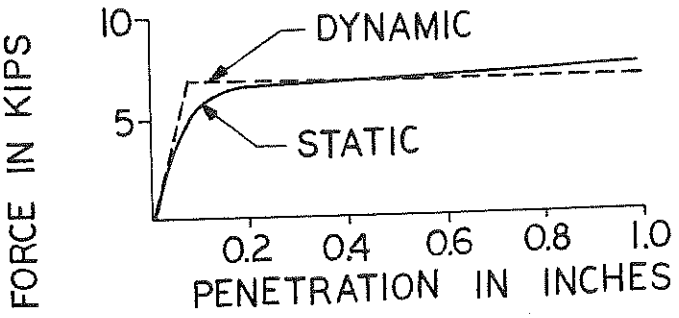

B. RI-50 SILT AND CLAY

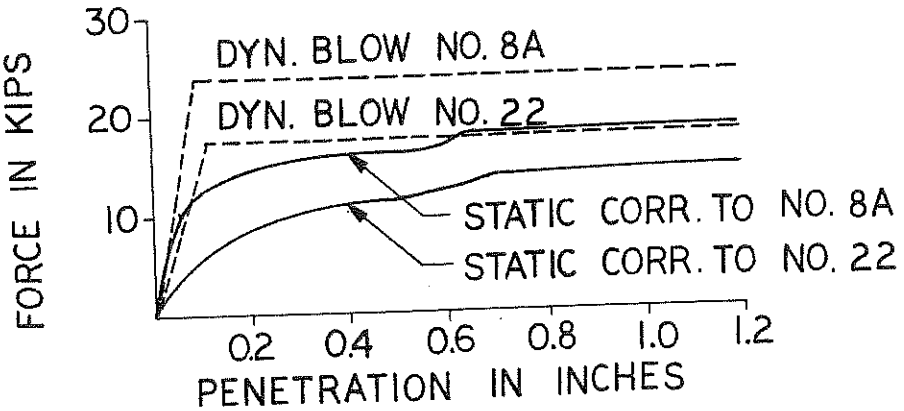

C. RI-60 GRANULAR SOIL

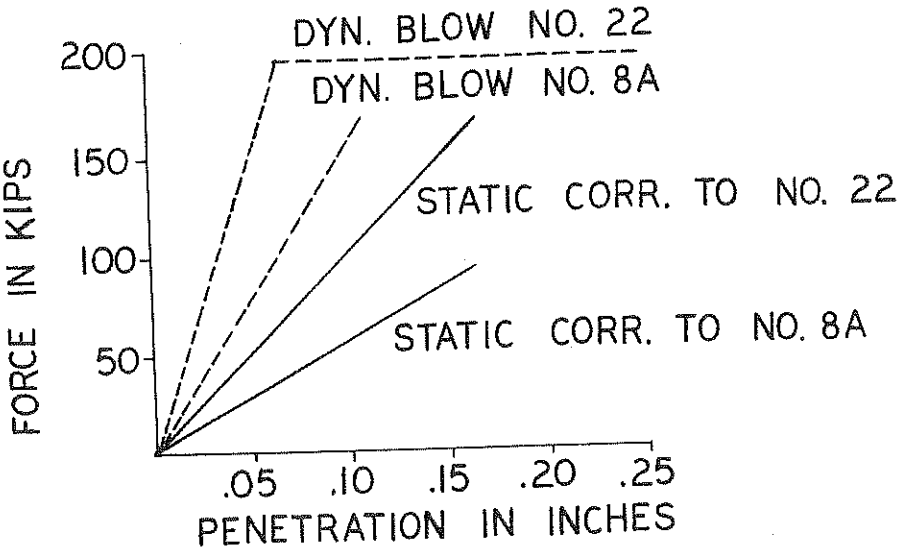

FIGURE 5.6: RESULTS FROM STATIC AND DYNAMIC PILE TIP MEASUREMENTS

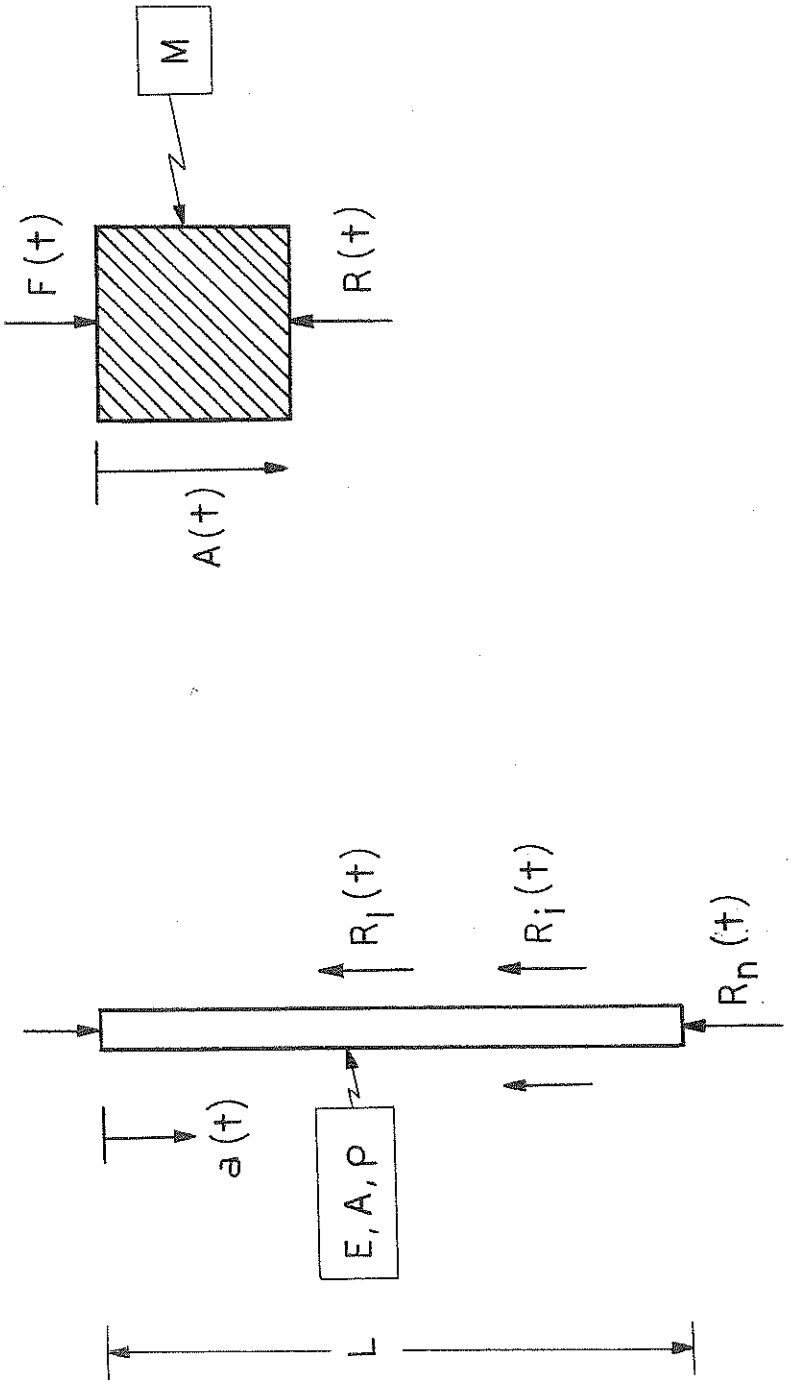

FIGURE 6.1: REAL PILE AND RIGID BODY MODEL

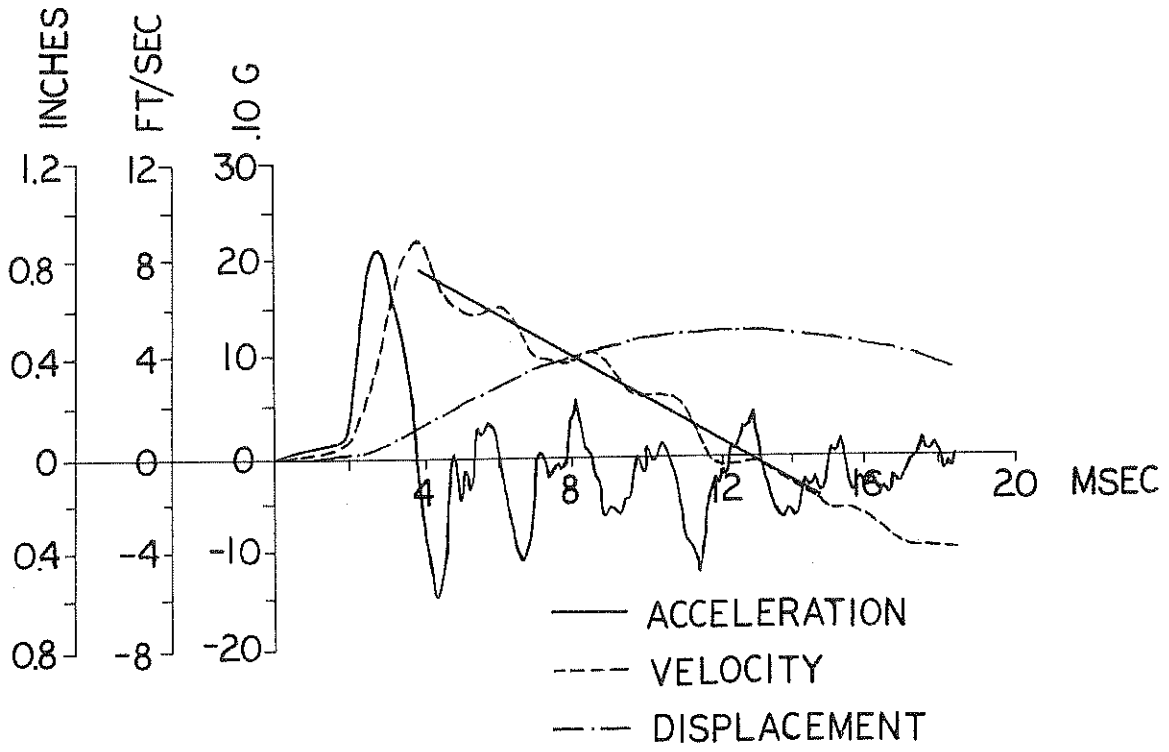

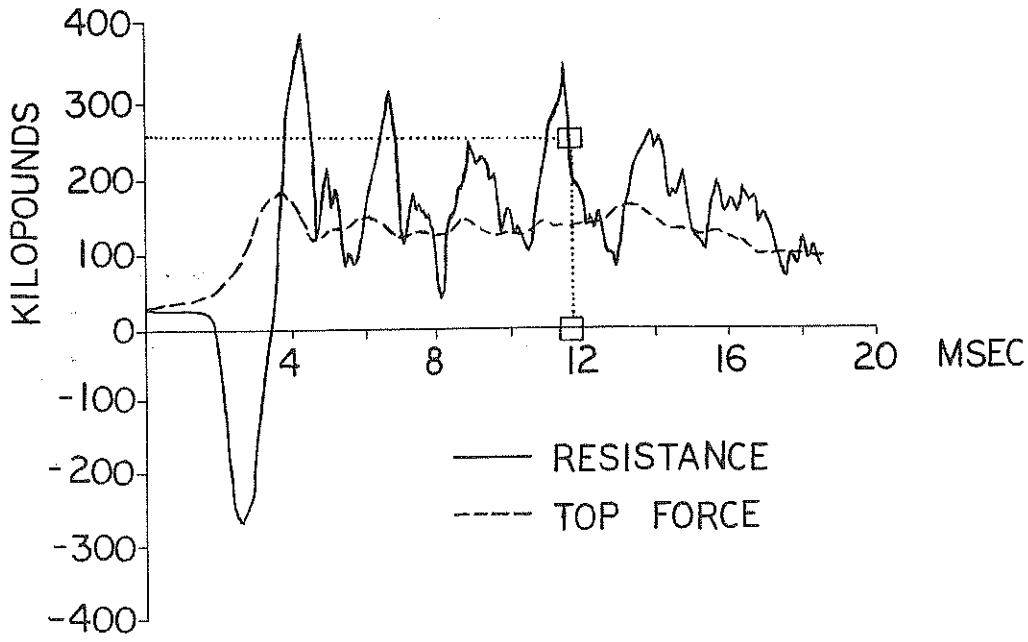

FIGURE 6.2: DYNAMIC RESULTS OF PILE F-50 AFTER DRIVING

(DATA SET NO. 7)

A. SHEAR AT BOTTOM END

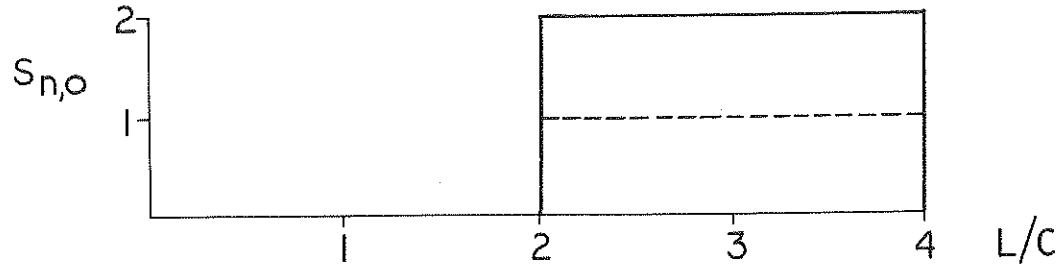

B. SHEAR AT $x = L/4$

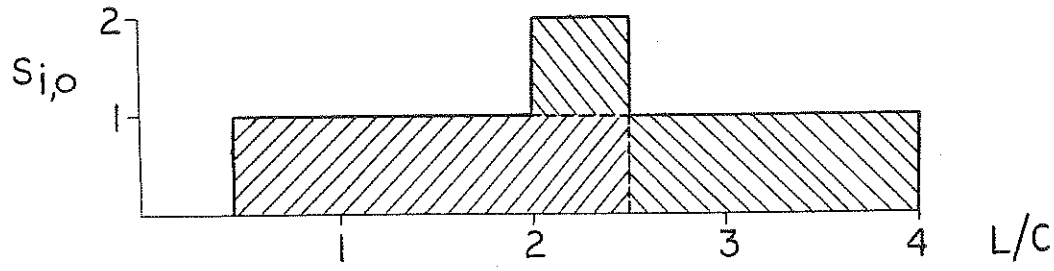

C. MODIFIED DELTA CURVE

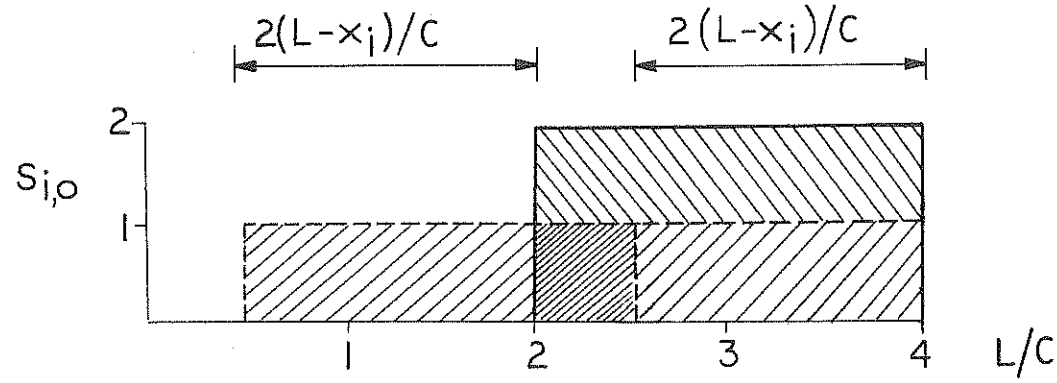

FIGURE 6.3: MODIFICATION OF RESISTANCE DELTA CURVE FOR SKIN SHEAR FORCE TO PRODUCE EQUIVALENT DELTA CURVE FOR BOTTOM SHEAR FORCE

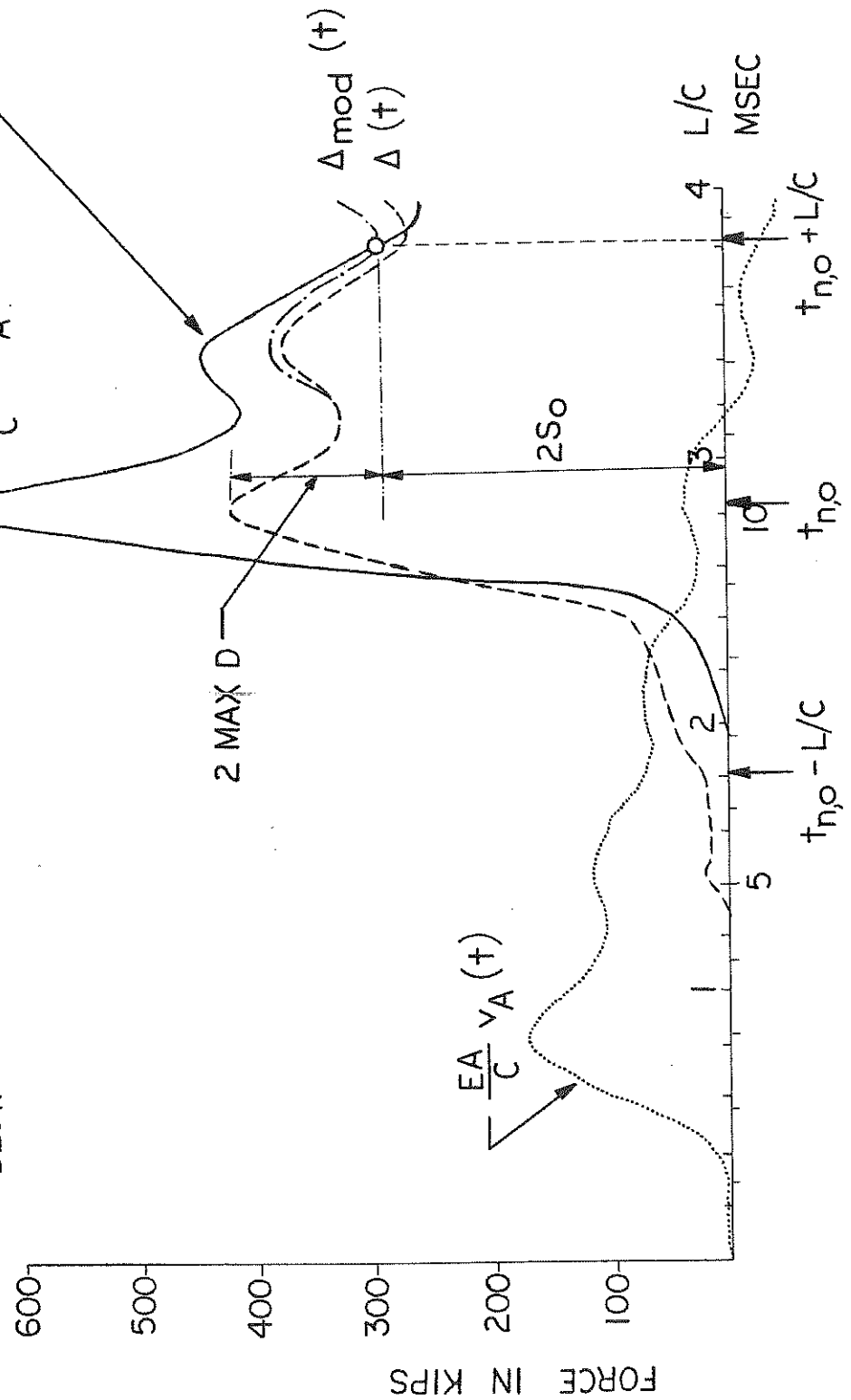

FIGURE 6.4: ILLUSTRATION OF PHASE III PREDICTION SCHEME

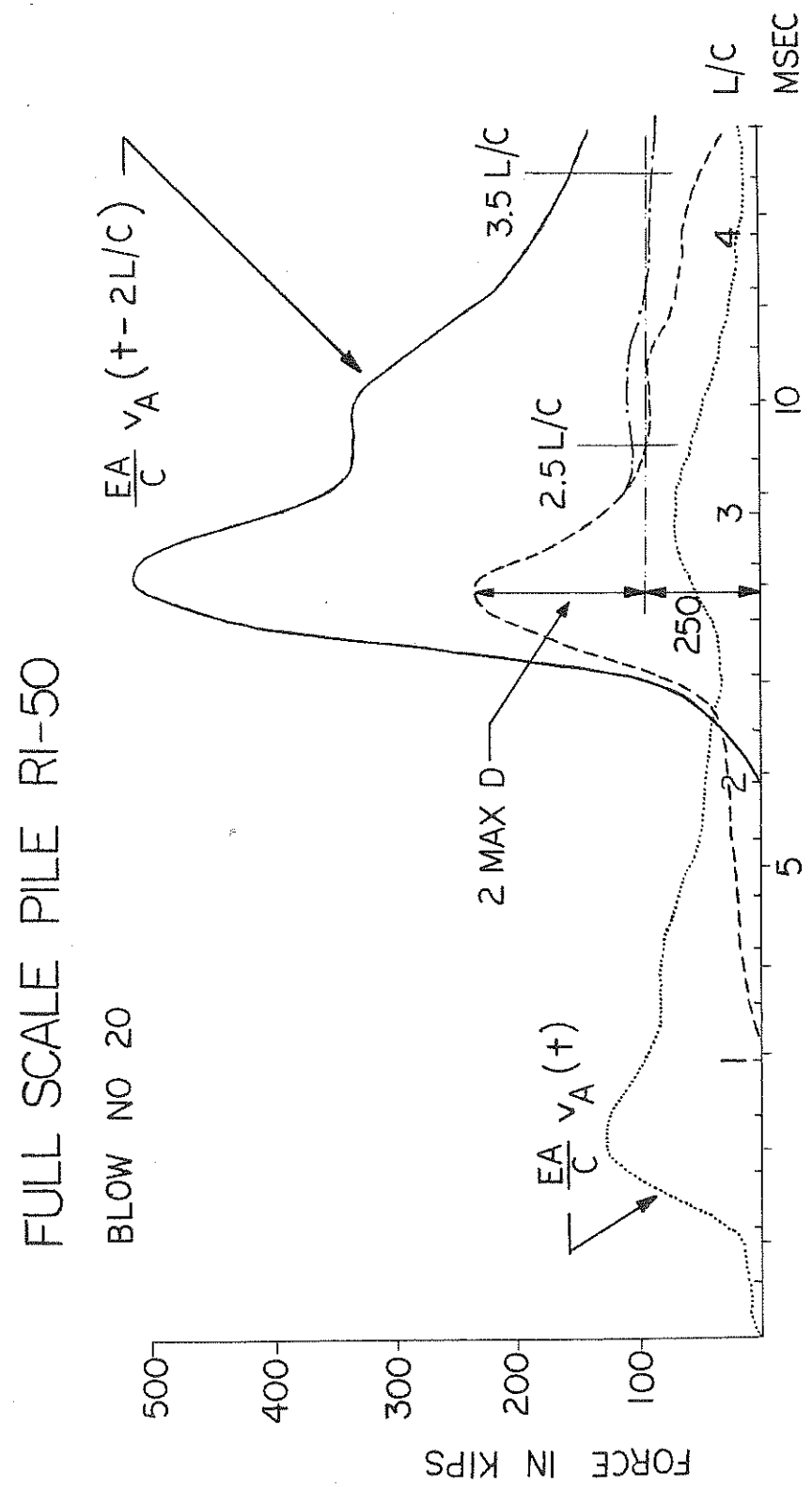

FIGURE 6.5: ILLUSTRATION OF PHASE III PREDICTION SCHEME FOR LOW DRIVING RESISTANCE